EMERGENCE OF COOPERATIVE BEHAVIOR

IN MICROBIAL CONSORTIA

by

Diana Ruth Schepens

A dissertation submitted in partial fulfillment
of the requirements for the degree

of

Doctor of Philosophy

in

Mathematics

MONTANA STATE UNIVERSITY
Bozeman, Montana

April 2018

ACKNOWLEDGEMENTS

I would like to acknowledge my advisor, Dr. Tomáš Gedeon, for all his support and mentorship during my time in the Ph.D. program; collaborators Dr. Jeff Heys, Dr. Ross Carlson, and Ashley Beck for their input and collaboration on the biological aspects of this project, committee members Dr. Lisa Davis and Dr. Tianyu Zhang for their support; and funding by a grant from the National Science Foundation NSF DSW-1361240.

TABLE OF CONTENTS

TABLE OF CONTENTS – CONTINUED

LIST OF TABLES

Table Page

LIST OF FIGURES

LIST OF FIGURES – CONTINUED

Figure Page

ABSTRACT

Cooperative microbial communities and their impact are ubiquitous in nature. The complexities of the cross-feeding interactions within such communities invite the application of mathematical models as a tool which can be used to investigate key influences in the emergence of cooperative behavior and increased productivity of the community. In this work, we develop and investigate a differential equation model of competition within a chemostat between four microbial strains utilizing a substrate to produce two necessary metabolites. The population of our chemostat includes a wild type strain that generalizes in producing both metabolites, two cross-feeding cooperator strains that each specialize in producing one of the two metabolites, and a cheater strain that produces neither metabolite.

Using numerical methods we consider three key characteristics of the microorganisms and investigate the impact on the emergence of mutual cross-feeding in the community. First, we investigate the impact that substrate input concentration and the rate and type (active vs. passive) of metabolite transport between cells has on the emergence of cooperation and multi-stabilities resulting from the competition. Second, we investigate the role that resource allocation within metabolic pathways plays in the results of the competition between cells with different metabolite production strategies. Introducing metabolite production cost into the model leads to new outcomes of the competition, including stable coexistence between different strains. Lastly, we examine the effect that an initial population of a non-cooperative cheater strain has on the outcome of competition. Our results show that the emergence of a cross-feeding consortia relies on the availability and efficient use of resources, ease of transport of metabolites between cells, and limited existence of cheaters.

CHAPTER ONE

INTRODUCTION

Cooperation between different species and phenotypes is observed frequently in natural systems. Examples of cooperative behavior on a larger scale include insects helping to pollinate plants [18,27] and human social and economic behavior [7,10,58]. Within microbial communities cooperation often takes the form of specialization in the production of essential resources and subsequent resource exchange in the form of cross-feeding [39, 40, 52]. Cooperating populations are able to more fully utilize available resources and thus may outcompete an homogenous population [14]. This seemingly contradicts classic resource-ratio theory [55] that an environment with a single limiting resource can support only a single population. Metabolic dependencies within diverse microbial communities encourage the coexistence of different species found within cooperative microbial groups [59].

Cross-feeding relationships between microbes can take various forms. One particular form is that of the producer-scavenger relationship in which one microbe consumes a metabolic byproduct of another microbe (Fig 1.1). An example of this can be seen with *E. coli* when one phenotype consumes glucose and produces an organic acid, such as lactic or acetic acid, and another phenotype consumes this organic acid as a scavenger [3, 28, 46, 56]. In this particular example, the shared benefits are mutual in that the producer provides resource for the scavenger and the scavenger helps mitigate the inhibitory pH effects of the excreted organic acid. In the case where the scavenger takes the form of a cheater, or individual that obtains resource without providing a benefit or resource in return, the benefits of cross-feeding are

asymmetric.

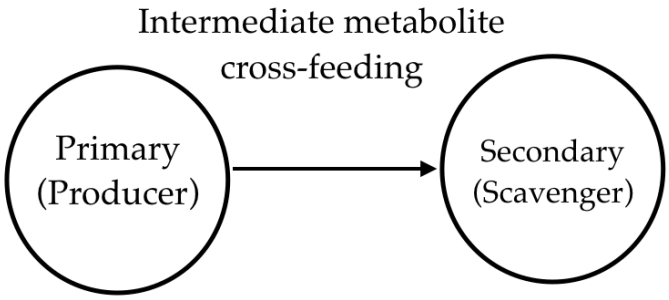

Figure 1.1: **Producer-scavenger cross-feeding.** Primary producer strain cross-feeds metabolic intermediary by-product to a secondary scavenger strain.

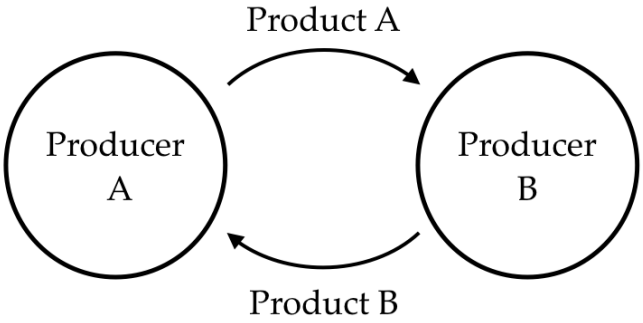

Figure 1.2: **Mutual cross-feeding.** Two producing strains exchange metabolic products.

The particular form of cross-feeding that we will focus on in this work is that of mutual cross-feeding- when individuals of a cross-feeding relationship produce a resource that is shared in exchange for resources received from other members (Fig 1.2). For example, rhizobia bacteria provide nitrogen fixing for legume plants, and the plant in turn provides organic acids as an energy source for the bacteria [19].

In light of the theory of evolution, every observed instance of cooperation is an event that asks for explanation: how does this benefit each participant in the

exchange? Given that cooperation was observed, is it more successful than other arrangements? Why is this arrangement more successful and what are the conditions that make cooperation successful?

Understanding the mechanisms that encourage cooperation in microbial communities has broad implications. Bacteria communities are found to cause a variety of chronic medical infections [13, 31], and the human microbiom has myriad health effects [24, 57], many of which have yet to be discovered. Microbial consortia play a role in water treatment plants [32], toxic site remediation [29, 30], and biofuel production [38, 57]. Biological and chemical engineers desire to engineer microbial communities in which biomass or byproduct production are optimized [5, 53]. Mathematical models play a critical role in broadening our knowledge of the functions and structures present in microbial communities.

One of the starting points for this work has been theoretical work [26], which studied the emergence of cooperative behavior in homogenous microbial populations and how it may lead to multicellularity. Researchers observe that there are many necessary cellular processes that are incompatible with each other, such as nitrogen fixing and photosynthesis in filamentous cyanobacteria [9, 47]. As a consequence, a cell has to temporarily separate these processes and performs only one of them at any given time. If two of such cells aggregate at a time when they perform complementary processes, and if the result of these processes can be shared, these two cells may form a cooperative unit that outperforms the original population. Ispolatov et al. [26] present a model that assumes that such propensity for co-localization is itself an evolvable trait, and show that under certain conditions on the shape of a cost-benefit function, the temporal segregation of mutually repressing processes indeed may lead to emergence of cooperation and multicellularity.

A recent paper by Gudelj et al. [22] studies the interaction of producer-scavenger

cross-feeding in microbial populations. They considered a mathematical model with two competing strains in a chemostat with a single limiting substrate. The metabolizing of the substrate is simplified to a two-reaction process corresponding to glycolysis and the TCA cycle. The first reaction metabolizes the substrate into an intercellular metabolic intermediate, which in the second reaction can be either completely metabolized, or excreted out of the cell as an extracellular metabolite. The extracellular intermediate metabolite can be imported by either microbe and metabolized. Each of the two strains specializes in metabolizing either the substrate or the extracellular intermediary. A bifurcation analysis of the system as a function of the input concentration of the substrate shows existence of multi-stability, where at high concentrations either strain can outcompete the other. In addition, there is a steady state that corresponds to stable coexistence of both species. The key observation in [22] is that microbial diversity can be supported by simple environments contradicting the competitive exclusion principle [20, 25].

Construction of synthetic cooperative interactions [37, 42, 43, 45, 61] similar to those modeled in this work have shown that cross-feeding consortia can be stable even when non-cooperative cells are present. Pande et al. [42, 43] engineered *E. coli* to be auxotrophic for each of four amino acids and to overproduce all other amino acids in order to simulate obligate cross-feeding communities. These cross-feeders were grown in various pairings and as co-cultures with wild-type and non-cooperative phenotypes. The theoretical results of our work closely resemble results of these experimental studies.

Using a mathematical model of competition in a chemostat, we investigate conditions that favor cooperation between four different microbial strains: wild type, two mutually cross-feeding strains, and cheaters. We examine more closely conditions that lead to stable polymorphisms, that is, a stable steady state with a coexistence of

different populations, such as those observed in Gudelj et al. [22]. In particular, we ask how the results of the competition depend on the type and rate of transport being used to move metabolites into and out of the cell, inflow concentration of substrate into the chemostat, and production cost of metabolites.

We incorporate metabolite production cost into the model by deriving a function that relates the cost of metabolite production to its production rate. Such a function should be expressed in terms of empirically measurable parameters [26], take into account investment into both substrates and enzymes that process them [54], reflect the belief that the process of evolution produced an optimally functioning cellular metabolism [50, 51], and contain an inefficiency penalty [26] that captures the incompatibility of cellular processes. A function that reflects the optimality assumption and contains an efficiency penalty has been proposed in [26], but it is not expressed in terms of measurable parameters. In our approach, we model a simple metabolic pathway that requires resource investment into both substrates and enzymes [54] as a sequence of Michealis-Menten reactions. We optimize the steady state production cost and find a function that describes this cost as a function of production rate and is expressed in terms of empirically measurable parameters. Our resulting cost function contains the desired inefficiency penalty as an emergent property of the model. Incorporation of this production cost into the model reflects the assumption that cells which incur low production costs have more resources available for growth which results in a fitness advantage over their competitors.

Models of microbial communities often assume that transport of metabolites is passive and thus proportional to a difference in concentrations. This may be done as a simplification, even though many essential resources require the use of a transmembrane protein. Therefore, our goal was to study the effect of both the rate of transport as well as the type of transport on the outcome of the competition.

We compare models utilizing either passive transport, which has been used in other microbial models [22, 34], or active transport, and observe significant differences in the results of the competition. The effect on the steady state composition of the population by the presence and initial concentration of obligatory auxotrophs (cheaters) is also examined.

We present our numerical analysis of the model in three parts. First we investigate how the rate and type of transport affects the outcome of competition in the chemostat between the four strains. In both models, we find that at low transport rate the wild type monoculture dominates the chemostat. However, the advantage of the wild type strain diminishes when the transport rate increases. These results are not surprising; limited transport hinders cooperation.

When the transport rate is increased in the active transport model, the wild type strain domination is not merely replaced by a state where the cooperative consortium wins. Rather, the system exhibits bistability of two coexisting stable steady states: in one only the wild type strain survives, in the other, only the cooperative consortium survives. The outcome of the competition depends on initial composition of the population. This interesting phenomena may have implications on spatially distributed microbial populations such as biofilms. Since the initial populations in small local niches can be considered random, one can expect to observe coexistence of wild type and cooperative consortia as spatially segregated local communities even though for the same parameters we would not observe coexistence in a well mixed chemostat .

In the passive transport model, an increased transport rate also results in the same bistability between a wild type dominated steady state and one with only the cooperative consortium. However, a further increase in transport rate gives rise to a third stable state, where no strain is able to survive. In this tri-stable regime the

outcome (wild type, consortium, or collapse) depends on initial population. Even further increase in transport rate leads to the loss of the wild type steady state resulting in bistability between population collapse and the cooperative consortium.

In the second part of our results, we include the production cost of resources into the model. Without the inclusion of this cost, there are no stable steady states where the cheater strain survives in coexistence with either wild type or cooperative strains. Yet, both in nature and in synthetic consortia [43] stable coexistence of populations is observed. When production cost is not included in our model, the growth rate for the cheater strain will be smaller than that of wild type, or either of the cooperator strains. The reason for this is that resource producing strains will naturally have a higher internal concentration of produced resource. However, producer strains must commit resources to produce metabolites that cannot be used elsewhere. To include this into the model we scale the growth rates of each strain by a function of the production cost incurred by that strain. We have previously derived such a function [48] from consideration of trade-off between investment into enzymes and substrates along a biochemical pathway and use this function to extend our chemostat model by scaling the growth rates of all producer strains. This scaling lowers the growth rate of overproducers and gives an advantage to cheaters which do not incur this cost, and to the wild type strain which does not overproduce metabolites [43].

With the inclusion of a cost function we see the emergence of stable polymorphisms and parameter regions with multi-stability for both passive transport and active transport models. However, the differences between these two models are accentuated by the inclusion of cost. The passive transport model with very high transport rate leads to population collapse, while in the active transport model, the wild type strain dominates. An additional observation seen only in the passive transport model is the dependence of steady states on the relative amount of cellular

resources that are invested in the production of exchanged resources. This observation is important for discussion if cooperative consortia are more likely to share an expensive product like amino acids, versus a less expensive resource like acetate or lactate. Our results suggest the importance of a cost-benefit trade off in the development of cooperative and diverse microbial communities.

In the final part of the numerical analysis we highlight the effect of cheaters and the role that they play in determining which of the stable steady states are attained from various initial conditions in bi-stable and tri-stable parameter regimes. We show that in both passive and active transport models an increase in the initial cheater population will weaken the cooperative consortium to the point where either wild type population dominates or the populations collapses. The effect of the presence of cheaters weakening cooperative behavior is also evident when we include the effect of production cost in the model. Even when cheaters and cooperators stably coexist at steady state, a high initial cheater population will weaken cooperation, leading to pure wild type population or population collapse.

Further study into the impact that cheaters have on the dynamics of the system could tie together results about the ability of spatial constraints to limit cheaters [42] and the effect of population density on cheaters [11]. In our model, an increase in the initial cheater population can weaken the cooperative behavior to the point where either wild type population dominates or the populations collapse, similar to simulations of two species populations [11]. Population collapse, caused by cells that uncontrollably leak essential resources observed in the passive transport model, as well as domination of non-producers has been observed in game theory models and experimental data from synthetic communities [61].

In addition to numerically analyzing the various forms of the model, we compare analytical results from a simplified version of the passive transport model without the

inclusion of production cost to the numerical results obtained from the original model. Qualitative behavior of the stable states is found to be similar, though coexistence states and states with population collapse show some differences that highlight the effects of simplifying assumptions.

Our investigations resulted in three important observations about the establishment of a cooperative consortium as a result of competition.

1. First, we found that the outcome of the competition as described by stable steady states, depends on the type and rate of transport. Surprisingly, the more simple passive transport model leads to more diverse behavior than the active transport model.

2. Second, the inclusion of metabolite production cost in the model gives rise to more diversity in the possible outcomes of the competition. With the inclusion of a cost function we see the emergence of a stable coexistence state of cheater and cooperator strains and parameter regions with multi-stability for both passive and active transport models. This agrees with theoretical results that even in the absence of the cooperator's ability to detect the presence of cheaters, and cheaters not being punished, a stable coexistence between cooperators and cheaters is possible [2, 21].

3. The third important observation is the role of cheaters in the outcome of the competition. In each variant of the model we observe that the presence of cheaters discourages cooperation and encourages either a mono-culture of the wild type strain, or population collapse. The effect of cheaters is even more noticeable when the metabolite production cost is included. This gives cheaters a growth advantage and increases their influence on the system.

Together these three observations from our model indicate that the ability of individuals to exchange resources easily and without the impediment of non-cooperating members plays a key role in the evolution of cooperative and diverse communities.

A most natural extension of our model would include spatial heterogeneity and evolvability of the strains. Bi-stability and multi-stability that we observe in our well-mixed chemostat model should give rise to spatially heterogenous communities. However, it is not clear what mixing conditions and critical size would lead to surviving mini-colonies that correspond to pure wild type, or pure cooperator consortium, or other coexistence steady states observed from our model. Experimental studies have shown that features of cooperative microbial communities, such as growth rate, can be enhanced via adaptive evolution [60]. While the four strains modeled in our study were fixed, integrating mutational capabilities of the strains to permit evolvability may give rise to different community compositions and interesting key traits, such as growth rate or the rate at which the cell produces metabolites, and would further enhance our understanding of microbial community structure and evolutionary trajectories.

CHAPTER TWO

METABOLITE PRODUCTION COST

In order to take metabolite production cost into account in our model we first need to derive a function that represents these costs. We assume that cells evolve their processes in order to optimize function and utilization of resources [5]. We consider the metabolic pathway used to produce a given metabolite and derive a cost function that optimizes the efficiency of this pathway. In particular, we examine tradeoff between cell investment into substrates and enzymes and assume that the cell can partition the use of essential resources into a combination of building enzymes and investing into substrates.

The work presented in this chapter has been published in [48]. Our results for pathway optimization are confirmed with model simulations and data from *E. coli* in [16]. We model a metabolic pathway by a system of differential equations. Since the metabolic process is needed to supply a cell with necessary resources and hence occur over short time scales we assume that steady state has been reached. Therefore, these equations will be analyzed at steady state. We first present the derivation of an optimal cost function for a single-step pathway and then generalize to a multi-step pathway.

2.1 Single-step Metabolic Pathway Cost Optimization

We begin with a single-step metabolic pathway that converts substrate S to product P using enzyme E

$$S + E \rightleftarrows C \rightarrow E + P,$$

simplified in notation to

$$S \xrightarrow{E} P.$$

The Michaelis-Menten equations for such a reaction are given by

$$\begin{aligned} \dot{S} &= S_0 - \frac{V_{max} S}{\kappa + S} \\ \dot{P} &= \frac{Y_{P/S} V_{max} S}{\kappa + S} - dP \end{aligned}$$

where S_0 is the influx of substrate S, dP is the decay rate of product P, $Y_{P/S}$ is the stoichiometric coefficient for the number of P molecules that can be produced from an S molecule, and $V_{max} = kE$ is the maximal rate of consumption of S. Variables S, P, and E represent concentrations of their respective molecules. At steady state we will have

$$\begin{aligned} S_0 &= \frac{V_{max} S}{\kappa + S} \\ \frac{Y_{P/S} V_{max} S}{\kappa + S} &= dP. \end{aligned}$$

We define flux through the pathway at steady state as the following function of E and S

$$A := \frac{Y_{P/S} k E S}{\kappa + S}.$$

For ease of analysis we define

$$\hat{k} := Y_{P/S} k,$$

giving the equation

$$A = \frac{\hat{k} E S}{\kappa + S}.$$

We examine tradeoff between cell investment into substrates and enzymes and

assume that the cell can partition the use of essential resources into a combination of building enzymes and investing into substrates. We will refer to this essential resource as carbon throughout but other essential resources such as nitrogen or sulfur could also be considered. If enzyme E requires a carbon atoms and substrate S requires b carbon atoms, then the total carbon investment for the enzymatic pathway is given by

$$C := aE + bS.$$

There are two ways to optimize the production of product P. Note that all parameters are assumed to be positive.

1. The cell can minimize investment into the pathway while maintaining a desired production rate.

$$\min_{\{E,S\}} C(E,S) \quad \text{subject to the constraints } \frac{\hat{k}ES}{\kappa + S} = A^*,\ S > 0$$

   where A^* is a fixed flux through the metabolic pathway.

2. The cell can maximize the flux through the pathway while maintaining a set investment cost.

$$\max_{\{E,S\}} A(E,S) \text{ subject to the constraints } aE + bS = C^*,\ S > 0$$

   where C^* is a fixed carbon investment.

We solve each of these constrained optimization problems using the method of Lagrange multipliers and then discuss how they are related. We note that from biological consideration it follows that all parameter values for these problems are positive.

2.1.1 Minimization of Investment Cost: Single-step Pathway

We first solve the optimization problem,

$$\min_{\{E,S\}}\{C(E,S) = aE + bS\} \quad \text{subject to the constraints } \frac{\hat{k}ES}{\kappa + S} = A^*,\ S > 0.$$

Using a Lagrange multiplier λ, we have the vector equation,

$$(a,b) = \lambda\left(\frac{\hat{k}S}{\kappa+S}, \frac{\hat{k}\kappa E}{(\kappa+S)^2}\right),$$

which gives us three equations,

$$a = \lambda\frac{\hat{k}S}{\kappa+S}, \tag{2.1}$$

$$b = \lambda\frac{\hat{k}\kappa E}{(\kappa+S)^2}, \tag{2.2}$$

$$A^* = \frac{\hat{k}ES}{\kappa+S}, \tag{2.3}$$

with three unknowns, E, S, λ. If we compare equations (2.1) and (2.3) we find,

$$\lambda = \frac{a}{A^*}E,$$

which expresses λ as a function of E. Substituting this into equation (2.2) finds,

$$b = (\frac{a}{A^*}E)\frac{\hat{k}\kappa E}{(\kappa+S)^2}.$$

When solved for E this gives,

$$E = \sqrt{\frac{bA^*}{a\hat{k}\kappa}}(\kappa+S), \text{ and} \tag{2.4}$$

$$E = -\sqrt{\frac{bA^*}{a\hat{k}\kappa}}(\kappa + S). \tag{2.5}$$

When we substitute (2.5) into equation (2.3), we find,

$$A^* = \frac{\hat{k}S}{\kappa + S}\left[-\sqrt{\frac{bA^*}{a\hat{k}\kappa}}(\kappa + S)\right],$$

which can be solved for the substrate concentration S,

$$S = -\sqrt{\frac{A^* a\kappa}{b\hat{k}}}.$$

Since this is a negative value for S it does not satisfy the constraint $S > 0$ and we know that (2.5) is not a solution for E of the optimization problem.

When we substitute (2.4) into equation (2.3), we find,

$$A^* = \frac{\hat{k}S}{\kappa + S}\left[\sqrt{\frac{bA^*}{a\hat{k}\kappa}}(\kappa + S)\right],$$

which can be solved for the unique positive substrate concentration S that minimizes cost for fixed flux A^*,

$$S = \sqrt{\frac{A^* a\kappa}{b\hat{k}}}.$$

Next, we substitute this into equation (2.4) for S to find the optimal enzyme concentration to be

$$E = \sqrt{\frac{bA^*}{a\hat{k}\kappa}}(\kappa + \sqrt{\frac{A^* a\kappa}{b\hat{k}}}) = \sqrt{\frac{A^* b\kappa}{a\hat{k}}} + \frac{A^*}{\hat{k}}.$$

We then apply the optimal concentrations of E and S to the cost function to find the minimum cost needed for production rate A^*,

$$C(A^*) = a(\sqrt{\frac{A^* b\kappa}{a\hat{k}}} + \frac{A^*}{\hat{k}}) + b\sqrt{\frac{A^* a\kappa}{b\hat{k}}} = \frac{a}{\hat{k}}A^* + 2\sqrt{\frac{\kappa ab}{\hat{k}}A^*}.$$

2.1.2 Maximization of Flux: Single-step Pathway

We now solve the alternate optimization problem of maximizing flux for a fixed cost:

$$\max_{\{E,S\}}\{A(E,S) = \frac{\hat{k}ES}{\kappa + S}\} \text{ subject to the constraints } aE + bS = C^*,\ S > 0.$$

Using Lagrange multiplier λ we get

$$\left(\frac{\hat{k}S}{\kappa + S}, \frac{\kappa\hat{k}E}{(\kappa + S)^2}\right) = \lambda(a, b)$$

which gives us three equations to solve for E, S, and λ.

$$\frac{\hat{k}S}{\kappa + S} = \lambda a, \tag{2.6}$$

$$\frac{\kappa\hat{k}E}{(\kappa + S)^2} = \lambda b, \tag{2.7}$$

$$Ea + Sb = C^*. \tag{2.8}$$

We begin by solving equation (2.6) for λ and substituting into equation (2.7) to find,

$$\frac{\kappa\hat{k}E}{(\kappa + S)^2} = \frac{b\hat{k}S}{a(\kappa + S)},$$

which we can solve for E giving,

$$E = \frac{b}{a\kappa}S(\kappa + S). \tag{2.9}$$

When we substitute equation (2.9) into equation (2.8) we find an equation that is quadratic in S,

$$\frac{b}{\kappa}S(\kappa + S) + Sb = C^*,$$

with unique positive root,

$$S = -\kappa + \kappa\sqrt{1 + \frac{C^*}{b\kappa}}. \tag{2.10}$$

Substituting (2.10) into equation (2.9) gives,

$$E = \frac{1}{a}(-b\kappa\sqrt{1 + \frac{C^*}{b\kappa}} + b\kappa + C^*). \tag{2.11}$$

Using the concentrations of S and E shown in equations (2.10) and (2.11) that maximize flux for fixed cost C^*, we find that the maximum flux value is then

$$A = \frac{\hat{k}}{a}\left(2b\kappa + C^* - 2b\kappa\sqrt{1 + \frac{C^*}{b\kappa}}\right).$$

2.1.2.1 Properties of Flux We now provide analysis of this function that shows the following results:

R1. More efficient enzymes result in higher flux for a fixed carbon investment;

R2. When the reaction slows down, the production rate will decrease;

R3. When more investment into S or E is needed, the overall flux will be lower for a fixed overall cost;

R4. Increasing investment into the pathway increases the optimal flux through the pathway.

To see how the flux value is affected by changes in the parameters, we consider the derivatives of A with respect to each parameter. First, we consider the derivative

with respect to $\hat{k}$ given by

$$\frac{\partial A}{\partial \hat{k}} = \frac{1}{a}\left(2b\kappa + C^* - 2b\kappa\sqrt{1+\frac{C^*}{b\kappa}}\right).$$

Since all parameters are positive it follows that

$$(2b\kappa)^2 + 4C^*b\kappa < (2b\kappa + C^*)^2,$$

with both sides of the inequality being positive. We square root both sides and rearrange terms to show that

$$0 < 2b\kappa + C^* - \sqrt{(2b\kappa)^2 + 4C^*b\kappa}. \tag{2.12}$$

This implies

$$\left(2b\kappa + C^* - 2b\kappa\sqrt{1+\frac{C^*}{b\kappa}}\right) > 0 \tag{2.13}$$

and thus,

$$\frac{\partial A}{\partial \hat{k}} > 0.$$

Parameter $\hat{k}$ is the catalytic rate of the Michaelis-Menten equations. Since $\frac{\partial A}{\partial \hat{k}} > 0$, the increase in the $\hat{k}$ value, i.e. more efficient enzymes, results in higher flux for a fixed carbon investment. This shows result **R1**.

Next, we consider the derivative of A with respect to κ,

$$\frac{\partial A}{\partial \kappa} = \frac{\hat{k}}{a}\left(2b - \frac{2b^2\kappa + C^*b}{\sqrt{b^2\kappa^2 + C^*b\kappa}}\right).$$

Rearranging (2.12) gives

$$1 < \frac{2b\kappa + C^*}{\sqrt{(2b\kappa)^2 + 4C^*b\kappa}},$$

which can be multiplied on both sides by $2b$ to find,

$$2b < \frac{2b^2\kappa + C^*b}{\sqrt{(b\kappa)^2 + C^*b\kappa}}.$$

This implies

$$\frac{\partial A}{\partial \kappa} < 0.$$

We conclude that when the half saturation constant for the reaction, κ, is increased, which represents a slower reaction, the production rate will decrease. This shows result **R2**.

To discuss the effects that the required investment level into substrates and enzymes has on flux, we find

$$\frac{\partial A}{\partial a} = -\frac{\hat{k}}{a^2}\left(2b\kappa + C^* - 2b\kappa\sqrt{1 + \frac{C^*}{b\kappa}}\right),$$
$$\frac{\partial A}{\partial b} = \frac{\hat{k}}{a}\left(2\kappa - \frac{2b\kappa^2 + C^*\kappa}{\sqrt{b^2\kappa^2 + C^*b\kappa}}\right).$$

Similar arguments to those previously presented can be used to show

$$\frac{\partial A}{\partial a} < 0,$$
$$\frac{\partial A}{\partial b} < 0.$$

Thus, if either substrate or enzyme require a greater investment of resource, the overall flux will be lower for a fixed overall cost. This shows result **R3**.

Lastly, we consider the derivative with respect to the fixed cost C^*,

$$\frac{\partial A}{\partial C^*} = \frac{\hat{k}}{a}\left(1 - \frac{b\kappa}{\sqrt{b^2\kappa^2 + C^*b\kappa}}\right).$$

Since we have that

$$\frac{b\kappa}{\sqrt{b^2\kappa^2 + C^* b\kappa}} < 1,$$

we know

$$\frac{\partial A}{\partial C^*} > 0.$$

Not surprisingly, this implies that when the cell increases investment into the pathway, the optimal flux through the pathway will also increase. This shows result **R4**.

2.2 Multi-step Metabolic Pathway Cost Optimization

We now assume that our metabolic pathway has n steps with substrates S_1, S_2,... S_n and enzymes E_1, E_2,... E_n. Increasing the number of steps in the pathway inposes more constraints on the optimization of producing product P. Substrate S_i is converted to substrate S_{i+1} by enzymatic reaction using enzyme E_i, and S_n is converted to product P.

$$S_1 \overset{E_1}{\to} S_2 \overset{E_2}{\to} \cdots \overset{E_{n-1}}{\to} S_n \overset{E_n}{\to} P$$

The Michaelis-Menten equations for these reactions are

$$\begin{aligned}
\dot{S}_1 &= S_0 - \frac{V_1 S_1}{\kappa_1 + S_1} \\
\dot{S}_2 &= \frac{Y_{S_2/S_1} V_1 S_1}{\kappa_1 + S_1} - \frac{V_2 S_2}{\kappa_2 + S_2} \\
&\vdots \\
\dot{S}_n &= \frac{Y_{S_n/S_{n-1}} V_{n-1} S_{n-1}}{\kappa_{n-1} + S_{n-1}} - \frac{V_n S_n}{\kappa_n + S_n} \\
\dot{P} &= \frac{Y_{P/S_n} V_n S_n}{\kappa_n + S_n} - dP
\end{aligned}$$

where $V_i = k_i E_i$ and stoichiometric coefficient Y_{S_{i+1}/S_i} represents the number of S_{i+1} molecules that can be produced from an S_i molecule. At steady state these equations yield

$$\begin{aligned}
S_0 &= \frac{V_1 S_1}{\kappa_1 + S_1} \\
\frac{Y_{S_2/S_1} V_1 S_1}{\kappa_1 + S_1} &= \frac{V_2 S_2}{\kappa_2 + S_2} \\
\frac{Y_{S_3/S_2} V_2 S_2}{\kappa_2 + S_2} &= \frac{V_3 S_3}{\kappa_3 + S_3} \\
&\vdots \\
\frac{Y_{S_n/S_{n-1}} V_{n-1} S_{n-1}}{\kappa_{n-1} + S_{n-1}} &= \frac{V_n S_n}{\kappa_n + S_n} \\
\frac{Y_{P/S_n} V_n S_n}{\kappa_n + S_n} &= dP.
\end{aligned}$$

We compile these equations to give us the relationship

$$dP = \frac{Y_{P/S_n} V_n S_n}{\kappa_n + S_n} = \frac{Y_{P/S_n} Y_{S_n/S_{n-1}} V_{n-1} S_{n-1}}{\kappa_{n-1} + S_{n-1}} = ... = \prod_{i=1}^{n-1} Y_{S_{i+1}/S_i} Y_{P/S_n} S_0,$$

or equivalently,

$$dP = \frac{Y_{P/S_n} k_n E_n S_n}{\kappa_n + S_n} = \frac{Y_{P/S_n} Y_{S_n/S_{n-1}} k_{n-1} E_{n-1} S_{n-1}}{\kappa_{n-1} + S_{n-1}} = ... = \prod_{i=1}^{n-1} Y_{S_{i+1}/S_i} Y_{P/S_n} S_0.$$

Analogous to the single-step equations we have constant steady state flux obtained from dP which we define as

$$A := dP.$$

Thus, we can write flux A as a function of any pair (S_i, E_i) for $i \in \{1, 2, ..., n\}$,

$$A = \frac{Y_{P/S_n} Y_{S_n/S_{n-1}} \cdots Y_{S_{i+1}/S_i} k_i E_i S_i}{\kappa_i + S_i}.$$

For ease of analysis we define

$$\hat{k_i} := Y_{P/S_n} Y_{S_n/S_{n-1}} \cdots Y_{S_{i+1}/S_i} k_i, \quad i \in \{1, 2, ..., n-1\},$$

and

$$\hat{k_n} := Y_{P/S_n} k_n,$$

which gives A as a function of any pair (S_i, E_i) for $i \in \{1, 2, ..., n\}$,

$$A = \frac{\hat{k_i} E_i S_i}{\kappa_i + S_i}.$$

If enzyme E_i requires a_i carbon atoms and substrate S_i requires b_i carbon atoms then the total carbon investment for the metabolic pathway is given by

$$C := \sum_{i=1}^{n} (E_i a_i + S_i b_i). \tag{2.14}$$

Consider a set of $n-1$ constraints,

$$\frac{\hat{k}_{i-1} E_{i-1} S_{i-1}}{\kappa_{i-1} + S_{i-1}} - \frac{\hat{k}_i E_i S_i}{\kappa_i + S_i} = 0 \text{ for } i = 2, ..., n. \tag{2.15}$$

With these common constraints we will consider two optimization problems, where all parameters are assumed to be positive.

1. Minimize investment into the pathway while maintaining a desired production

rate.

$$\min_{\{E_i,S_i,i=1,...,n\}} C(E_i,S_i) \qquad \text{subject to } n-1 \text{ constraints in (2.15) and}$$
$$\frac{\hat{k_1}E_1S_1}{\kappa_1+S_1} = A^*,$$
$$S_i > 0 \text{ for } i = 1,...,n.$$

where A^* is a fixed flux through the metabolic pathway.

2. Maximize the flux through the pathway while maintaining a set investment cost.

$$\max_{E_1,S_1} A(E_1,S_1) \qquad \text{subject to } n-1 \text{ constraints in (2.15) and}$$
$$\sum_{i=1}^{n} E_ia_i + S_ib_i = C^*,$$
$$S_i > 0 \text{ for } i = 1,...,n.$$

where C^* is a fixed carbon investment. Here we choose to let A be a function of S_1 and E_1.

2.2.1 Minimization of Investment Cost: Multi-step Pathway

We solve the first optimization, the minimization of cost for a fixed flux, using Lagrange multipliers.

$$\min_{\{E_i,S_i,i=1,...,n\}} C(E_i,S_i) \quad \text{subject to constraints}$$
$$\frac{\hat{k}_iE_iS_i}{\kappa_i+S_i} = A^* \text{ for } i = 1,...,n,$$
$$S_i > 0 \text{ for } i = 1,...,n.$$

Using Lagrange multipliers λ_i we obtain vector equation,

$$\begin{aligned}(a_1, b_1, a_2, b_2, ...) &= \lambda_1 \left(\frac{\hat{k}_1 S_1}{\kappa_1 + S_1}, \frac{\hat{k}_1 \kappa_1 E_1}{(\kappa_1 + S_1)^2}, 0, 0, ... \right) \\ &+ \lambda_2 \left(0, 0, \frac{\hat{k}_2 S_2}{\kappa_2 + S_2}, \frac{\hat{k}_2 \kappa_2 E_2}{(\kappa_2 + S_2)^2}, 0, ... \right) \\ &+ \cdots + \lambda_n \left(0, 0, ..., \frac{\hat{k}_n S_n}{\kappa_n + S_n}, \frac{\hat{k}_n \kappa_n E_n}{(\kappa_n + S_n)^2} \right).\end{aligned}$$

This can be written as a system of equations for $i = 1, ..., n$

$$a_i = \lambda_i \frac{\hat{k}_i S_i}{\kappa_i + S_i} \tag{2.16}$$

$$b_i = \lambda_i \frac{\hat{k}_i \kappa_i E_i}{(\kappa_i + S_i)^2} \tag{2.17}$$

$$A^* = \frac{\hat{k}_i E_i S_i}{\kappa_i + S_i}. \tag{2.18}$$

We solving these similarly to the above in section 2.1 for $i = 1, ..., n$.

If we compare equations (2.16) and (2.18) we find

$$\lambda_i = \frac{a_i}{A^*} E_i,$$

which expresses λ_i as a function of E_i. Substituting this into equation (2.17) finds,

$$b_i = (\frac{a_i}{A^*} E_i) \frac{\hat{k}_i \kappa_i E_i}{(\kappa_i + S_i)^2}. \tag{2.19}$$

Equation (2.18) and the constraint $S_i > 0$ implies that E_i must also be positive. We solve (2.19) for the unique positive solution for E_i,

$$E_i = \sqrt{\frac{b_i A^*}{a_i \hat{k}_i \kappa_i}} (\kappa_i + S_i). \tag{2.20}$$

We substitute this into equation (2.18) to find,

$$A^* = \frac{\hat{k}_i S_i}{\kappa_i + S_i}\left[\sqrt{\frac{b_i A^*}{a_i \hat{k}_i \kappa_i}}(\kappa_i + S_i)\right],$$

which can be solved for the substrate concentration S_i that minimizes cost for fixed flux A^*,

$$S_i = \sqrt{\frac{A^* a_i \kappa_i}{b_i \hat{k}_i}}.$$

Next, we substitute this into equation (2.20) for S_i to find the optimal enzyme concentration to be

$$E_i = \sqrt{\frac{b_i A^*}{a_i \hat{k}_i \kappa_i}}(\kappa_i + \sqrt{\frac{A^* a_i \kappa_i}{b_i \hat{k}_i}}) = \sqrt{\frac{A^* b_i \kappa_i}{a_i \hat{k}_i}} + \frac{A^*}{\hat{k}_i}.$$

Thus, the minimum investment for fixed production rate, A^*, will be

$$C = \sum_{i=1}^{n}(E_i a_i + S_i b_i) = \sum_{i=1}^{n}\left(\frac{a_i}{\hat{k}_i}A^* + 2\sqrt{\frac{\kappa_i a_i b_i}{\hat{k}_i}A^*}\right). \tag{2.21}$$

2.2.1.1 Properties of Cost Function The optimal metabolite production cost function in (2.21) as a function of production rate will be applied to a chemostat model in chapters 3 and 5. Thus, understanding some properties of this function will add to our understanding of its effects on our model. To determine how optimal cost will change with respect to each parameter we find the derivatives of C with respect to each parameter.

The analysis of this function shows the following results:

R5. More efficient enzymes result in lower investment cost for fixed flux;

R6. When the reaction slows down the investment cost will increase;

R7. When more investment into S or E is needed the total cost will be higher

to achieve a fixed flux.

R8. Increasing flux through the pathway increases the investment cost.

We first look at the effect of the efficiency of enzymes on cost. The derivative of cost with respect to $\hat{k_i}$ for $i \in \{1, 2, ...n\}$ is

$$\frac{\partial C}{\partial \hat{k_i}} = -\left(\frac{a_i}{\hat{k_i^2}} A^* + \sqrt{\frac{\kappa_i a_i b_i}{\hat{k_i^3}} A^*}\right).$$

Given that all parameters are assumed to be positive, it is clear that

$$\frac{\partial C}{\partial \hat{k_i}} < 0.$$

Thus, when enzyme E_i is more efficient, i.e. $\hat{k_i}$ is increased, then the total cost of the metabolic pathway optimized for fixed flux will decrease. This shows result **R5**.

In contrast, the derivative of cost with respect to saturation constant for the i^{th} reaction for $i \in \{1, 2, ...n\}$ is given by

$$\frac{\partial C}{\partial \kappa_i} = \sqrt{A^* \frac{a_i b_i}{\hat{k_i} \kappa_i}} > 0.$$

When κ_i increases and the i^{th} reaction is slowed, a higher investment of carbon will be needed in order to achieve the desired production rate. This shows result **R6**.

The derivatives of cost with respect to required investment into each enzyme and substrate are given by

$$\begin{aligned} \frac{\partial C}{\partial a_i} &= \frac{A^*}{\hat{k_i}} + \sqrt{A \frac{\kappa_i b_i}{a_i \hat{k_i}}} \\ \frac{\partial C}{\partial b_i} &= \sqrt{A^* \frac{\kappa_i a_i}{b_i \hat{k_i}}} \end{aligned}$$

Both of these derivatives are positive, which implies that when the cell has an increase in the amount of resource it must necessarily invest into enzymes or substrates, it will require a greater overall investment in order to achieve the same flux through the pathway. This shows result **R7**.

Lastly, the derivative with respect to flux,

$$\frac{\partial C}{\partial A^*} = \sum_{i=1}^{n} \left[\frac{a_i}{\hat{k}_i} + \frac{1}{\sqrt{A^*}} \sqrt{\frac{\kappa_i a_i b_i}{\hat{k}_i}} \right] > 0,$$

not surprisingly, implies that when flux through the metabolic pathway is increased, the investment cost necessary to maintain that flux also increases. This shows result **R8**.

We also consider how the optimal enzyme and substrate concentrations will be affected by a change in flux.

$$\begin{aligned} \frac{\partial E_i}{\partial A^*} &= \frac{1}{2} \sqrt{\frac{\kappa_i b_i}{\hat{k}_i a_i A^*}} + \frac{1}{\hat{k}_i} \\ \frac{\partial S_i}{\partial A^*} &= \frac{1}{2} \sqrt{\frac{\kappa_i a_i}{\hat{k}_i b_i A^*}} \end{aligned}$$

As we expected, both of these derivatives are positive indicating an increase in the respective concentrations when the desired production rate is increased. Considering

$$\frac{\frac{\partial E_i}{\partial A^*}}{\frac{\partial S_i}{\partial A^*}} = \frac{\frac{1}{2}\sqrt{\frac{\kappa_i b_i}{\hat{k}_i a_i A^*}} + \frac{1}{\hat{k}_i}}{\frac{1}{2}\sqrt{\frac{\kappa_i a_i}{\hat{k}_i b_i A^*}}} = \frac{b_i}{a_i} + 2\sqrt{A^* \frac{b_i}{\kappa_i \hat{k}_i a_i}},$$

if we assume that investment into enzymes is much higher than investment into substrates, $a_i >> b_i$ for $i = 1, ..., n$, then

$$\frac{\frac{\partial E_i}{\partial A^*}}{\frac{\partial S_i}{\partial A^*}} = \epsilon + 2\sqrt{\epsilon}\sqrt{A^*} \sqrt{\frac{1}{\kappa_i \hat{k}_i}}.$$

If this ratio is > 1, then a greater flux will require a greater enzyme concentration. If this ratio is < 1, then a greater flux will require a greater substrate concentration.

We now consider the characteristics of the cost function given in (2.21) as a function of flux. These results have been published in [48].

$$C = \sum_{i=1}^{n} \left(\frac{a_i}{\hat{k}_i} A^* + 2\sqrt{\frac{\kappa_i a_i b_i}{\hat{k}_i} A^*} \right).$$

As mentioned previously

$$\frac{\partial C}{\partial A^*} = \sum_{i=1}^{n} \left[\frac{a_i}{\hat{k}_i} + \frac{1}{\sqrt{A^*}} \sqrt{\frac{\kappa_i a_i b_i}{\hat{k}_i}} \right] > 0.$$

The second derivative is given by

$$\frac{\partial^2 C}{\partial {A^*}^2} = -\frac{1}{2} \sum_{i=1}^{n} \left[\frac{1}{\sqrt{{A^*}^3}} \sqrt{\frac{\kappa_i a_i b_i}{\hat{k}_i}} \right] < 0.$$

We observe that $C(A^*)$ is an increasing, convex function of flux (Fig 2.1). As a consequence, to achieve a two-fold increase in flux the cell will need less than a two-fold increase in cost; in other words,

$$C(2A^*) < 2C(A^*).$$

Thus, if specialists are able to overproduce a product at a higher production rate and share with other members of the community, the overall cost to the community will be lower than if individual cells produce their own product and do not share.

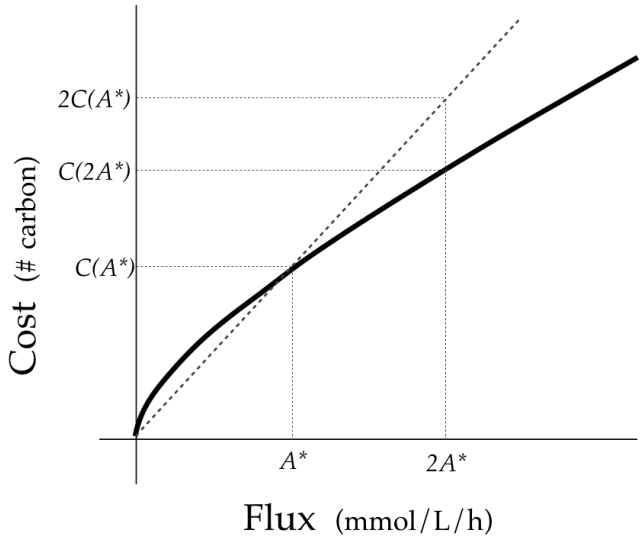

Figure 2.1: **Metabolite production cost function.** Production cost is plotted as a function of flux.

2.2.2 Maximization of Flux: Multi-step Pathway

We now consider the second method a cell can use to optimize the utilization of resource - maximizing flux for a fixed investment cost, C^*.

$$\max_{E_1,S_1} A(E_1, S_1) \text{ subject to } n \text{ constraints}$$

$$\sum_{i=1}^{n} E_i a_i + S_i b_i = C^*,$$

$$\frac{\hat{k}_{i-1} E_{i-1} S_{i-1}}{\kappa_{i-1} + S_{i-1}} - \frac{\hat{k}_i E_i S_i}{\kappa_i + S_i} = 0 \text{ for } i = 2, ..., n,$$

$$S_i > 0 \text{ for } i = 1, ..., n.$$

Using Lagrange multipliers $\mu_i\,, i = 1, ..., n$ we get

$$\left(\frac{\hat{k}_1 S_1}{\kappa_1 + S_1}, \frac{\kappa_1 \hat{k}_1 E_1}{(\kappa_1 + S_1)^2}, 0, 0, ...\right) = \mu_1(a_1, b_1, a_2, b_2, a_3, ...)$$
$$+\mu_2 \left(\frac{\hat{k}_1 S_1}{\kappa_1 + S_1}, \frac{\kappa_1 \hat{k}_1 E_1}{(\kappa_1 + S_1)^2}, -\frac{\hat{k}_2 S_2}{\kappa_2 + S_2}, -\frac{\kappa_2 \hat{k}_2 E_2}{(\kappa_2 + S_2)^2}, 0, 0, ..\right)$$
$$+\mu_3 \left(0, 0, \frac{\hat{k}_2 S_2}{\kappa_2 + S_2}, \frac{\kappa_2 \hat{k}_2 E_2}{(\kappa_2 + S_2)^2}, -\frac{\hat{k}_3 S_3}{\kappa_3 + S_3}, -\frac{\kappa_3 \hat{k}_3 E_3}{(\kappa_3 + S_3)^2}, 0, 0, ..\right) + \cdots$$
$$+\mu_{n-1} \left(..., \frac{\hat{k}_{n-2} S_{n-2}}{\kappa_{n-2} + S_{n-2}}, \frac{\kappa_{n-2} \hat{k}_{n-2} E_{n-2}}{(\kappa_{n-2} + S_{n-2})^2}, -\frac{\hat{k}_{n-1} S_{n-1}}{\kappa_{n-1} + S_{n-1}}, -\frac{\kappa_{n-1} \hat{k}_{n-1} E_{n-1}}{(\kappa_{n-1} + S_{n-1})^2}, 0, 0\right)$$
$$+ \cdots + \mu_n \left(0, ..., \frac{\hat{k}_{n-1} S_{n-1}}{\kappa_{n-1} + S_{n-1}}, \frac{\kappa_{n-1} \hat{k}_{n-1} E_{n-1}}{(\kappa_{n-1} + S_{n-1})^2}, -\frac{\hat{k}_n S_n}{\kappa_n + S_n}, -\frac{\kappa_n \hat{k}_n E_n}{(\kappa_n + S_n)^2}\right).$$

which gives us the systems of equations to solve,

$$\frac{\hat{k}_1 S_1}{\kappa_1 + S_1} = \mu_1 a_1 + \mu_2 \frac{\hat{k}_1 S_1}{\kappa_1 + S_1} \tag{2.22}$$
$$\frac{\kappa_1 \hat{k}_1 E_1}{(\kappa_1 + S_1)^2} = \mu_1 b_1 + \mu_1 \frac{\kappa_1 \hat{k}_1 E_1}{(\kappa_1 + S_1)^2} \tag{2.23}$$
$$0 = \mu_1 a_i - \mu_i \frac{\hat{k}_i S_i}{\kappa_i + S_i} + \mu_{i+1} \frac{\hat{k}_i S_i}{\kappa_i + S_i} \tag{2.24}$$
$$0 = \mu_1 b_i - \mu_i \frac{\kappa_i \hat{k}_i E_i}{(\kappa_i + S_i)^2} + \mu_{i+1} \frac{\kappa_i \hat{k}_i E_i}{(\kappa_i + S_i)^2} \tag{2.25}$$
$$\text{for } i = 2, .., n-1$$
$$0 = \mu_1 a_n - \mu_n \frac{\hat{k}_n S_n}{\kappa_n + S_n} \tag{2.26}$$
$$0 = \mu_1 b_n - \mu_n \frac{\kappa_n \hat{k}_n E_n}{(\kappa_n + S_n)^2} \tag{2.27}$$
$$\sum_{i=1}^{n} E_i a_i + S_i b_i = C^* \tag{2.28}$$
$$\frac{\hat{k}_{i-1} E_{i-1} S_{i-1}}{\kappa_{i-1} + S_{i-1}} - \frac{\hat{k}_i E_i S_i}{\kappa_i + S_i} = 0 \text{ for } i = 2, ..., n. \tag{2.29}$$

Rather than explicitely solve the system of equations (2.22) - (2.29) we prove

the following result.

Theorem 1. *The constrained minimization problem solved in section 2.2.1 gives optimal cost as a unique function of flux, $C = f(A)$. The constrained maximization problem in section 2.2.2 gives optimal flux as a function of cost, $A = g(C)$. Functions f and g are inverse functions, i.e. $f(g(C)) = C$ and $g(f(A)) = A$.*

Proof. We prove the theorem by first showing that the two optimization problems result in the same system of $3n+1$ equations with $3n+2$ variables. Solving equation (2.22) for a_1 we find

$$a_1 = \frac{1-\mu_2}{\mu_1}\frac{\hat{k}_1 S_1}{\kappa_1 + S_1}.$$

Similarly, solving equation (2.24) for a_i finds

$$a_i = \frac{\mu_i - \mu_{i+1}}{\mu_1}\frac{\hat{k}_i S_i}{\kappa_i + S_i} \text{ for } i = 2, .., n-1,$$

and solving equation (2.26) for a_n finds

$$a_n = \frac{\mu_n}{\mu_1}\frac{\hat{k}_n S_n}{\kappa_n + S_n}.$$

We proceed similarly for b_i equations. Comparing the system of equations (2.16)-(2.18) with equations (2.22)-(2.29), shows that under the following relationships between the Lagrange multipliers the two sets of equations are the same.

$$\lambda_1 = \frac{1-\mu_2}{\mu_1} \tag{2.30}$$

$$\lambda_i = \frac{\mu_i - \mu_{i+1}}{\mu_1} \text{ for } i = 2, ..., n-1 \tag{2.31}$$

$$\lambda_n = \frac{\mu_n}{\mu_1}. \tag{2.32}$$

Clearly, for a given collection $\{\mu_1, \ldots, \mu_n\}$ there is a unique corresponding collection

of $\{\lambda_1, \ldots, \lambda_n\}$. Conversely, given a collection $\{\lambda_1, \ldots, \lambda_n\}$ we now explicitly solve for $\{\mu_1, \ldots, \mu_n\}$. From (2.32) we have

$$\frac{\mu_n}{\mu_1} = \lambda_n, \tag{2.33}$$

and from (2.31), for $i = 2, ..., n-1$, we find

$$\frac{\mu_i}{\mu_1} = \lambda_i + \frac{\mu_{i+1}}{\mu_1}.$$

It follows by induction that for $i = 2, ..., n-1$,

$$\frac{\mu_i}{\mu_1} = \sum_{j=i}^{n} \lambda_j. \tag{2.34}$$

We substitute this into equation (2.30) for $i = 2$ to find

$$\frac{1}{\mu_1} = \lambda_1 + \sum_{j=2}^{n} \lambda_j = \sum_{j=1}^{n} \lambda_j,$$

or equivalently

$$\mu_1 = \frac{1}{\sum_{j=1}^{n} \lambda_j}.$$

We then substitute this into equation (2.33) and (2.34) to find, for $i = 2, ..., n$,

$$\mu_i = \frac{\sum_{j=i}^{n} \lambda_j}{\sum_{j=1}^{n} \lambda_j}.$$

It follows that there is a bijection between collection $\{\lambda_1, \ldots, \lambda_n\}$ and a collection $\{\mu_1, \ldots, \mu_n\}$. Under this correspondence the system of equations for unknowns E_i, S_i, λ_i, and either C as a function of fixed A (section 2.2.1) or A as a function of fixed C (section 2.2.2), are the same.

2.2.1 system of equations Minimize C for fixed flux A	2.2.2 system of equations Maximize A for fixed cost C
$a_1 = \lambda_1 \dfrac{\hat{k}_1 S_1}{\kappa_1 + S_1}$	$a_1 = \dfrac{1-\mu_2}{\mu_1} \dfrac{\hat{k}_1 S_1}{\kappa_1 + S_1}$
$b_1 = \lambda_1 \dfrac{\hat{k}_1 \kappa_1 E_1}{(\kappa_1 + S_1)^2}$	$b_1 = \dfrac{1-\mu_2}{\mu_1} \dfrac{\hat{k}_1 \kappa_1 E_1}{(\kappa_1 + S_1)^2}$
$a_2 = \lambda_2 \dfrac{\hat{k}_2 S_2}{\kappa_2 + S_2}$	$a_2 = \dfrac{\mu_2 - \mu_3}{\mu_1} \dfrac{\hat{k}_2 S_2}{\kappa_2 + S_2}$
$b_2 = \lambda_2 \dfrac{\hat{k}_2 \kappa_2 E_2}{(\kappa_2 + S_2)^2}$	$b_2 = \dfrac{\mu_2 - \mu_3}{\mu_1} \dfrac{\hat{k}_2 \kappa_2 E_2}{(\kappa_2 + S_2)^2}$
$\vdots$	$\vdots$
$a_n = \lambda_n \dfrac{\hat{k}_n S_n}{\kappa_n + S_n}$	$a_n = \dfrac{\mu_n}{\mu_1} \dfrac{\hat{k}_n S_n}{\kappa_n + S_n}$
$b_n = \lambda_n \dfrac{\hat{k}_n \kappa_n E_n}{(\kappa_n + S_n)^2}$	$b_n = \dfrac{\mu_n}{\mu_1} \dfrac{\hat{k}_n \kappa_n E_n}{(\kappa_n + S_n)^2}$
$0 = \dfrac{\hat{k}_{i-1} E_{i-1} S_{i-1}}{\kappa_{i-1} + S_{i-1}} - \dfrac{\hat{k}_i E_i S_i}{\kappa_i + S_i}$	$0 = \dfrac{\hat{k}_{i-1} E_{i-1} S_{i-1}}{\kappa_{i-1} + S_{i-1}} - \dfrac{\hat{k}_i E_i S_i}{\kappa_i + S_i}$
for $i = 2, ..., n$	for $i = 2, ..., n$
$A = \dfrac{\hat{k}_1 E_1 S_1}{\kappa_1 + S_1}$	$A = \dfrac{\hat{k}_1 E_1 S_1}{\kappa_1 + S_1}$
$C = \sum_{i=1}^{n} E_i a_i + S_i b_i$	$C = \sum_{i=1}^{n} E_i a_i + S_i b_i$

In section 2.2.1 we solved this system of equations for E_i, S_i, λ_i, and $C = f(A)$. Now consider the solution

$$C = f(A) = \sum_{i=1}^{n} \left(\frac{a_i}{\hat{k}_i} A + 2\sqrt{\frac{\kappa_i a_i b_i}{\hat{k}_i} A} \right).$$

to this system of equations (2.16)-(2.18), defined for positive values of flux A. Note that this solution exists and is unique when A and S_i are positive.

Furthermore, we have shown in section 2.2.1.1 that f is differentiable and

$$\frac{df}{dA} = \sum_{i=1}^{n} \left[\frac{a_i}{\hat{k}_i} + \frac{1}{\sqrt{A}} \sqrt{\frac{\kappa_i a_i b_i}{\hat{k}_i}} \right] > 0. \tag{2.35}$$

Thus, f is strictly increasing, and therefore is an injective function from its domain, $A > 0$. Since $f(A)$ is clearly not bounded above and $f(0) = 0$, the function $f : \mathbf{R}^+ \to \mathbf{R}^+$ is surjective. Therefore, $f : \mathbf{R}^+ \to \mathbf{R}^+$ is bijective and the inverse function $A = f^{-1}(C)$ exists.

Since we have shown the system of equations (2.22)-(2.29) is the same system as equations (2.16)-(2.18), and is solved uniquely by $C = f(A)$, then (2.22)-(2.29) has as a solution $A = g(C)$, where $g = f^{-1}$, $f(g(C)) = C$, and $g(f(A)) = A$.

□

CHAPTER THREE

CHEMOSTAT MODEL

We develop a model of a chemostat with four strains: cheaters, wild type, A-cooperator, and B-cooperator (Fig. 3.1). We assume that each phenotype has a fixed strategy for producing necessary secondary metabolites A and B from primary substrate S in a chemostat. Strains that cannot produce either A or B need to import that metabolite from the external environment. All strains can export metabolites they produce to the external environment. The wild type strain produces both A and B, cheater strain produces neither and must import both A and B from the environment, while each of the cooperator strains produces only one of the two metabolites (i.e. A-cooperator produces only A), and must import the other metabolite from the external environment.

3.1 Mass Balance Equations Model

The foundation of our model is the mass balance equations of the chemostat. We will denote by $X_\emptyset, X_{ab}, X_a, X_b$ concentrations of cheater, wild type, A-cooperator, and B-cooperator strains, respectively. The equations governing growth of each population are given by

$$\frac{dX_\gamma}{dt} = (\mu_\gamma - d)X_\gamma, \tag{3.1}$$

where the subscript $\gamma \in \{\emptyset, a, b, ab\}$ will always stand for a particular strain. Constant d is the population decay from death and washout of the chemostat and μ_γ is the strain-specific growth rate dependent on variable concentrations A_γ, B_γ, and S,

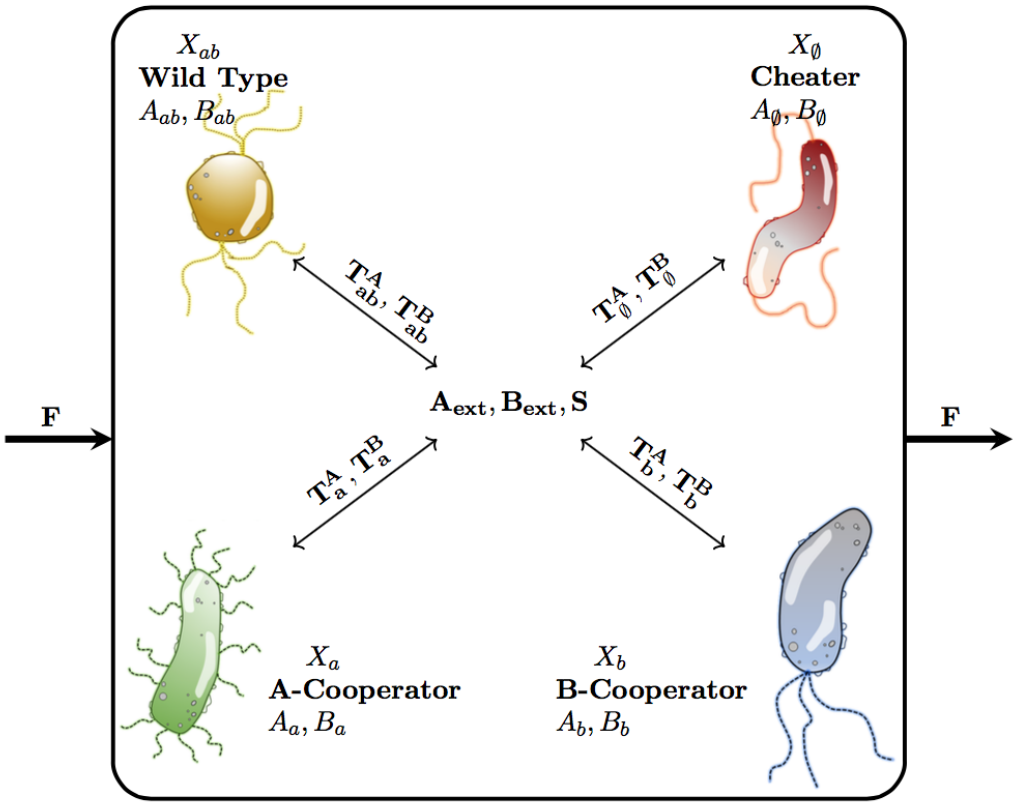

Figure 3.1: **Chemostat model.** Four types of cells grow within a well mixed, controlled volume chemostat of total volume V_T, with dilution rate $J = \frac{F}{V_T}$. Cells use phenotype specific strategy for producing metabolites A and B from substrate S and are able to import and export both metabolites. Wild type strain produces both A and B, cheater strain will produce neither A nor B, and cooperator strains known as A-cooperator and B-cooperator will produce only A and only B respectively. Metabolites A and B and substrate S are all necessary for cell growth.

governed by equations (3.7) and (3.11),

$$\mu_\gamma = \mu_{max,\gamma} \frac{A_\gamma}{K_\gamma^A + A_\gamma} \frac{B_\gamma}{K_\gamma^B + B_\gamma} \frac{S}{K_\gamma^S + S}. \tag{3.2}$$

Constants $\mu_{max,\gamma}, K_\gamma^A, K_\gamma^B$, and K_γ^S are, in general, specific for each strain. Parameter μ_{max} denotes the maximum growth rate of the cell, and K_γ^A, K_γ^B, and K_γ^S are half saturation rates. Note that metabolites A and B and substrate S are all required for growth. Variables A_γ and B_γ denote the internal concentration of A and B, respectively, for strains $\gamma \in \{\emptyset, ab, a, b\}$.

The mass balance equations for internal concentration A_γ has the form

$$\frac{d(A_\gamma V_\gamma)}{dt} = P_\gamma^A X_\gamma V_T - D_\gamma^A X_\gamma V_T - T_\gamma^A X_\gamma V_T. \tag{3.3}$$

Here V_T is the constant total volume of the chemostat and V_γ is the total internal volume for strain of type γ. Function P_γ^A is the rate at which the cell produces metabolite A, function D_γ^A is the demand, or rate at which the cell utilizes metabolite A, and function T_γ^A is the transport of metabolite A into and out of the cell. The equation for B_γ will be analogous.

To remove the volume dependency, we apply the product rule to the left hand side of equation (3.3) to find

$$\frac{d(A_\gamma V_\gamma)}{dt} = \frac{d(A_\gamma)}{dt} V_\gamma + \frac{d(V_\gamma)}{dt} A_\gamma,$$

which gives

$$\frac{dA_\gamma}{dt} = \frac{1}{V_\gamma} \left(\frac{d(A_\gamma V_\gamma)}{dt} - \frac{dV_\gamma}{dt} A_\gamma \right). \tag{3.4}$$

We introduce parameter β_γ representing the density of a cell of strain γ. The

mass and internal volume of cells of strain γ will be proportional,

$$\beta_\gamma := \frac{X_\gamma V_T}{V_\gamma}. \tag{3.5}$$

This implies

$$V_\gamma = \frac{X_\gamma V_T}{\beta_\gamma} \quad \text{and} \quad \frac{dV_\gamma}{dt} = \frac{V_T}{\beta_\gamma}\frac{dX_\gamma}{dt}.$$

Using equations (3.1) in equation (3.4) we then have

$$\frac{dA_\gamma}{dt} = \frac{\beta_\gamma}{X_\gamma V_T}\left(\frac{d(A_\gamma V_\gamma)}{dt} - \frac{V_T}{\beta_\gamma}\frac{dX_\gamma}{dt}A_\gamma\right).$$

We combine this result with (3.1) and (3.3) to find

$$\frac{dA_\gamma}{dt} = \frac{\beta_\gamma}{X_\gamma V_T}(P_\gamma^A X_\gamma V_T - D_\gamma^A X_\gamma V_T - T_\gamma^A X_\gamma V_T - \frac{V_T}{\beta_\gamma}(\mu_\gamma - d)X_\gamma A_\gamma). \tag{3.6}$$

Note that there is a removable discontinuity in equation (3.6) when $X_\gamma = 0$, which we remove to obtain the equation for internal concentration,

$$\frac{dA_\gamma}{dt} = \beta_\gamma(P_\gamma^A - D_\gamma^A - T_\gamma^A) - (\mu_\gamma - d)A_\gamma. \tag{3.7}$$

The metabolite production rate is proportional to the amount of substrate available

$$P_\gamma^A = Y_{P,\gamma}^A \frac{S}{K_\gamma^S + S}$$

where $Y_{P,\gamma}^A$ is strain specific production and K_γ^S is a strain-specific affinity constant. The demand is determined by consumption for growth and non-growth,

$$D_\gamma^A = Y_{D,\gamma}^A \mu_\gamma + K_{D,\gamma}^A.$$

$K^A_{D,\gamma}$ is a non-growth constant assumed to be small.

One of the central questions we address is the role of transport on the outcome of the competition in the chemostat. In particular, we are interested in whether the type of transport that is needed for a particular metabolite affects the competition between the strains. We consider both passive transport and active transport. Passive transport is when metabolites are able to flow freely along the concentration gradient into and out of the cell. Active transport, on the other hand, requires the cell to expend energy in order to move a metabolite across the cell membrane and can be done against the concentration gradient. An example of active transport is when a cell uses a transmembrane protein to move a substance across the membrane. This type of transport is necessary to transport large molecules that cannot passively diffuse through the cell wall, or for molecules that have charge such as organic acids [33].

To model passive transport we assume that the rate of the transport is proportional to difference between internal and external concentrations of a given metabolite with proportionality constant q^{Ap}_γ.

$$T^A_\gamma = q^{Ap}_\gamma (A_\gamma - A_{ext}) \quad , \quad \gamma \in \{\emptyset, ab, a, b\}. \tag{3.8}$$

In order to model active transport, we assume that there is a desired concentration of each metabolite in the cell denoted by $\hat{A}_\gamma$. We assume that the active transport of a metabolite from inside the cell to the external environment happens only when the internal concentration exceeds the desired concentration. The rate of transport is proportional to the product of this difference and a saturating function of the internal concentration. This latter function models saturation of the transporters in the cell wall needed to export the metabolite. Conversely, importing the metabolite from the external environment into the cell happens only when internal concentration is below

the desired concentration. The rate of transport is proportional to the product of this difference and a saturating function of the external concentration. We model active transport rate of metabolite A as

$$T_\gamma^A = \begin{cases} -q_\gamma^{Ai} \frac{(\hat{A}_\gamma - A_\gamma)}{\hat{A}_\gamma} \left[\frac{A_{ext}}{K_{\gamma,i}^A + A_{ext}} \right], & A_\gamma < \hat{A}_\gamma \\ q_\gamma^{Ax} \frac{(A_\gamma - \hat{A}_\gamma)}{\hat{A}_\gamma} \left[\frac{A_\gamma}{K_{\gamma,x}^A + A_\gamma} \right], & A_\gamma > \hat{A}_\gamma \end{cases} \tag{3.9}$$

In general, the parameters used in modeling both types of transport are strain specific.

Next, we represent the external concentration of metabolite A. The mass balance equation for external concentration of A is given by,

$$\frac{dA_{ext}V_T}{dt} = FA_{in} - FA_{ext} + \sum_\gamma T_\gamma^A X_\gamma V_T.$$

Parameter A_{in} is the concentration of A being added to the chemostat from an external source, and T_γ^A is the transport rate of A into and out of a cell. We will assume that the total volume of the chemostat, V_T, will remain constant, and that the chemostat has volumetric flow rate F. Thus, we can divide this equation by total volume, and let $J = \frac{F}{V_T}$ represent the dilution rate of the chemostat, to find the equation for A_{ext}.

$$\frac{dA_{ext}}{dt} = J(A_{in} - A_{ext}) + \sum T_\gamma^A X_\gamma. \tag{3.10}$$

The equation for external concentration of metabolite B will be similar.

Lastly, we let S denote the concentration of substrate S. This substrate is the resource that the cells need in order to grow and to produce A and B, such as glucose or lactose. We assume that the substrate is uniformly distributed throughout the system. Thus, internal and external concentrations of the substrate are not distinguished. The

mass balance equation for S is

$$\frac{dSV_T}{dt} = FS_{in} - FS - \sum \frac{1}{Y_{A/S}} P_\gamma^A X_\gamma V_T - \sum \frac{1}{Y_{B/S}} P_\gamma^B X_\gamma V_T - \sum \frac{1}{Y_{X/S}} \mu_\gamma X_\gamma V_T.$$

We again divide both sides of this equation by the constant total volume of the chemostat to find the equation for S,

$$\frac{dS}{dt} = J(S_{in} - S) - \sum \frac{1}{Y_{A/S}} P_\gamma^A X_\gamma - \sum \frac{1}{Y_{B/S}} P_\gamma^B X_\gamma - \sum \frac{1}{Y_{X/S}} \mu_\gamma X_\gamma. \tag{3.11}$$

Parameter S_{in} is the concentration of S being added to the chemostat. Parameters $Y_{A/S}$ and $Y_{B/S}$ are yield coefficients for producing A and B from S. We assume that the rate of biomass production of different strains from substrate S is proportional to growth rate with yield coefficient $\frac{1}{Y_{X/S}}$.

3.1.1 Model Equations Summary

We provide a summary of the mass balance equations model for reference. These equations are for $\gamma \in \{\emptyset, ab, a, b\}$ which gives us a system of 15 ordinary differential equations.

$$
\begin{aligned}
\frac{dX_\gamma}{dt} &= (\mu_\gamma - d)X_\gamma \\
\frac{dA_{ext}}{dt} &= J(A_{in} - A_{ext}) + \sum T_\gamma^A X_\gamma \\
\frac{dB_{ext}}{dt} &= J(B_{in} - B_{ext}) + \sum T_\gamma^B X_\gamma \\
\frac{dA_\gamma}{dt} &= \beta_\gamma(P_\gamma^A - D_\gamma^A - T_\gamma^A) - (\mu_\gamma - d)A_\gamma \\
\frac{dB_\gamma}{dt} &= \beta_\gamma(P_\gamma^B - D_\gamma^B - T_\gamma^B) - (\mu_\gamma - d)B_\gamma \\
\frac{dS}{dt} &= J(S_{in} - S) - \sum \frac{1}{Y_{A/S}} P_\gamma^A X_\gamma - \sum \frac{1}{Y_{B/S}} P_\gamma^B X_\gamma - \sum \frac{1}{Y_{X/S}} \mu_\gamma X_\gamma
\end{aligned}
$$

where

$$
\begin{aligned}
\mu_\gamma &= \mu_{max,\gamma} \frac{A_\gamma}{K_\gamma^A + A_\gamma} \frac{B_\gamma}{K_\gamma^B + B_\gamma} \frac{S}{K_\gamma^S + S} \\
P_\gamma^A &= Y_{P,\gamma}^A \frac{S}{K_\gamma^S + S} \\
P_\gamma^B &= Y_{P,\gamma}^B \frac{S}{K_\gamma^S + S} \\
D_\gamma^A &= Y_{D,\gamma}^A \mu_\gamma + K_{D,\gamma}^A \\
D_\gamma^B &= Y_{D,\gamma}^B \mu_\gamma + K_{D,\gamma}^B
\end{aligned}
$$

Active Transport:

$$
T_\gamma^A = \begin{cases} -q_\gamma^{Ai} \frac{(\hat{A}_\gamma - A_\gamma)}{\hat{A}_\gamma} \left[\frac{A_{ext}}{K_{\gamma,i}^A + A_{ext}} \right], & A_\gamma < \hat{A}_\gamma \\ q_\gamma^{Ax} \frac{(A_\gamma - \hat{A}_\gamma)}{\hat{A}_\gamma} \left[\frac{A_\gamma}{K_{\gamma,x}^A + A_\gamma} \right], & A_\gamma > \hat{A}_\gamma \end{cases}
$$

$$
T_\gamma^B = \begin{cases} -q_\gamma^{Bi} \frac{(\hat{B}_\gamma - B_\gamma)}{\hat{B}_\gamma} \left[\frac{B_{ext}}{K_{\gamma,i}^B + B_{ext}} \right], & B_\gamma < \hat{B}_\gamma \\ q_\gamma^{Bx} \frac{(B_\gamma - \hat{B}_\gamma)}{\hat{B}_\gamma} \left[\frac{B_\gamma}{K_{\gamma,x}^B + B_\gamma} \right], & B_\gamma > \hat{B}_\gamma \end{cases}
$$

Passive Transport:

$$
\begin{aligned}
T_\gamma^A &= q_\gamma^{Ap}(A_\gamma - A_{ext}) \\
T_\gamma^B &= q_\gamma^{Bp}(B_\gamma - B_{ext})
\end{aligned}
$$

Analysis of this model can be found in chapter 5.

3.2 Cost Application to Mass Balance Equation Model

To produce A and B a cell must commit resources that it cannot use elsewhere. As different strains use unique production strategies this commitment of resources can lead to differences in the efficiency and functionality of the cell. One difference may be seen in the maximal growth rate of the cell as amino acid over production leads to significant fitness costs [43]. A strain such as the cheater strain does not incur production costs, thus would be able to use its energy and resources elsewhere and may have a higher maximal growth rate. To account for the production expense we scale the maximal growth rate of each strain by the cost of metabolite production. We have previously derived such a function in chapter 2 section 2.2.1 from consideration of trade-off between investment into the enzymes and substrates of a given pathway. We use this function here.

In section 2.2.1, we have shown that the minimal cost for a cell to produce a metabolite substrate S at rate A^* using an n-step pathway is

$$C = \sum_{i=1}^{n}(E_i a_i + S_i b_i) = \sum_{i=1}^{n}\left(\frac{a_i}{\hat{k}_i}A^* + 2\sqrt{\frac{\kappa_i a_i b_i}{\hat{k}_i}A^*}\right).$$

In the context of our optimization problem, production rate $A^*[=]\frac{mmol_A}{L\cdot h}$. This corresponds to production rate P^A from our mass balance equation model. Since production rate $P^A[=]\frac{mmol_A}{g\cdot h}$, we convert to the same units as A^* by multiplying by cell density $\beta[=]\frac{g}{L}$. Thus, in applying this cost function to our model, $A^* = \beta P^A$.

The optimal cost of producing metabolite using an n-step pathway at rate P^A

is given by

$$C(P^A) = \sum_{i=1}^{n} \left(\frac{a_i}{\hat{k}_i} \beta P^A + 2\sqrt{\frac{\kappa_i a_i b_i}{\hat{k}_i} \beta P^A} \right) = \sum_{i=1}^{n} \left(\frac{a_i}{\hat{k}_i} \right) \beta P^A + \sum_{i=1}^{n} \left(2\sqrt{\frac{\kappa_i a_i b_i}{\hat{k}_i}} \right) \sqrt{\beta P^A}.$$

We define parameters η^A and ζ^A as follows,

$$\eta^A := \sum_{i=1}^{n} \left(\frac{a_i}{\hat{k}_i} \right) \beta \quad \text{and} \quad \zeta^A := \sum_{i=1}^{n} \left(2\sqrt{\frac{\kappa_i a_i b_i}{\hat{k}_i}} \right) \sqrt{\beta}.$$

Then, the cost for producing a metabolite at rate P^A can be written as

$$C(P^A) = \eta^A P^A + \zeta^A \sqrt{P^A}.$$

For our strain specific cell, $\gamma \in \{\emptyset, ab, a, b\}$ with cell density β_γ, the production of metabolites A and B at rates P_γ^A and P_γ^B, respectively, is given by

$$C_\gamma(P_\gamma^A, P_\gamma^B) = \left(\eta_\gamma^A P_\gamma^A + \zeta_\gamma^A \sqrt{P_\gamma^A} \right) + \left(\eta_\gamma^B P_\gamma^B + \zeta_\gamma^B \sqrt{P_\gamma^B} \right), \tag{3.12}$$

where

$$\eta_\gamma^A := \sum_{i=1}^{n} \left(\frac{a_i}{\hat{k}_i} \right) \beta_\gamma \quad \text{and} \quad \zeta_\gamma^A := \sum_{i=1}^{n} \left(2\sqrt{\frac{\kappa_i a_i b_i}{\hat{k}_i}} \right) \sqrt{\beta_\gamma},$$

under the assumption that the pathways to produce A and B are independent. We use this cost function to build a scaling function with which to scale the maximum growth rate of each strain.

Since the cheater strain does not produce either of the metabolites A and B, $C_\emptyset = 0$. The A-producer will have cost function with only the first terms of equation (3.12), $C_a = (\eta_a^A P_a^A + \zeta_a^A \sqrt{P_a^A})$, the cost for the B-producer, C_b ,will only contain the second terms, and the cost for wild type, C_{ab}, will contain both terms.

In addition to costs associated with the production of metabolites A and B, each

cell has a basic maintenance cost. We assume that this cost is a multiple of the wild type cost of producing A and B,

$$M = \alpha C_{ab}\,, \tag{3.13}$$

and is the same for all strains.

The average of the total cost for all four strategies is

$$C_{Avg} := \frac{1}{4}\Big((C_\emptyset + M) + (C_a + M) + (C_b + M) + (C_{ab} + M)\Big) = \frac{C_\emptyset + C_a + C_b + C_{ab}}{4} + M. \tag{3.14}$$

From this we create a scaling factor that compares each strain's total cost to the average cost for a cell.

$$\kappa_\gamma = \frac{C_\gamma + M}{C_{Avg}}. \tag{3.15}$$

Note that $\kappa_\gamma > 1$ if the strain's cost is higher than the average total cost for all four strategies, C_{avg}, and $\kappa_\gamma < 1$ if the strain's cost is lower than the average total cost for all four strategies. We scale the growth in such a way that a lower than average cost yields a relatively faster growth rate, and a higher than average cost yields a slower growth rate. The scaled growth function is given by

$$\mu_\gamma = \frac{1}{\kappa_\gamma}\mu_{max,\gamma}\frac{A_\gamma}{K_\gamma^A + A_\gamma}\frac{B_\gamma}{K_\gamma^B + B_\gamma}\frac{S}{K_\gamma^S + S}. \tag{3.16}$$

Note that if the metabolic cost associated with A and B is a small fraction of the overall maintenance cost for the cell, then α will be large and κ_γ will be close to 1. Analysis of the model with cost scaled growth rate can be found in chapter 5 section 5.2.

CHAPTER FOUR

METHODS

4.1 Numerical Methods

To analyze our model we used a combination of MATLAB [36], AUTO [15] accessed within XPPAUT [17] . We use the parameters described in sections 4.2 and 4.3. These parameters made our system stiff, thus we use variable-step, variable-order solver ode15s within MATLAB. In XPP we use Gear method to solve our system and estimate positive steady states. We use these steady states as initial conditions from which from which to do the continuation in AUTO. The Gear method is a variable stepsize solver that is useful for integrating stiff systems. Once we have found a steady state in XPP we perform an arc length continuation in AUTO to numerically obtain the bifurcation diagrams we are interested in. To confirm our numerical results we compare solutions from both XPP and MATLAB, as well as confirm solutions to the steady state equations and stability using the eigenvalues of the Jacobian at those equilibria using Mathematica [1].

As a reference and for reproducibility, we provide the *.ode files used with XPP and AUTO in appendix B.

4.2 Simplifying Assumptions

Our original mass balance equation model has 100 parameters, with 17 additional parameters for the cost scaled model. We apply the following simplifying assumptions to our mass balance equation model for the numerical analysis.

A1. Symmetry of Metabolites. We assume that metabolites A and B are symmetric. Explicitly, this gives the following equivalencies for all $\gamma \in \{\emptyset, ab, a, b\}$,

$$\begin{aligned}
&K^A_\gamma = K^B_\gamma, \quad A_{in} = B_{in}, \quad Y^A_{P,a} = Y^B_{P,b}, \quad Y^A_{P,b} = Y^B_{P,a},\\
&Y^A_{D,\gamma} = Y^B_{D,\gamma}, \quad K^A_{D,\gamma} = K^B_{D,\gamma}, \quad q^{Ai}_\gamma = q^{Bi}_\gamma, \quad q^{Ax}_\gamma = q^{Bx}_\gamma,\\
&K^A_{\gamma,i} = K^B_{\gamma,i}, \quad K^A_{\gamma,x} = K^B_{\gamma,x}, \quad \hat{A}_\gamma = \hat{B}_\gamma, \quad q^{Ap}_\gamma = q^{Bp}_\gamma, \quad Y_{A/S} = Y_{B/S}.
\end{aligned}$$

When our initial conditions are also symmetric in relation to A and B,

$$X_a(0) = X_b(0),\ A_\emptyset(0) = B_\emptyset(0),\ A_{ab}(0) = B_{ab}(0),\ A_a(0) = B_b(0),\ A_b(0) = B_a(0),$$

then for all time we have,

$$X_a(t) = X_b(t),\ A_\emptyset(t) = B_\emptyset(t),\ A_{ab}(t) = B_{ab}(t),\ A_a(t) = B_b(t),\ A_b(t) = B_a(t).$$

A2. Strain Specific Parameters. We assume that all parameters except production rate of metabolites A and B, $Y^A_{P,\gamma}$ and $Y^B_{P,\gamma}$, are not strain specific. Explicitly we define these parameters for metabolite A in the following way,

$$\begin{aligned}
&\mu_{max} := \mu_{max,\gamma}, \quad K^A := K^A_\gamma, \quad K^S := K^S_\gamma, \quad \beta := \beta_\gamma,\\
&Y^A_D := Y^A_{D,\gamma}, \quad K^A_D := K^A_{D,\gamma}, \quad q^{Ai} := q^{Ai}_\gamma, \quad q^{Ax} := q^{Ax}_\gamma,\\
&K^A_i := K^A_{\gamma,i}, \quad K^A_x := K^A_{\gamma,x}, \quad \hat{A} := \hat{A}_\gamma, \quad q^{Ap} := q^{Ap}_\gamma.
\end{aligned}$$

Parameters related to metabolite B are analogous.

A3. Parameters set to 0. We assume that metabolites A and B are not being added into the chemostat from an external source. We also assume that consumption of A and B for non-growth is very small [44] and will be assumed to be 0 for all

strains. Thus,

$$A_{in} = 0, \quad , B_{in} = 0, \quad K^A_{D,\gamma} = 0, \quad K^B_{D,\gamma} = 0.$$

A4. Transport Parameters. We assume that the proportionality constant for import and export of A and B by active transport is equal for all strains.

$$q^{Ai}_\gamma = q^{Ax}_\gamma, \quad q^{Bi}_\gamma = q^{Bx}_\gamma.$$

Furthermore, under assumptions A1 and A2, we define non-strain specific parameter in the passive transport model

$$q := q^{Ap}_\gamma = q^{Bp}_\gamma.$$

Under assumptions A1, A2, and the first part of A4, we define non-strain specific parameter in the active transport model

$$q := \frac{q^{Ai}_\gamma}{\hat{A}_\gamma} = \frac{q^{Bi}_\gamma}{\hat{B}_\gamma} = \frac{q^{Bx}_\gamma}{\hat{B}_\gamma} = \frac{q^{Ax}_\gamma}{\hat{A}_\gamma}.$$

A5. Cost Parameters. In extension of assumptions A1 and A2 we assume that cost function parameters are not strain specific and are symmetric for A and B. Explicitly for all $\gamma \in \{\emptyset, ab, a, b\}$ this is,

$$\eta^A := \eta^A_\gamma = \eta^B_\gamma,$$
$$\zeta^A := \zeta^A_\gamma = \zeta^B_\gamma.$$

4.3 Parameter Estimates

Our full model without simplifying assumptions, but including the parameters associated with the metabolic cost function, has as many as 100 different parameters. Under the simplifying assumptions made in section 4.2, which assume that all but a few parameters are not strain-specific and that parameters relating to A and B are symmetric, the number of parameters is reduced to 21. We now describe these parameters and estimate their values based on experimental data and the literature, with input from collaborators A. Beck and R. Carlson from the department of Chemical and Biological Engineering.

4.3.1 Population Growth and Decay

Parameters related to growth and decay of the population are μ_{max}, K^A, K^S, and d. Function μ_γ representing strain-specific growth rate has three variables, A_γ, B_γ and S, and four parameters which are assumed to not be strain-specific under the assumption A2 in section 4.2: μ_{max}, K^A, K^B, and K^S. Parameter μ_{max} represents the maximal growth rate of the cell, which is estimated by the maximal growth rate of *E. coli* on M9 minimal media [6]. Half saturation constants K^A and K^B, assumed to be equal under our symmetry assumption A1, have a range which is estimated using values for amino acids arginine, lysine, proline, serine, and threonine (see supplemental spreadsheet AAPathwayParameters.xlsx for details). The range of estimated K^A values spanned two orders of magnitude; thus, we chose a midrange value, $K^A = 0.023$ mM. Half saturation constant K^S is estimated based on glucose [23,35]. Decay rate d includes both chemostat washout and death rate of cells. Thus, we estimate it to be slightly larger than a dilution rate of the chemostat.

Parameter	Estimated range or value	Value used in simulations
μ_{max}	$0.6\,\frac{1}{\text{h}}$	$0.6\,\frac{1}{\text{h}}$
K^A	$0.0042 - 0.23$ mM	0.023 mM
K^S	$1 - 10 \times 10^{-3}$ mM	10^{-3} mM
d	$0.1 - 0.4\,\frac{1}{\text{h}}$	$0.2\,\frac{1}{\text{h}}$

4.3.2 Internal Metabolite Production and Demand

Demand function D_γ^A is proportional to growth rate with constant Y_D^A, assumed not to be strain-specific. To compute this parameter we first find the relative abundance of each amino acid as reported in [41]. Assuming that cells are between 50 and 70 percent protein [12] we compute demand in millimoles of amino acid and grams of cell dry weight, by

$$(\%\text{ protein})(\frac{\text{mmol}_{AA}}{\text{g cdw}})(\text{rel. abund.}\frac{\text{mmol}_A}{\text{mmol}_{AA}}) = Y_D^A\frac{\text{mmol}_A}{\text{g cdw}}.$$

This gives us a low estimate of $0.05\,\frac{\text{mmol}_A}{\text{g cdw}}$ and a high estimate of $0.80\,\frac{\text{mmol}_A}{\text{g cdw}}$. We chose an intermediate value of $Y_D^A = 0.25\,\frac{\text{mmol}_A}{\text{g cdw}}$ for our simulations.

Amino acid	Abundance $\frac{\mu\text{mol}_{AA}}{\text{1g cdw}}$	Relative abundance $\frac{\text{mmol}_{A}}{\text{mmol}_{\text{Total } AA}}$
tryptophan	54	0.01
cysteine	87	0.02
histidine	90	0.02
tyrosine	131	0.03
methionine	146	0.03
phenylalanine	176	0.03
serine	205	0.04
proline	210	0.04
asparagine	229	0.05
aspartate	229	0.05
threonine	241	0.05
glutamate	250	0.05
glutamine	250	0.05
isoleucine	276	0.05
arginine	281	0.06
lysine	326	0.06
valine	402	0.08
leucine	428	0.08
alanine	488	0.10
glycine	582	0.11

Function P_{γ}^{A}, representing metabolite production rate, uses parameter $Y_{P,\gamma}^{A}$ which is a strain-specific metabolite production coefficient. Production rate for the wild type strain is estimated as a product of the demand and the growth rate. For *E. coli* average growth rate is estimated to be approximately $0.4\frac{1}{h}$, estimated from

steady state equality with typical dilution rate d. Thus, production rate for wild type is given by

$$Y^A_{P,ab}\frac{\text{mmol}_A}{\text{g cdw}\cdot\text{h}} = 0.25\frac{\text{mmol}_A}{\text{g cdw}}(0.4\frac{1}{\text{h}}) = 0.1\frac{\text{mmol}_A}{\text{g cdw}\cdot\text{h}}.$$

Overproducing auxotrophs have been shown to produce amino acids at a rate four times as fast as wild type [43], and specialists have been observed to overproduce at a rate as much as 14 times that of wild type [4]. In preliminary numerical analysis of this model we observe that cooperation occurs when cooperator strains produce at a rate faster than 2.68 times that of the wild type strain. Thus, we chose the metabolite production coefficient for cooperator A (A-producer) to be four times that of the wild type. Since neither the cheater nor cooperator B produce metabolite A, production coefficient for these strains will be 0.

Parameter	Estimated range or value	Value used in simulations
Y^A_D	$0.05 - 0.80\ \frac{mmol_A}{gcdw}$	$0.25\ \frac{mmol_A}{gcdw}$
$Y^A_{P,ab}$	$0.02 - 0.32\ \frac{mmol_A}{gcdw\cdot h}$	$0.1\ \frac{mmol_A}{gcdw\cdot h}$
$Y^A_{P,a}$	$0.08 - 4.48\ \frac{mmol_A}{gcdw\cdot h}$	$0.4\ \frac{mmol_A}{gcdw\cdot h}$
$Y^A_{P,b}$		$0\ \frac{mmol_A}{gcdw\cdot h}$
$Y^A_{P,\emptyset}$		$0\ \frac{mmol_A}{gcdw\cdot h}$

4.3.3 Substrate

The parameter denoting biomass yield from S, $Y_{X/S}$, is computed by the following,

$$Y_{X/S} = \frac{0.45\,cmol_X}{cmol_S}\cdot\frac{cmol_S}{30\,g_S}\cdot\frac{180\,g_S}{mol_S}\cdot\frac{24.5\,g_X}{cmol_X} = 66.15\,\frac{g_X}{mol_S}$$

where molecular weight of S is estimate using glucose.

The yield coefficient for producing A from S was computed with the estimation

that 50 to 70 percent of the cell is protein [12], S represents glucose, and by using the molecular weight of five sample amino acids. The molecular weight of glucose is given by $180\,\frac{\mathrm{g}_S}{\mathrm{mol}_S}$. Then $Y_{A/S}$ is computed using the following equation and the values in the table below. We again chose an intermediate value for our simulations.

$$\frac{\mathrm{g}_A}{\mathrm{g}_S}\cdot\frac{\mathrm{g}_S}{\mathrm{mol}_S}\cdot\frac{\mathrm{mol}_A}{\mathrm{g}_A}=Y_{A/S}\frac{\mathrm{mol}_A}{\mathrm{mol}_S}$$

Amino acid	Molecular weight $\frac{\mathrm{g}_S}{\mathrm{mol}_S}$	Range for $Y_{A/S}\frac{\mathrm{mol}_A}{\mathrm{mol}_S}$
arginine	174.2	0.517-0.724
lysine	146.2	0.616-0.862
threonine	119.1	0.756-1.059
proline	115.1	0.782-1.095
serine	105.1	0.857-1.200

Parameter S_{in} has an estimated range of $5.6 - 55.6\,\frac{\mathrm{mmol}_S}{\mathrm{L}}$, equivalent to $1 - 10\,\frac{\mathrm{g}}{\mathrm{L}}$ glucose. Since the lowest value in this range was close to the transition from region V to II in Fig 5.1b we chose the value to be slightly higher for the passive transport examples without application of production cost (Fig 5.3, 5.7, 5.8). All active transport examples in the sections 5.1 and 5.1.1 (Figs 5.1b, 5.2) and all three examples of the cost scaled model in the third section of our results (Figs 5.4, 5.5, 5.6) use $S_{in} = 5.6\frac{\mathrm{mmol}_S}{\mathrm{L}}$.

Parameters	Estimated range or value	Value used in simulations
$Y_{X/S}$	$66.15\times10^{-3}\,\frac{\mathrm{g\ cdw}}{\mathrm{mmol}_S}$	$66.15\times10^{-3}\,\frac{\mathrm{g\ cdw}}{\mathrm{mmol}_S}$
$Y_{A/S}$	$0.517 - 1.2\,\frac{\mathrm{mmol}_A}{\mathrm{mmol}_S}$	$0.909\,\frac{\mathrm{mmol}_A}{\mathrm{mmol}_S}$
S_{in}	$5.6 - 55.6\,\frac{\mathrm{mmol}_S}{\mathrm{L}}$	$5.6\,\frac{\mathrm{mmol}_S}{\mathrm{L}}$, $8\,\frac{\mathrm{mmol}_S}{\mathrm{L}}$

4.3.4 Transport

There are five parameters associated with the transport functions, each assumed to not be strain-specific and to satisfy our symmetry assumptions i.e. transport of A will have the same parameters as transport of B. For the passive case the transport is proportional to the difference between internal and external concentrations of metabolite with proportionality constant q^{Ap}. For active transport our proportionality constant is q^A. These parameters will be investigated throughout this paper and values are specified when necessary.

The desired internal concentration used for active transport is $\hat{A}$. Estimated internal concentrations were taken from [8] for five sample amino acids and summarized in the following table. For our numerical simulations we chose the intermediate value associated with proline.

Amino acid	Concentration mM
serine	0.07
threonine	0.18
proline	0.39
lysine	0.41
arginine	0.57

Half saturation constant of K_i^A for import into the cell and half saturation constant for export out of the cell K_x^A are also assumed to not be strain-specific. We estimate the half saturation constant for export by multiplying the half saturation constant for import by the cell density $\beta = 1000\,\frac{\text{g cdw}}{\text{L}}$. We estimate them using five sample amino acids with values from BRENDA [49] and chose the intermediate value for proline for our simulations.

Amino acid	K_i^A mM	K_x^A mM
serine	0.568×10^{-3}	0.568
lysine	1.126×10^{-3}	1.126
arginine	4.088×10^{-3}	4.088
proline	5.957×10^{-3}	5.957
threonine	7.030×10^{-3}	7.030

We summarize the fixed transport parameters here:

Parameter	Estimated range or value	Value used in simulations
$\hat{A}$	$0.07 - 0.57$ mM	0.39 mM
K_i^A	$0.568 \times 10^{-3} - 7.03 \times 10^{-3}$ mM	5.957×10^{-3} mM
K_x^A	$0.568 - 7.03$ mM	5.957 mM
β	1000 $\frac{\text{g cdw}}{\text{L}}$	1000 $\frac{\text{g cdw}}{\text{L}}$

4.3.5 Other Chemostat Parameters

Our model allows for an inflow of metabolites A and B into the chemostat with concentration given by A_{in} and B_{in}. To simplify our analysis and to guarantee that any metabolite in the system was made by one of the producer strains we chose these to both be 0 mM. Dilution rate of the chemostat will be slightly less than population decay d described previously.

Parameters	Estimated range or value	Value used in simulations
A_{in}	≥ 0 mM	0 mM
J	$0.1 - 0.4\,\frac{1}{\text{h}}$	$0.19\,\frac{1}{\text{h}}$

4.3.6 Production Cost

Parameters for the cost function are computed in the supplemental spreadsheet AAPathwayParameters.xlsx for five different amino acids. We use parameters from

proline for both A and B under our symmetry assumptions.

Parameter	Estimated range or value	Value used in simulations
η^A	$9.27 \times 10^5 - 1.91 \times 10^7 \frac{\#_{\text{carbon}} \cdot \text{g cdw} \cdot \text{h}}{\text{mmol}_A}$	$3.65 \times 10^6 \frac{\#_{\text{carbon}} \cdot \text{L} \cdot \text{h}}{\text{mmol}_A}$
ζ^A	$1.68 \times 10^3 - 1.12 \times 10^5 \#_{\text{carbon}} \sqrt{\frac{\text{g cdw} \cdot \text{h}}{\text{mmol}_A}}$	$3.51 \times 10^4 \#_{\text{carbon}} \sqrt{\frac{\text{L} \cdot \text{h}}{\text{mmol}_A}}$

CHAPTER FIVE

NUMERICAL RESULTS

We now provide numerical results from the model under assumptions A1 - A5 with parameters chosen to be biologically relevant described in section 4.3. To maintain symmetry in the system under these assumptions, we impose symmetric initial conditions,

$$X_a(0) = X_b(0),\ A_a(0) = B_b(0),\ A_b(0) = B_a(0),\ A_{ext}(0) = B_{ext}(0).$$

Under symmetry assumptions A1 and A5 with these initial conditions, the two cooperator strains will always have the same population concentration $X_a(t) = X_b(t)$ and symmetric concentrations $A_a(t) = B_b(t), A_b(t) = B_a(t)$, and $A_{ext}(t) = B_{ext}(t)$ for all $t > 0$.

We use software XPPAUT [17] with AUTO [15] to numerically explore three questions:

- How does passive transport and active transport between intra- and extracellular compartment affect the outcome of competition between the four phenotypes?
- How does the inclusion of the cost of metabolite production affect the outcome of the competition?
- What effect does the presence of the cheater strain have on competition?

We will describe the results by showing which stable steady states, representing different microbial populations, exist in various parameter regimes. Steady states will

be described using the following conventions. Pure wild type steady state (WT) is the steady state at which the only population is that of the wild type strain; there are no cooperators, or cheaters. Pure cooperator steady state (CO) is the steady state at which the only remaining populations are the two cooperator strains; there are no wild type or cheater strains. By symmetry assumptions, both cooperator strains must be present at the same concentration. The coexistence of wild type and cooperators (WT/CO) steady state contains a mixed population of wild type and cooperator strains while there is no cheater strain. Coexistence of wild type and cheaters (WT/CH) contains a mixed population of wild type and cheater strains with no cooperators. The coexistence of cooperators and cheaters (CO/CH) contains a mixed population of cooperator and cheater strains with no wild type strain. Finally, the steady state where all population concentrations are zero (D) describes population collapse.

5.1 Mass Balance Equation Model Results

We select biologically relevant parameter ranges to investigate for q and input substrate concentration S_{in}, and fix biologically justified values for all other parameters (see section 4.3 for details). Steady state behavior is examined as a function of q and S_{in} in these ranges and the results compared for passive and active transport.

In Fig 5.1, we present two-dimensional bifurcation diagrams where the axes represent transport parameter q and input substrate concentration S_{in}, and where each curve represents a bifurcation affecting a steady state. Dotted curves denote bifurcations that occur either in the nonphysical region (one of the concentrations is negative) or do not change the stability of physical steady states. Solid curves denote bifurcations involving a change in stable steady states. Therefore, only solid curves in

the figure separate regions with potentially different sets of physically relevant stable steady states. The table in Fig 5.1 summarizes the set of stable steady states in each two-dimensional region bounded by solid curves.

The diagrams in Fig 5.1 indicate that the dynamics for the passive transport model may be much richer than for the active transport model. To investigate these differences further, we discuss these diagrams in detail and provide one-dimensional cross-sections through each diagram (Figs 5.2, 5.3) where we elucidate the sequence of bifurcations that happen as we increase transport parameter q at fixed values of S_{in}.

5.1.1 Active Transport

As seen in Fig 5.1a, the active transport mass balance equation model has only two different regions of stable equilibrium. For low transport rates the only stable steady state is WT. In region I, the transport rates are too low for the cooperator strains to gain enough metabolite from the environment. Since growth is a function of both necessary resources A and B, and substrate S, all auxotrophs will have a lower fitness than the wild type strain that produces both metabolites. Higher transport rates allow the cooperator strains to compete with the wild type strain, and the bistability in region II indicates that the winner of this competition is determined by the initial concentrations of each strain. In section 5.3, we further explore the basins of attraction for parameter regions with bistability such as this one.

Consider a horizontal cross section of the diagram for active transport in Fig 5.1a for $S_{in} = 5.6$ mM (Fig 5.2). We choose $S_{in} = 5.6$ mM as it correlates to having 1 g/L of glucose, a typical substrate used to grow microbes such as *E.coli*. For $0 < q < 0.272$ we observe monostability where the only steady state is pure wild type population (WT). For $q > 0.272$ there is bistability of WT and a stable steady state of pure

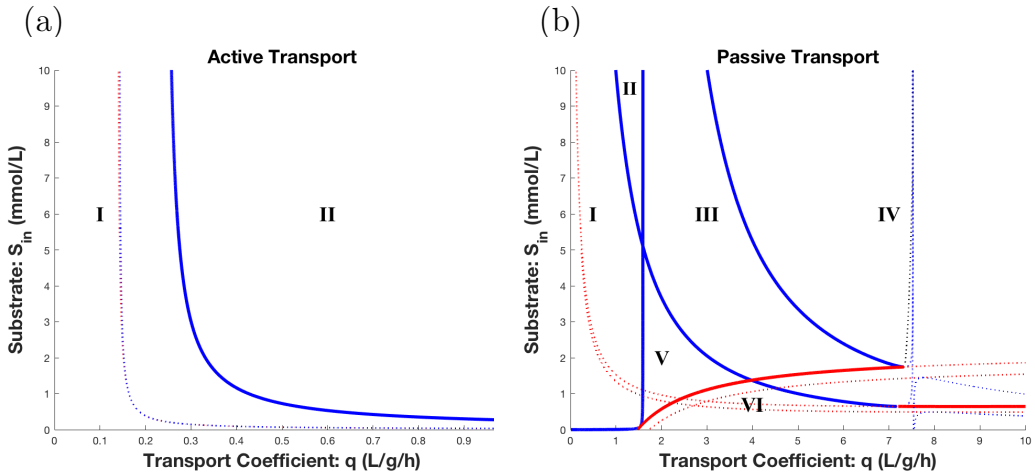

Region	Stable steady states
I	WT
II	WT, CO
III	WT, CO, D
IV	CO, D
V	WT, D
VI	D

Figure 5.1: **Two-dimensional bifurcation diagrams.** Bifurcation diagram in transport coefficient q and substrate inflow concentration S_{in} for active transport model (a) and passive transport model (b). Boundary point bifurcations (blue), saddle-node bifurcations (red), and Hopf bifurcations (black) are either solid lines, to indicate a change in physical stable steady states, or dotted to denote a bifurcation that does not affect the physical stable steady states. The table details which physical steady states are stable in each labeled region bounded by solid curves.

cooperative consortia (CO). At $q = 0.272 \frac{\text{L}}{\text{g·h}}$ there is a transcritical bifurcation where a stable but nonphysical coexistence curve of WT/CO intersects an unstable curve of pure cooperators (CO) to give rise to a physical unstable curve WT/CO and stable steady state CO.

Similar diagrams would be found for cross sections at any value of $S_{in} > 0$. For our results we considered S_{in} to represent glucose as a commonly found substrate in microbial systems. Many chemostat experiments use $1 - 10$ g/L of glucose which corresponds to $5.6 - 56$ mM for the units used in our model. If we were to run our two-dimensional diagram out to large values of q we would see that the curve separating regions I and II in Fig 5.1 crosses the horizontal axis at $q = 245 \frac{\text{L}}{\text{g·h}}$. While this value is extreme and may not be biologically possible, it indicates that even with a very limited food source, increasing the efficiency of transport is one way in which cooperation is able to emerge.

5.1.2 Passive Transport

The passive transport model indicates a much richer dynamics as seen in Fig 5.1b. Similar to the behavior seen with active transport, the wild type strain is the dominate strain for region I with low transport rate. As transport rate is increased there are two possible behaviors. Above substrate input concentration $S_{in} = 5.105$ mM, there is first bistability of WT and the cooperative consortium (CO) in region II. This is followed by tristability region III with the additional stable state of population collapse (D). Below $S_{in} = 5.105$ mM, there is first bistability of WT and population collapse (D) in region V, followed by the same tristable region III.

To give the differences of these progressions some context, consider glucose as an example substrate for the chemostat. Typical microbial growth experiments with *E.coli* have a glucose concentration of between 1 and 10 g/L (see appendix A for

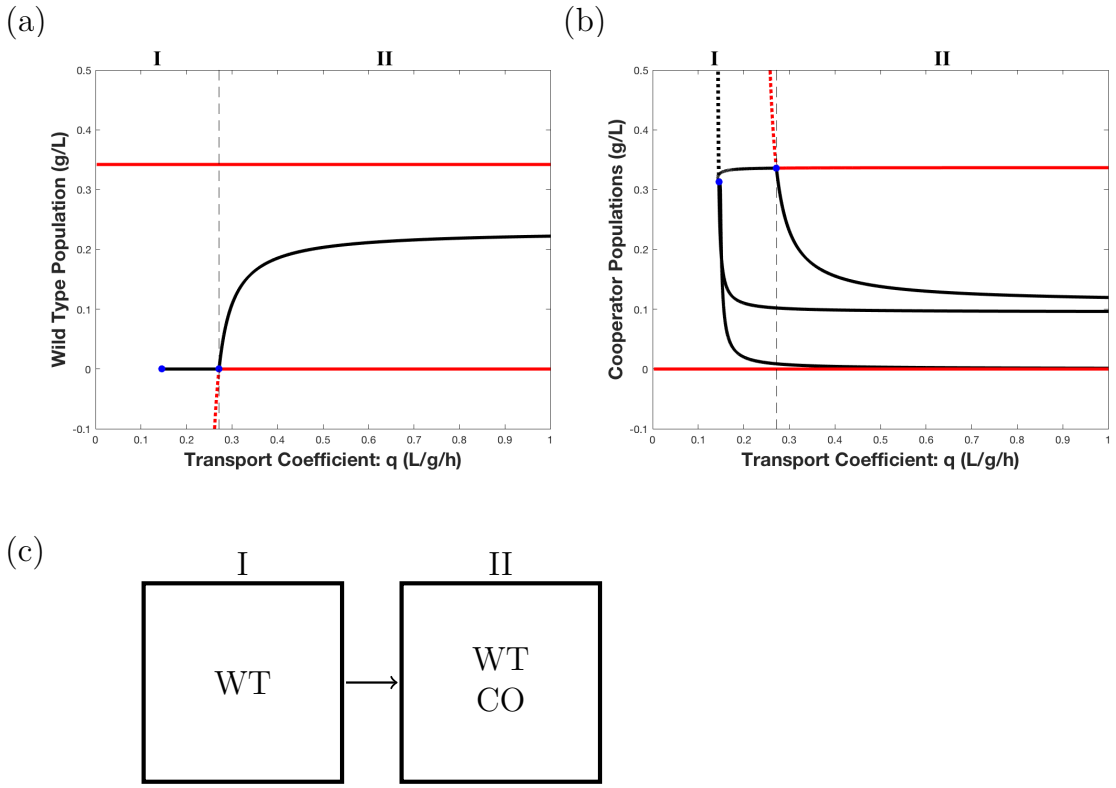

Figure 5.2: **Active transport - One-dimensional bifurcation diagram with $\mathbf{S_{in} = 5.6}$ mM.** A one-dimensional cross section of Fig 5.1a in transport parameter q for substrate inflow concentration $S_{in} = 5.6$ mM. Projection of phase space shows steady states for (a) wild type population and (b) cooperator population. The graphs show stable steady states (red), unstable steady states (black), non-physical stable steady states (red dashed), and non-physical unstable steady states (black dashed). Bifurcations are denoted by blue dots. Regions labeled in (a) and (b) correspond to diagram (c) showing the physical stable steady states possible in each interval of q. As transport parameter q increases, behavior shifts from monostability to bistability.

example batch culture experiments). When converted using the molecular weight of glucose, 180 g/mol, this is equivalent to substrate concentration being between 5.56 mM and 55.56 mM. Thus, the regions above $S_{in} = 5.105$ mM would represent a growth experiment that isn't glucose limited. The regions below $S_{in} = 5.105$ mM would indicate that resources are scarce and exemplify a glucose limited scenario. In the extreme substrate limited system, such as in region VI of Fig 5.1b, the only stable steady state is population collapse (D).

Region IV of Fig 5.1b is a region of bistability between the pure cooperative consortium (CO) and population collapse (D). For higher values of S_{in} this bistability occurs after tristability as transport rate increases. This indicates that better transport of metabolites for a system that is not substrate limited leads to more cooperative behavior. In parameter regions where input substrate concentration is limited, but is still enough to sustain a population, the transport efficiency is not required to be as high to outcompete the wild type strain and establish bistability of CO and D, replacing the tristability seen in region III. Region VI represents a region with very low input substrate concentration where no population is able to grow well enough, even with efficient transport, to prevent population collapse.

As an example of behavior for the passive transport model we provide a cross section of the diagram in Fig 5.1b at $S_{in} = 8$ mM (Fig 5.3). This diagram will be similar to a cross section at $S_{in} = 5.6$mM, but we chose a higher S_{in} value to make it clear that we are providing a cross section from the upper portion of Fig 5.1b. When $0 < q < 1.1628$, we observe monostability where WT is the only stable steady state. For $1.1628 < q < 1.591$, there is a region of bistability between WT and CO, and for $1.591 < q < 3.3018$, there is tristability of WT, CO, and D. For large values of the transport parameter, $q > 3.3018$, we have only two stable steady states CO and D. Each of these three bifurcations is a transcritical bifurcation.

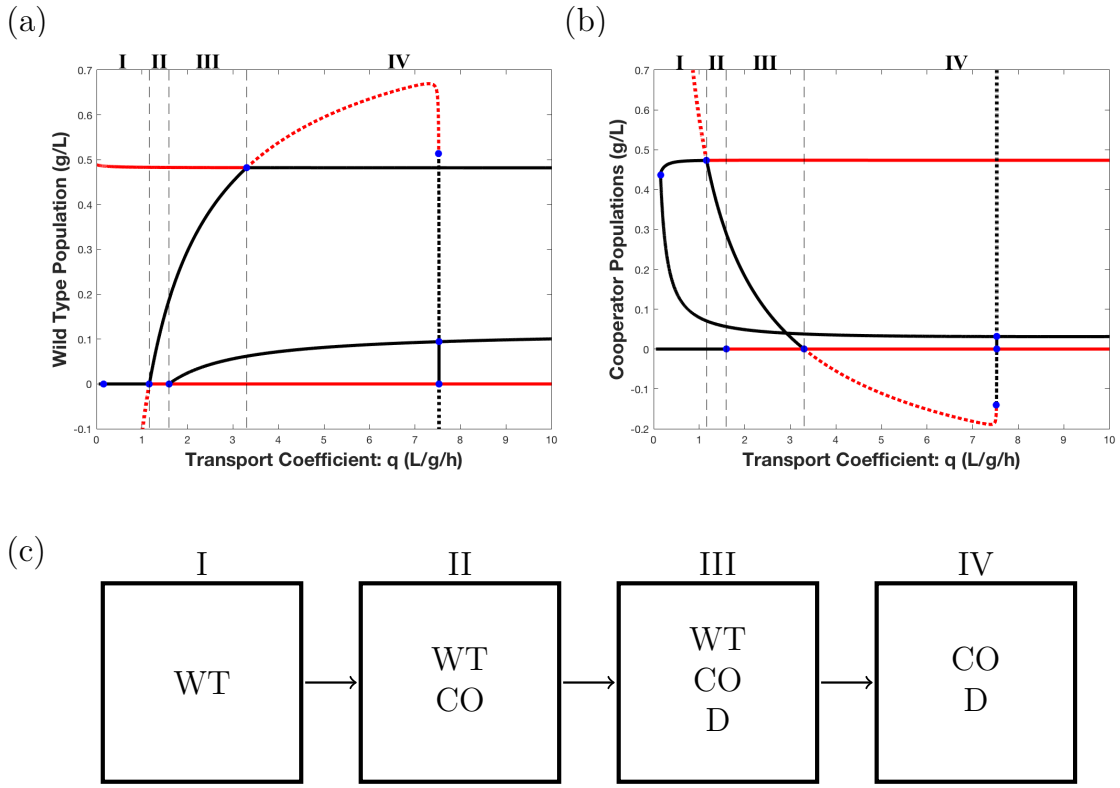

Figure 5.3: **Passive transport - One-dimensional bifurcation diagram with $\mathbf{S_{in} = 8}$ mM.** A one-dimensional cross section of Fig 5.1b in transport parameter q for substrate inflow concentration $S_{in} = 8$ mM. Projection of phase space shows steady states for (a) wild type population and (b) cooperator population. The graphs show stable steady states (red), unstable steady states (black), non-physical stable steady states (red dashed), and non-physical unstable steady states (black dashed). Bifurcations are denoted as blue dots. Regions labeled in (a) and (b) correspond to diagram (c) showing the physical stable steady states possible in each interval of q. As transport parameter q increases, behavior shifts from monostability to bistability to tristability, and then back to bistability.

To summarize, in both active and passive transport models at low transport rate the wild type population outcompetes the other phenotypes. At higher transport rate a stable steady state of pure cooperators emerges. This is consistent with the idea that in order for the cells to cooperate transport must be above a critical value. Unique to the passive transport model is the existence of a stable steady state D where population collapses. This steady state is stable for $q > 1.591$ for any positive input resource concentration $S_{in} > 0$. We propose that stable state D exists when the passive transport rate is so high that strains have difficulty utilizing any metabolites that they produce before it is exported from the cell, or when resources are scarce. With cheaters present to utilize the exported metabolites, the community can be weakened to the point of collapse if the initial population of wild type or cooperator strains is low. We further analyze the effect of cheaters on the system in section 5.3.

5.2 Cost-scaled Model Results

In the previously discussed results there are no physical stable steady states where the cheater strain survives. The main reason is that the growth rate of the cheater strain is smaller than the growth rate of any of the producer strains, since the internal concentration of either A or B, or both, will be lower for the cheater strain than for either wild type or cooperator strains. The growth rate is proportional to the product of the internal concentration of A, internal concentration of B, and the concentration of S; thus, the cheater strain always loses in a competition with a producer strain when they have the same maximal growth rate, μ_{max}. Importantly, the model above does not take into account production costs of A and B. To produce A and B, a cell must invest resources that it cannot then use elsewhere. To account for this expense, we scale the maximal growth rate of each strain by a function of the cost of metabolite production (section 3.2).

The scaling of growth rate described in section 3.2 gives a growth advantage to cheaters whose total cost is lower than the average total cost. Whether a growth advantage or disadvantage is given to the wild type and cooperator strains depends on the parameters chosen for the cost function and rate at which each strain produces metabolites. We estimate our cost function parameters from the metabolic pathways of chosen amino acids in section 4.3. We assume that the cooperators produce the metabolite at a rate four times as fast as the wild type. The multiplicative constant that describes the rate with which each cooperator overproduces the single metabolite compared to the wild type may be an important constant that determines the outcome of the competition. Our preliminary simulations indicate that in order for cooperators to win at any transport rate they must produce at more than twice the rate of the wild type. For the results presented here we chose an overproduction rate of four times that of the wild type and we leave the investigation of the overproduction multiplier for future work. With the selection of parameters presented in section 4.3, the wild type strain is given a slight growth advantage, though not as much of an advantage as the cheater strain, and the overproducing cooperator strain is given a slight disadvantage by our production cost scaling.

5.2.1 Active Transport

We first present a one dimensional bifurcation diagram, with respect to transport parameter q, of the active transport model with the cost function applied to growth rate and fixed inflow substrate concentration $S_{in} = 5.6$ mM . The behavior is similar to the behavior of the unscaled model with one exception- at higher transport values there is an additional steady state that represents the coexistence of cheaters and cooperators (CH/CO). This steady state is born in a transcritical bifurcation at $q = 2.209 \frac{\mathrm{L}}{\mathrm{g \cdot h}}$ where a stable CO steady state and an unstable CH/CO intersect to give rise

to stable CH/CO and unstable CO. This new coexistence state, CH/CO, disappears in a degenerate vertical line of limit point bifurcations at $q = 4.399\frac{\mathrm{L}}{\mathrm{g}\cdot\mathrm{h}}$. For $q > 4.399$ only the stable state WT persists (Fig 5.4).

By using active transport, cells only export metabolites that are in excess of the desired internal concentration. Thus, producers are able to maintain a minimal concentration of whichever metabolite they produce. This capability has the effect of protecting the wild type population so that WT can persist as a stable steady state at all values of transport parameter q. In the progression from region I to region IV, we see that as transport is increased, CO becomes a stable steady state. In region III, this state is invaded by cheaters resulting in a coexistence steady state CH/CO. In region IV, we see that further strengthening of cheaters by faster transport drives cooperators to extinction and the only stable steady state is pure wild type population (WT) (Fig 5.4).

5.2.2 Passive Transport

We consider two scenarios of the passive transport model with the included metabolic production cost scaling. In section 3.2 we defined the maintenance cost for the cell to be proportional to the cost of production of A and B incurred by the wild type strain, $M = \alpha C_{ab}$. The overall metabolic cost to the cell of strategy γ is then $C_\gamma + M$. A low value for α represents the situation where the metabolic pathways to make A and B are a larger proportion of the cell's operations and thus A and B are relatively *expensive* to make. When α is large, then the proportion of the cost of making A and B to the overall metabolic cost is small and thus A and B are relatively *cheap* to make. We note that the two qualitative scenarios detailed below change at $\alpha^* := 284.2$. Therefore, if the overall metabolic cost is more than about 280 times production of A and B, or equivalently, production of A and B is

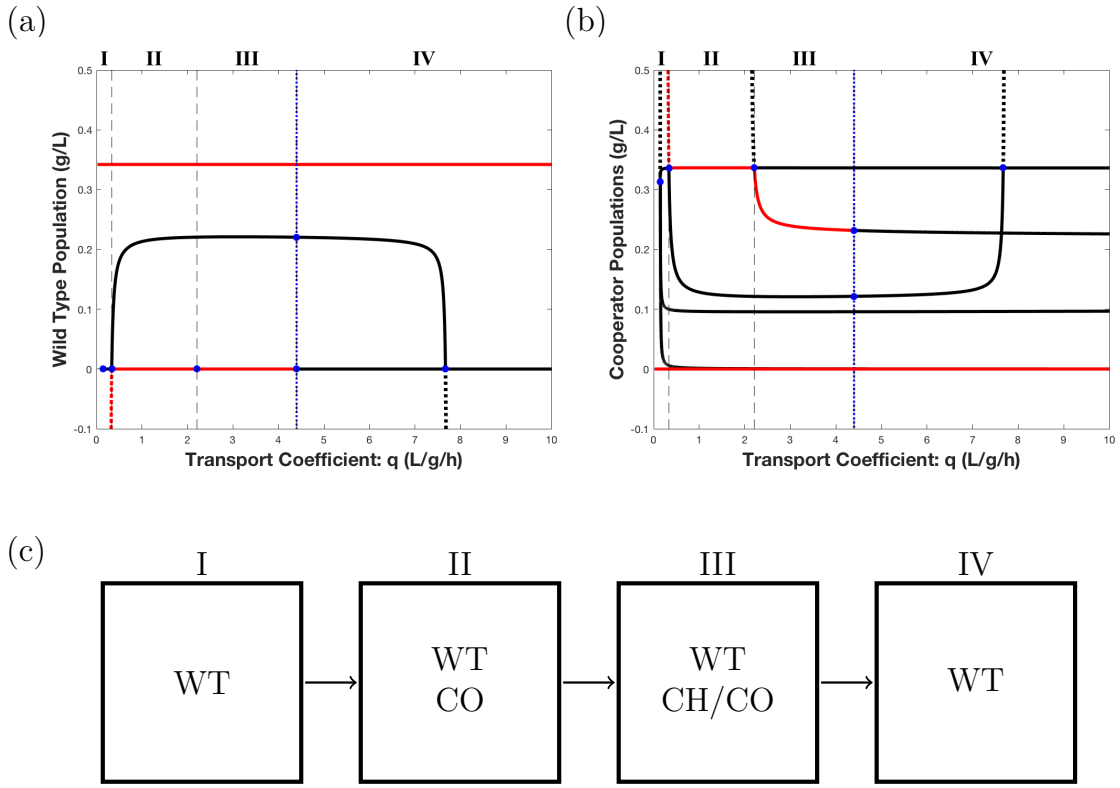

Figure 5.4: **Active transport with metabolite cost for $\mathbf{S_{in} = 5.6}$ mM** One-dimensional bifurcation diagrams in q with inflow substrate concentration $S_{in} = 5.6$ mM showing steady states for (a) wild type population and (b) cooperator population. The graphs show stable steady states (red), unstable steady states (black), non-physical stable steady states (red dashed), and non-physical unstable steady states (black dashed). Bifurcations are denoted as blue dots. Regions labeled in (a) and (b) correspond to diagram (c) showing the physical stable steady states possible in each. Regions I and II are similar to those seen in Fig 5.2. As transport parameter q increases, behavior shifts from monostability to two different bistability regions, ending with a region of monostability where only wild type persist. There is a degenerate line of steady states where all four phenotypes coexist between regions III and IV.

less than about 0.4 % of the overall metabolic cost, metabolites are cheap. If the overall metabolic cost is less than 280 times production of A and B, i.e. production of A and B is more than about 0.4 % of the overall metabolic cost, the metabolites are expensive. In the analysis of the active transport model with cost scaling we did not distinguish between these two scenarios. This is because the bifurcation diagram and stable steady states for the active transport model with cost scaling did not have any qualitative difference when analyzed for cheap metabolites versus expensive metabolites. The results of the passive transport model with cost scaling show a significant difference between expensive and cheap metabolites and are thus analyzed separately.

When A and B are expensive to make, $\alpha < 284.2$, we observe several new stable coexistence steady states, which are illustrated in Fig 5.5 for $\alpha = 60$ and $S_{in} = 5.6$ mM. The first four regions for transport parameter $q < 11.385$ recapitulate the behavior of the passive transport model with no cost scaling in Fig 5.3. Solutions in region V, when $11.385 < q < 64.007$, will converge to either a stable coexistence state WT/CO or the population will collapse to state D. When $64.007 < q < 69.136$, there is bistability of WT and D, and then for $69.136 < q < 163.62$ bistability of WT/CH and D. Finally, when $q > 163.62$ the only stable steady state is population collapse (Fig 5.5).

The passive transport model with expensive metabolites (Fig 5.5) is the most complex of the three presented in this section, because the effects of the metabolite cost scaling differ more between the strains, which leads to a broader range of behaviors. In this case, the metabolite production cost scaling gives significant advantage to both wild type and cheater strains over cooperators. There are two different behavior scenarios observed in Fig 5.5c. The first four regions recapitulate the behavior of the model with no metabolite cost (Fig 5.3). Here the increased

transport rate leads to gradual replacement of wild type strain by cooperator strains. In region V, the increased transport allows the cheater strain to consume more of the metabolites and inhibit cooperation between the two cooperator strains. This weakens the cooperators and allows the wild type strain to come back, first with coexistence of WT/CO in region V, and then to outcompete cooperators in region VI. However, even though the wild type strain has a growth advantage over cooperators from the inclusion of cost, the cheater strain has even greater advantage, and at higher transport it can successfully invade the wild type strain to coexist as WT/CH in region VII before causing population collapse at very high transport rates.

Now we discuss the second scenario where A and B are cheap relative to the overall metabolic cost, i.e. $\alpha > 284.2$. We select $\alpha = 1000$ and $S_{in} = 5.6$ mM (Fig 5.6). In this case, we again see the first four regions are analogous to those seen in Fig 5.3. For higher transport rate, $224.59 < q < 2683.4$, we observe the emergence of coexistence state CH/CO, which exhibits bistability with steady state D. For very high transport rates, $q > 2683.4$, the only stable steady state is population collapse D (Fig 5.6).

The passive transport model for relatively cheap metabolites (Fig 5.6) has similar behavior as we saw with active transport, where a pure cooperator state (CO) gives way to coexistence state CH/CO which is then driven to extinction by further increasing of transport rate and concurrent strengthening of cheaters. There are two main differences between the behavior seen in this scenario and the active transport case. First, when transport rate is high enough, population collapse (D) is the only stable steady state. State D is not seen in the active case because of the protection that the wild type strain has from exporting more metabolite than desirable. Second, since the wild type strain is not protected by passive transport, once the transport rate reaches a critical value ($q = 3.901$ for the example in Fig 5.6) the wild type strain

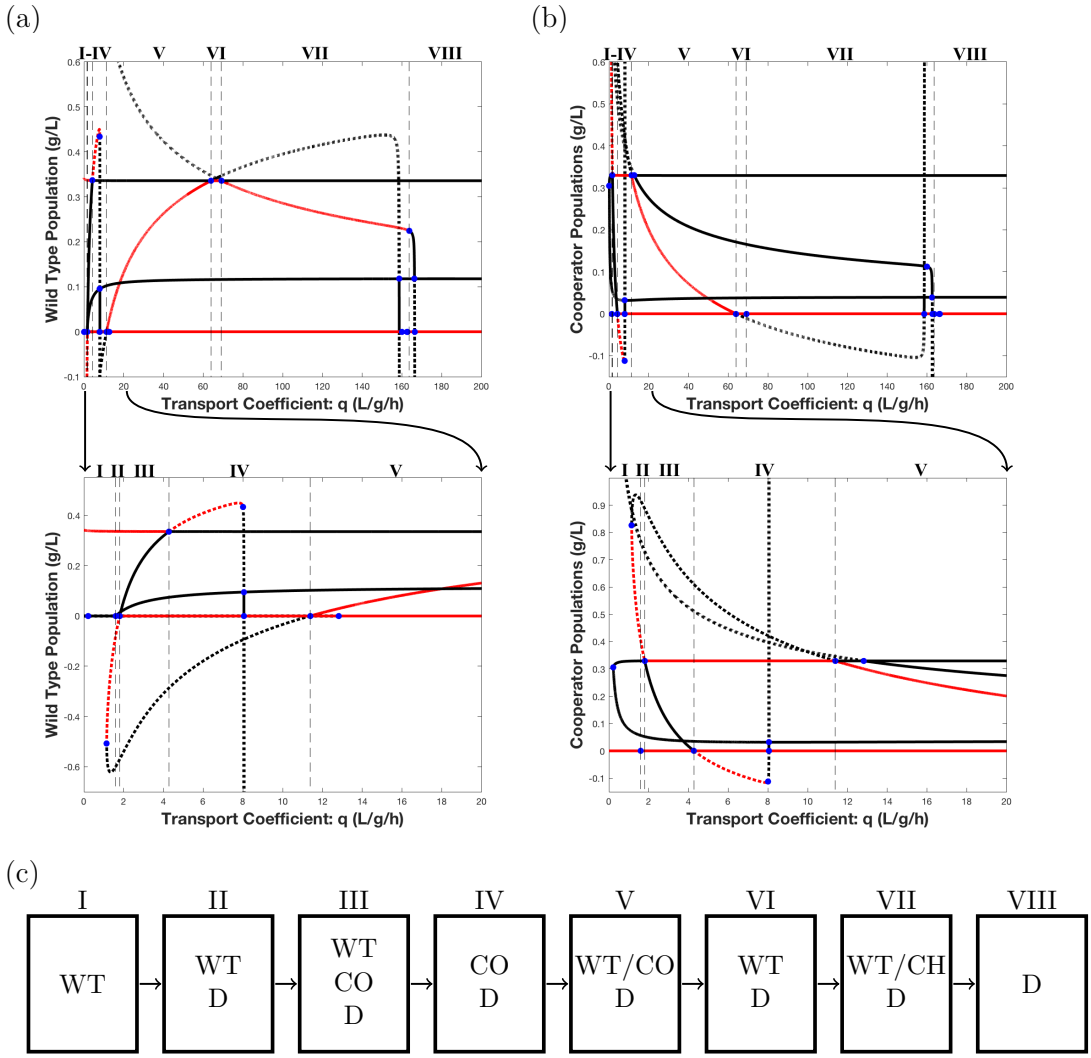

Figure 5.5: **Passive transport model with metabolic cost: Expensive metabolites.** Bifurcation diagrams in q for $\alpha = 60$ and inflow substrate concentration $S_{in} = 5.6$ mM, showing steady states for (a) wild type population and (b) cooperator population. The graphs show stable steady states (red), unstable steady states (black), non-physical stable steady states (red dashed), and non-physical unstable steady states (black dashed). Bifurcations are denoted as blue dots. Regions I-IV are expanded in the lower diagrams and their sequence recapitulates the behavior without the cost function (Fig 5.3). Regions labeled in (a) and (b) correspond to diagram (c) showing the stable steady states possible in each. As transport parameter q increases, behavior shifts from monostability to bistability to tristability, followed by 4 different regions of bistability and finally population collapse for $q > 163.62$.

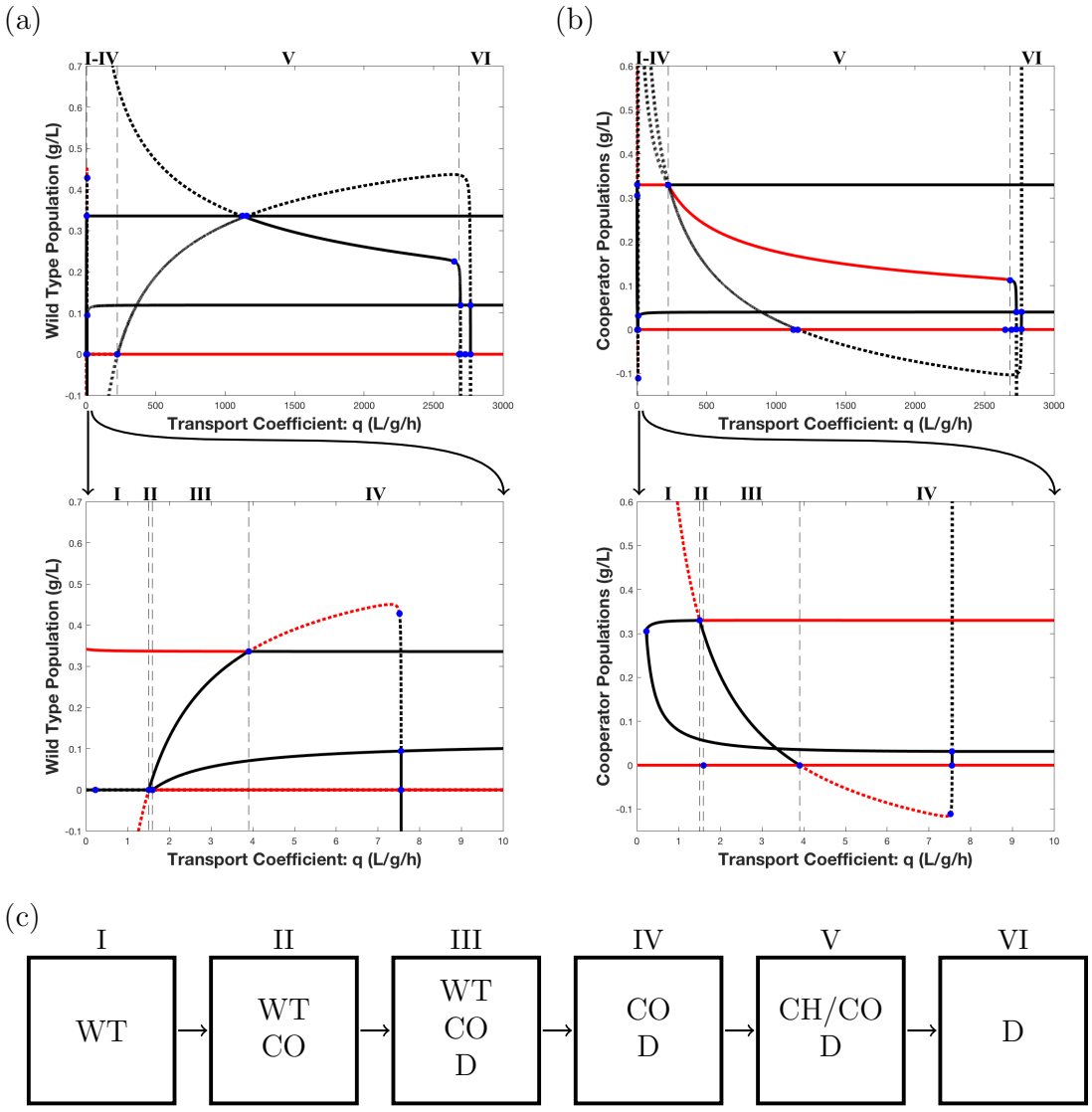

Figure 5.6: **Passive transport model with metabolite cost: Cheap metabolites.** Bifurcation diagrams in q for $\alpha = 1000$ and inflow substrate concentration $S_{in} = 5.6$ mM showing steady states for (a) wild type population and (b) cooperator population, showing stable steady states (red), unstable steady states (black), non-physical stable steady states (red dashed), and non-physical unstable steady states (black dashed). Regions I-IV are expanded in lower diagrams and their sequence recapitulates the behavior without the cost function (Fig 5.3). Regions labeled in (a) and (b) correspond to those in diagram (c) which shows all stable steady states in each region. As transport parameter q increases, behavior shifts from monostability to bistability to tristability, followed by two different regions of bistability and finally population collapse for $q > 2648.4$.

is no longer able to outcompete cooperators or cheaters and stable state WT does not persist. When α is large, as it is in the scenario of a relatively cheap metabolite, the cost scaling constant κ_γ is close to 1 for each phenotype γ. Therefore, any advantage that wild type has over an overproducing cooperator based on cost of production is insufficient to counteract the weakening effect of cheaters. Thus, in the passive transport model with cheap metabolites A and B, at high transport rate, such as in region VI, the advantage of cheaters drives both cooperators and wild type to extinction. The only stable state at high transport rates is population collapse (D) (Fig 5.6).

All three bifurcation diagrams previously discussed from the models with metabolite production cost scaling exhibit some common trends. Clearly, in all three cases the cheater population gains competitive advantage by the inclusion of metabolite production cost, since only producer strains incur this cost. As the transport coefficient increases, more metabolites are available to cheaters because of more rapid export by producing strains and more efficient import by the cheater strain. Similar to what we will see in section 5.3, when the cheater strain is strengthened, as in the case of accounting for metabolite production cost or with fast transport rates, the cooperator strains are weakened. Cheaters also weaken the wild type strain, though to a lesser extent.

5.3 Effect of Cheaters on Population Dynamics

5.3.1 Cheater Effect on Original Model

In our analysis of the original mass balance equation model in section 5.1 we observe that the cheater population does not survive at any of the stable steady states. This motivates the question, what effect does the cheater population have on the population dynamics of the model? In this section, we provide numerical examples

showing how the cheater population changes basins of attraction in parameter regions with multistability for both the original model and the cost scaled model.

If cheaters do not exist at any stable steady states, why do we include them in the model? One reason to include cheaters into the original model is because, although they may not affect which steady states exist, the identity of the basin of attraction of steady states depends on initial cheater concentration. As a numerical example of this influence we chose parameters from two regions of the diagram in Fig 5.1 and provide illustrations of the effect cheaters have on the final outcome of competition.

To illustrate this effect, we choose parameters for the passive transport model from a region with tristability (region III in Fig 5.1b)with $S_{in} = 8$ mM, $q = 2\,\frac{\mathrm{L}}{\mathrm{g\cdot h}}$, see section 4.3 for more parameter details) of pure cooperator consortia (CO), pure wild type population (WT), and population collapse (D). We begin with no initial cheater population, $X_\emptyset(0) = 0$ (Fig 5.7a), and observe the three steady states achieved from various positive initial wild type and cooperator concentrations. As the initial cheater population is increased to $X_\emptyset(0) = 2$ (Fig 5.7b), and then to $X_\emptyset(0) = 4$ (Fig 5.7c), the range of initial values for which population collapses (D, red) or wild type dominates (WT, green) increases.

For a different illustration of the same phenomena, we choose an initial concentration marked with a star in Fig 5.7a - c,

$$X_{ab}(0) = 0.01, \quad X_a(0) = 0.1, \quad X_b(0) = 0.1.$$

Note that our symmetry assumptions require both cooperator strains to have the same initial conditions. The solution curves for these initial concentrations are plotted beneath the corresponding basin of attraction diagram (Fig 5.7). For no initial cheater

population the initial populations lie within the region converging to CO (blue). This corresponds to the solution curve for cooperators (solid, blue) reaching positive steady state while wild type (dashed, green) and cheaters (dotted, red) approach 0 (Fig 5.7d). When the initial cheater population is increased to $X_\emptyset(0) = 2$, the marked initial condition is in a region of initial conditions that converge to a pure wild type population (WT, green). We see this illustrated with the solution curves as the wild type population (dashed, green) is the only one to reach a positive steady state value (Fig 5.7e). Finally, for $X_\emptyset(0) = 4$, all three solution curves decay to zero (Fig 5.7f) and the initial concentration is in a region of initial conditions that converge to population collapse (D, red).

The third row of Fig 5.7 displays the information from Fig 5.7a-c in the form of the proportion of wild type population out of the total producer population, i.e.

$$\frac{X_{ab}(0)}{X_{ab}(0) + 2X_a(0)}.$$

These diagrams reinforce the finding that an increased initial cheater concentration leads to higher chance of population collapse. Note that the in order to outcompete other strains when cheaters are present, the cooperator population needs to start as a majority of the producer population (Fig 5.7g-i).

In Fig 5.8, we fix parameters for the passive transport model from a region with bistability of CO and D (region IV in Fig 5.1b with $S_{in} = 8\text{mM}, q = 10\frac{\text{L}}{\text{g·h}}$, see section 4.3 for more parameter details). Increasing the initial concentration of cheaters weakens the cooperators, making population collapse more likely. There are only two steady states, CO (blue) and D (red), for this choice of parameters. As initial cheater population is raised from $X_\emptyset(0) = 0$ (Fig 5.8a) to $X_\emptyset(0) = 1$ (Fig 5.8b), and then to $X_\emptyset(0) = 2.5$ (Fig 5.8c) we see that the range of initial populations converging

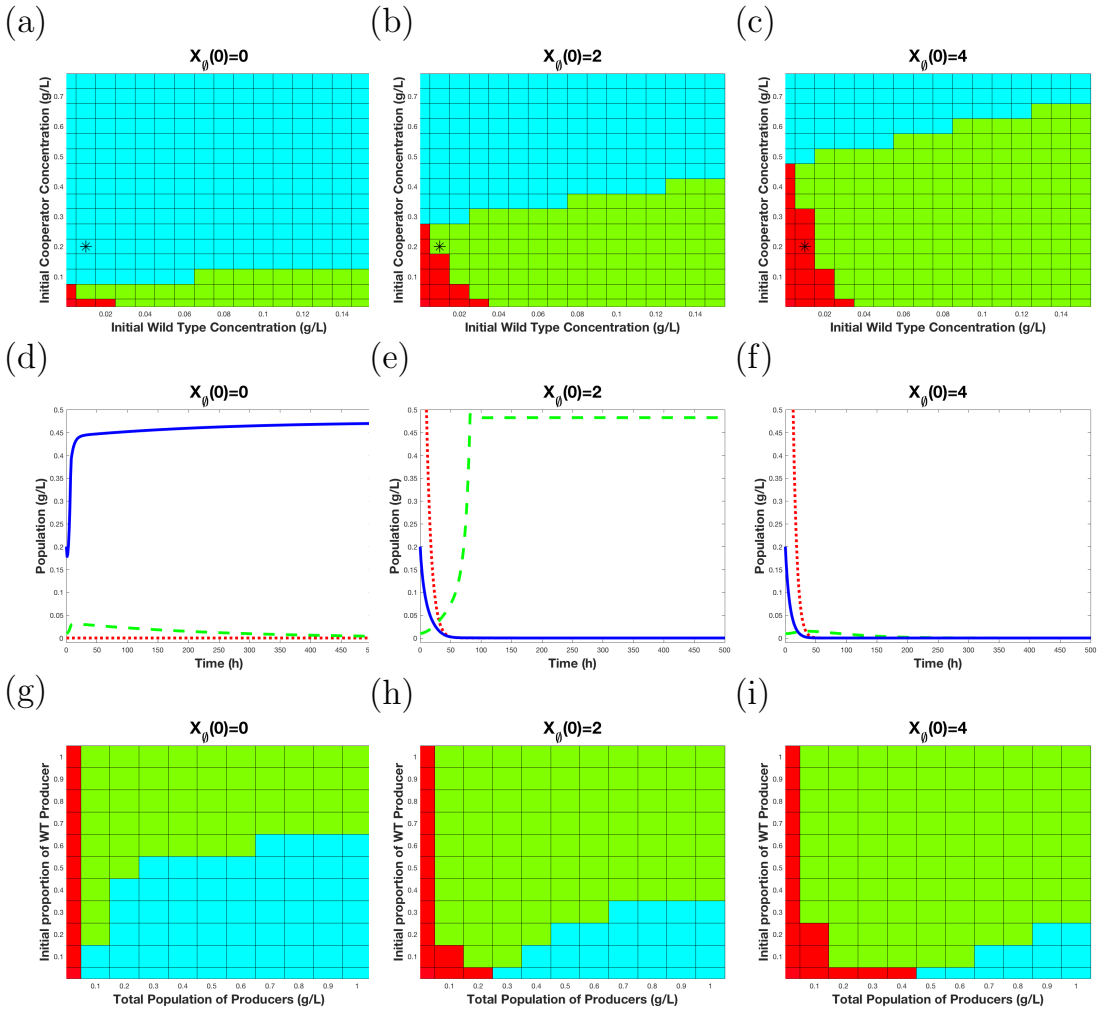

Figure 5.7: **Effect of Cheaters on Tristability Basins of Attraction for Passive Transport Model.** Basins of attraction for cooperators (blue), wild type (green), and population collapse (red) given increasing levels of initial cheater population. Parameters were selected for passive transport model from tristable parameter region III in Fig 5.1b with $S_{in} = 8\text{mM}, q = 2\frac{\text{L}}{\text{g}\cdot\text{h}}$ and cheater population set at (a)$X_\emptyset(0) = 0$, (b)$X_\emptyset(0) = 2$, and (c)$X_\emptyset(0) = 4$. Non-cooperative regions of population collapse or wild type domination expand as initial cheater population is increased. Solution curves corresponding to the marked initial populations in (a)-(c) are plotted beneath their corresponding basin of attraction diagram, (d)-(f) wtih cooperator population (solid, blue), wild type population (dashed, green), and cheater population (dotted, red). Total producer population and the proportion of which is wild type are shown in (g)-(i) with competition outcome at steady state colored as in (a)-(c).

to population collapse increases. Another important observation from Fig 5.8 is that a higher initial wild type population can lower the threshold of initial cooperator population under which there is population collapse. This is because the wild type population can help support and feed the cheater population, and in the case where there are no cheaters, the wild type cells can support cooperator populations. This takes stress off of the cooperator populations and allows them to thrive enough to avoid population collapse. In the case where there are no cheaters (Fig 5.8a), even a small amount of cooperators can invade the initial wild type population so long as the overall population is high enough.

To see the effect of cheaters illustrated with solution curves we choose an initial concentration marked with a star in Fig 5.8a - c,

$$X_{ab}(0) = 0.1, \quad X_a(0) = 0.05, \quad X_b(0) = 0.05.$$

The solution curves are plotted below their respective basin of attraction diagram with wild type (dashed, green), cooperators (solid, blue), and cheaters (dotted, red). As we can see in Fig 5.8d, when there are no cheaters the cooperators outcompete the wild type strain. In Fig 5.8e, the initial condition selected is close to the boundary between basins of attraction and there is significant delay before the population reaches the steady state of pure cooperator consortium. When there is a initial high amount of cheaters (Fig 5.8c,f) all populations decay to zero.

The last row of Fig 5.8 displays the same outcomes as in the first row but with respect to total producer population and the proportion which is wild type strain,

$$\frac{X_{ab}(0)}{X_{ab}(0) + 2X_a(0)}.$$

From Fig 5.8g-i we see that very small initial producer populations will lead to collapse

even when no cheaters are present. Slightly larger producer populations can survive if the wild type strain is not too dominant. Interestingly, if the total population is above the threshold for collapse, even an initial producer population that is almost entirely wild type will lead to a pure cooperative consortium. The protection against cheaters by the dominating wild type strain demonstrates that there is strength in numbers, and that a competing wild type strain can help prevent total population collapse and encourage the emergence of cooperation.

Lastly, we provide an example for the active transport model. For the mass balance equation model with active transport there is only one region of multistability. We choose parameters from region II in 5.1a of $S_{in} = 5.6$ mM and $q = 2\,\frac{\mathrm{L}}{\mathrm{g\cdot h}}$, and observe stable steady states of wild type (WT, green) and cooperators (CO, blue). A main difference between the passive and active models is that in the active model, cells only export excess metabolite. Thus, cheaters are not able to "steal" resources from wild type or cooperators by depleting the external concentration and forcing producer cells to export. This protects the community from a population collapse. Cheaters still weaken cooperators by consuming the external metabolites that the cooperators need to receive from their producing counterpart. In the case of active transport, the wild type population no longer supports cheaters or cooperators but rather protects themselves by only exporting excess metabolite. As initial cheater population is raised from $X_\emptyset(0) = 0$ (Fig 5.9a) to $X_\emptyset(0) = 0.1$ (Fig 5.9b), and then to $X_\emptyset(0) = 0.25$ (Fig 5.9c), we see that the range of initial populations leading to cooperation decreases and is replaced by initial populations that result in the wild type strain winning the competition.

The third row of Fig 5.9 displays the information from Fig 5.9a-c in the form of the proportion of wild type population out of the total producer population. These diagrams reinforce the finding that an increased initial cheater concentration lessens

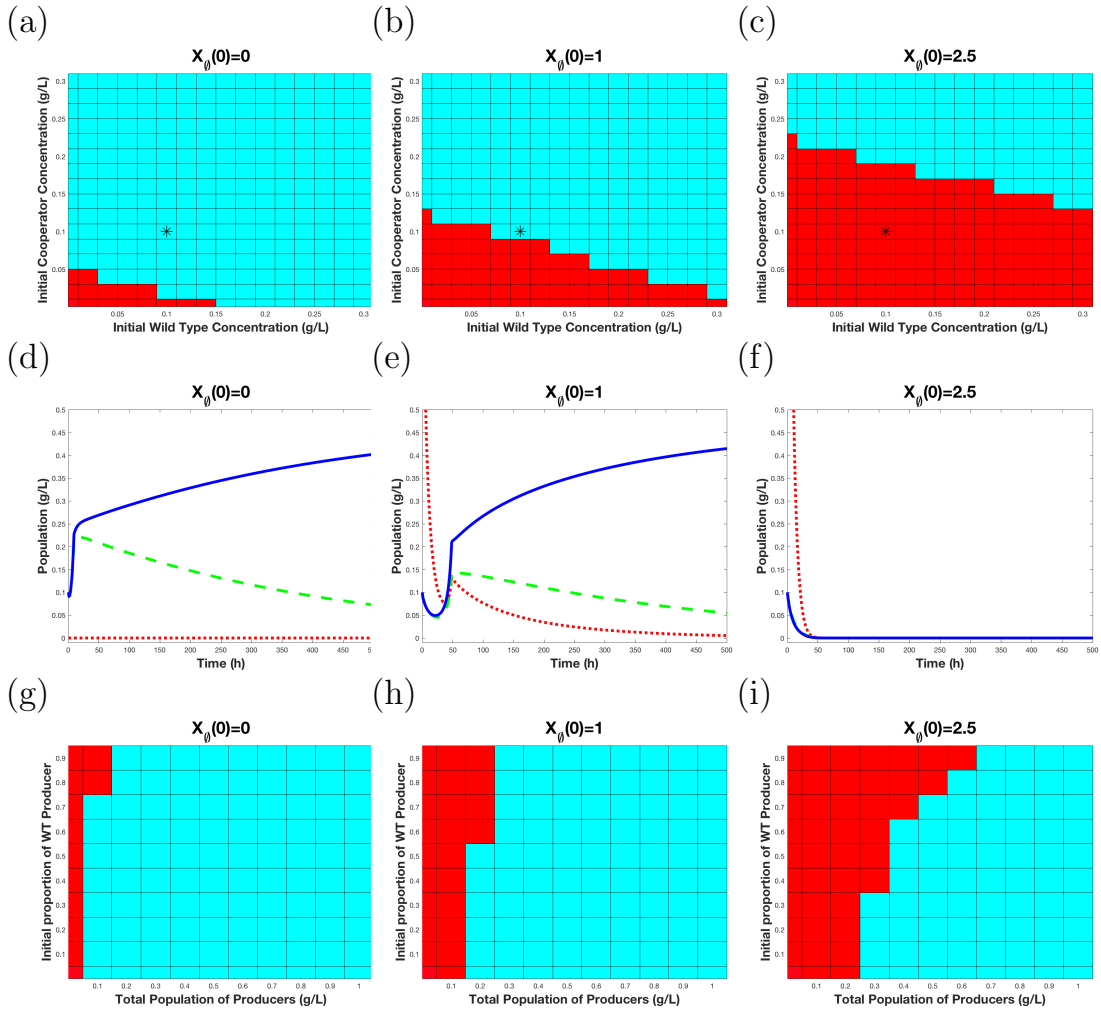

Figure 5.8: **Effect of Cheaters on Bistability Basins of Attraction for Passive Transport Model.** Blue (red) denotes the range of initial conditions that converge to CO (D) steady state. Parameters were selected for passive transport model from bistability region IV in Fig 5.1b with $S_{in} = 8$ mM, $q = 10 \frac{\text{L}}{\text{g·h}}$ and cheater population set at (a) $X_\emptyset(0) = 0$, (b)$X_\emptyset(0) = 1$, and (c) $X_\emptyset(0) = 2.5$. Non-cooperative regions of collapse expand as initial cheater population is increased. Solution curves corresponding to the marked initial populations in (a)-(c) are plotted beneath their corresponding basin of attraction diagram, (d)-(f) for cooperator population (solid, blue) and cheater population (dotted, red). Note that as the basin for population collapse increases, there is an delay in reaching steady state for the cooperator population solution curve in (e). Total producer population and the proportion of which is wild type are shown in (g)-(i) with competition outcome at steady state colored as in (a)-(c).

the chance of cooperation. When cheaters are present, the cooperator population needs to start as a majority of the producer population in order to outcompete the cooperators (Fig 5.9g-i).

The overall effect of the cheaters in the mass balance equation model with both passive and active transport is to weaken the cooperators, and to a lesser extent the wild type, to the point where the cooperators are not able to outcompete the wild type strain or there is population collapse. In both passive and active transport models, even though initial cheater populations affect the outcome of the competition, at every steady state the cheater population is zero.

5.3.2 Cheater Effect on Cost Scaled Model

In section 5.2 we see in the results from the cost scaled model for both passive and active transport the addition of coexistence states. Now that cheaters have the possibility of coexisting with wild type or cooperator strains do they still have the same effect of weakening cooperative behavior?

We first investigate by choosing parameters for the active transport model with cost scaling from region III of Fig 5.4 of $S_{in} = 5.6$ mM and $q = 1.3 \frac{\text{L}}{\text{g·h}}$. Similar to what we saw in section 5.3.1, as initial cheater population increases from $X_\emptyset(0) = 0.001$ (Fig 5.10a) to $X_\emptyset(0) = 0.1$ (Fig 5.10b), and then to $X_\emptyset(0) = 0.2$ (Fig 5.10c) the region of initial conditions that converge to pure wild type population at steady state increases.

To see the effect of cheaters illustrated with solution curves we choose an initial concentration marked with a star in Fig 5.10a - c,

$$X_{ab}(0) = 0.04, \quad X_a(0) = 0.07, \quad X_b(0) = 0.07.$$

The solution curves are plotted below their respective basin of attraction diagram with

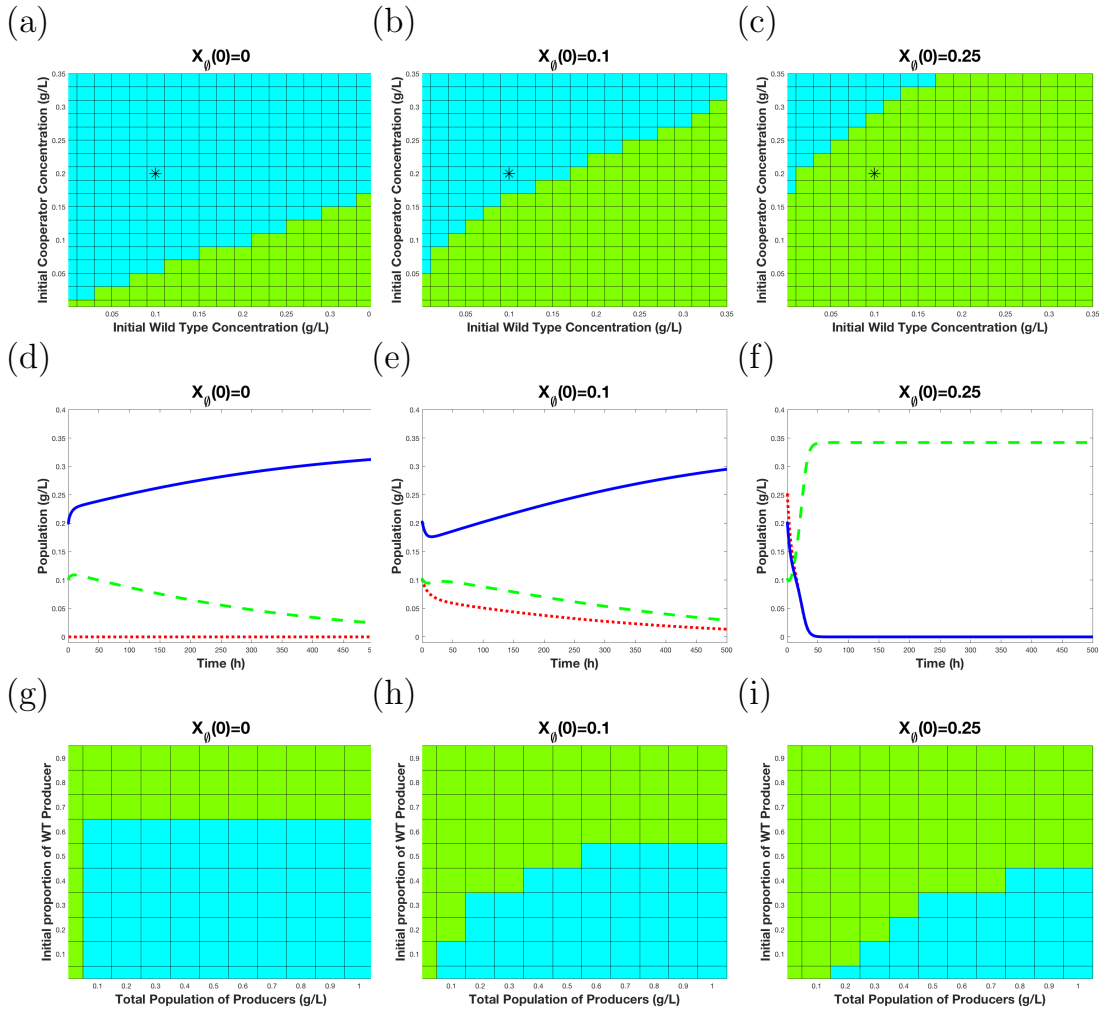

Figure 5.9: **Effect of Cheaters on Bistability Basins of Attraction for Active Transport Model.** Basins of attraction for cooperators (blue) and wild type (green) given increasing levels of initial cheater population. Parameters were selected for active transport model from bistability region II in Fig 5.1a withS_{in} = 5.6 mM and $q = 2\frac{\text{L}}{\text{g}\cdot\text{h}}$ and cheater population set at (a)$X_\emptyset(0) = 0$, (b) $X_\emptyset(0) = 0.1$, and (c) $X_\emptyset(0) = 0.25$. Non-cooperative regions of pure wild type population expand as initial cheater population is increased. Solution curves corresponding to the marked initial populations in (a)-(c) are plotted beneath their corresponding basin of attraction diagram, (d)-(f) for cooperator population (solid, blue) and cheater population (dotted, red). Note that as the basin for population collapse increases, there is an delay in reaching steady state for the cooperator population solution curve in (e). Total producer population and the proportion of which is wild type are shown in (g)-(i) with competition outcome at steady state colored as in (a)-(c).

wild type (dashed, green), cooperators (solid, blue), and cheaters (dotted, red). In Fig 5.10d, we observe that even with initially very few cheaters, the cooperators are able to outcompete the wild type and the cheater population grows to a stable coexistence state with the cooperators. For an increased initial cheater population (Fig 5.10e) the cooperators are somewhat weaken and the wild type population initially increase, though they are ultimately outcompeted by the cooperator and cheater populations. Finally, for high initial cheater population (Fig 5.10f) the cooperators are weakened to the point where wild type is able to dominate leading to a pure wild type population steady state.

To investigate the effect of the initial cheater population in the passive transport model with cost scaling we consider parameters from region V in Fig 5.5 of $S_{in} = 5.6$ mM and $q = 30\,\frac{\mathrm{L}}{\mathrm{g{\cdot}h}}$. Not surprisingly, when initial cheater population increases from $X_\emptyset(0) = 0$ (Fig 5.11a) to $X_\emptyset(0) = 0.2$ (Fig 5.11b) and to $X_\emptyset(0) = 0.4$ (Fig 5.11c), the range of initial conditions leading to population collapse increases. The behavior seen in Fig 5.11 is reminiscent of Fig 5.8 though in this case there is coexistence between wild type and cooperators and not just pure cooperator steady state.

The two examples provided here give further indication that the presence of an initial cheater population serves to weaken cooperators and lead to non-cooperative states of pure wild type or population collapse. This behavior continues even when there are stable coexistence states and stable states in which the cheater population is not zero. The effect of the cheaters on the cooperator population is clearly visible in comparing the trajectory of the cooperator solution curve (blue,solid) in Fig 5.10d and e and in Fig 5.11d and e. For both of these figures, when there is low cheater population (Fig 5.10d, Fig 5.11d), the cooperator population initially grows before reaching steady state. For the increased cheater population (Fig 5.10e, Fig 5.11e), this initial growth is visibly lessened, indicating that the cooperator strain is weakened by

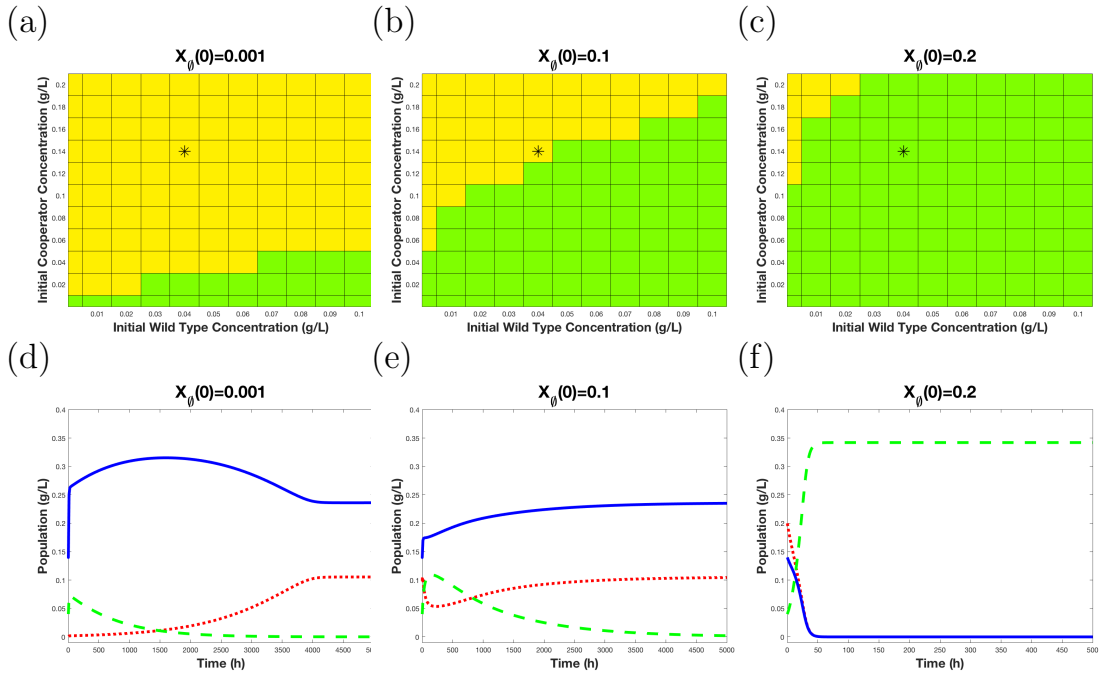

Figure 5.10: **Effect of Cheaters on Bistability Basins of Attraction for Active Transport Model with Cost Scaling.** Basins of attraction for CO/CH (yellow) and wild type (green) given increasing levels of initial cheater population. Parameters were selected for passive transport model with cost scaling from bistability region III in Fig 5.4 with$S_{in} = 5.6$ mM and $q = 1.3\,\frac{\mathrm{L}}{\mathrm{g\cdot h}}$ and cheater population set at (a)$X_\emptyset(0) = 0.001$, (b) $X_\emptyset(0) = 0.1$, and (c) $X_\emptyset(0) = 0.2$. Non-cooperative regions of wild type expand as initial cheater population is increased. Solution curves corresponding to the marked initial populations in (a)-(c) are plotted beneath their corresponding basin of attraction diagram, (d)-(f) for cooperator population (solid, blue), wild type population (dashed, green), and cheater population (dotted, red).

the presence of more cheaters.

5.3.3 Summary of Results

Based on our numerical investigations of our model, we conclude that

1. The outcome of the competition between wild type, A-cooperators, B-cooperators, and cheaters depends on the type and rate of metabolite transport. Active transport allows producers to keep sufficient amount of resources they produce, allowing for survival of the wild type strain for high rates of transport, and less

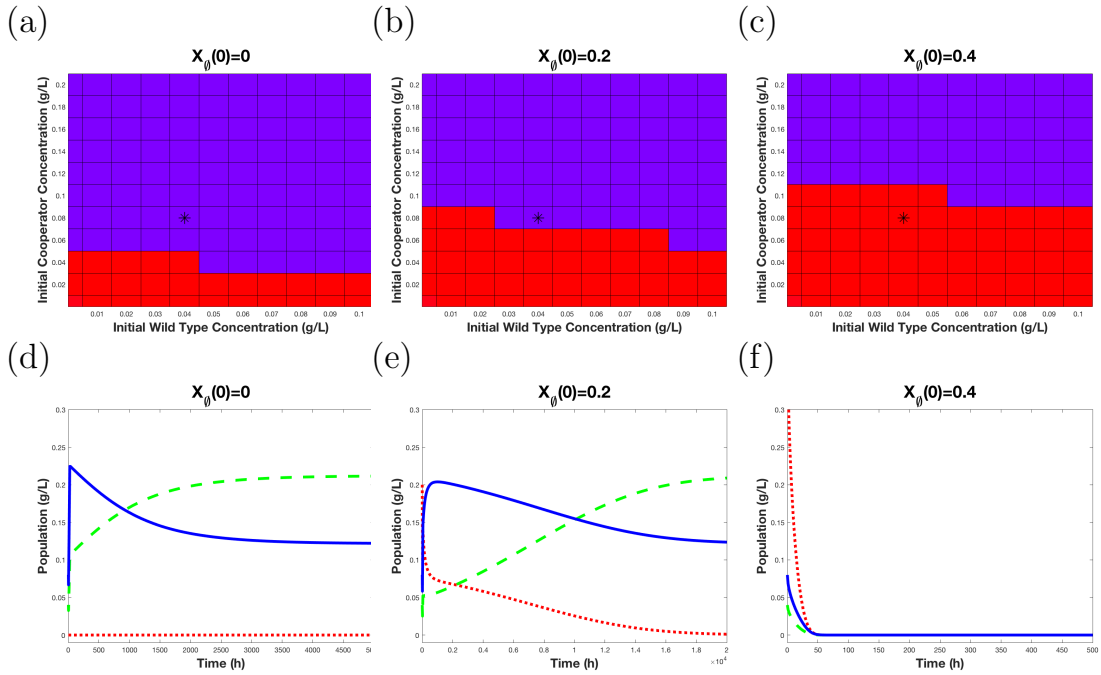

Figure 5.11: **Effect of Cheaters on Bistability Basins of Attraction for Passive Transport Model with Cost Scaling.** Basins of attraction for WT/CO (purple) and population collapse (red) given increasing levels of initial cheater population. Parameters were selected for passive transport model with cost scaling from bistability region V in Fig 5.5 withS_{in} = 5.6 mM and $q = 30\,\frac{\mathrm{L}}{\mathrm{g{\cdot}h}}$ and cheater population set at (a)$X_\emptyset(0) = 0$, (b) $X_\emptyset(0) = 0.2$, and (c) $X_\emptyset(0) = 0.4$. Non-cooperative regions of population collapse expand as initial cheater population is increased. Solution curves corresponding to the marked initial populations in (a)-(c) are plotted beneath their corresponding basin of attraction diagram, (d)-(f) for cooperator population (solid, blue), wild type population (dashed, green), and cheater population (dotted, red).

variety in steady states for different parameter regions. In the passive transport model, collapse of the population is possible at high transport rates.

2. Cost of metabolite production affects the competition. Inclusion of cost into the model makes cheaters more competitive, since they do not incur a production cost. As a result, there are stable equilibria where cheaters coexist with either cooperators, or wild type strains.

3. In all models, cheaters affect the ultimate outcome of the competition, even if they are not able to outcompete other strains. The presence of the cheater strain serves to weaken cooperation. Since cooperators depend on resource exchange through the external environment, the cheaters are able to consume exchanged metabolites without contributing benefit to the system.

CHAPTER SIX

SIMPLIFIED MODEL ANALYSIS

The model detailed in chapter 3, with and without the cost function scaling, contains many nonlinearities. Thus, finding steady states and analyzing their stability is difficult. Numerical analysis of many dynamical behaviors seen in this system can be found in chapter 5, and we now provide analysis of a simplified version of the passive transport model without cost scaling.

6.1 Linearization of Hill Functions

The first step in simplifying the model is done by linearizing all Hill functions. This assumes that the metabolic and chemical processes are not saturated. This assumption allows us to explicitly analyze the behavior of the system when resource consumption is in the linear regime.

For cell with strategy $\gamma \in \{\emptyset, ab, a, b\}$, simplified growth rate function is

$$\mu_\gamma = \mu_{max,\gamma} \frac{A_\gamma}{K_\gamma^A} \frac{B_\gamma}{K_\gamma^B} \frac{S}{K_\gamma^S} =: \mu_m A_\gamma B_\gamma S,$$

and simplified metabolite production rate function is

$$P_\gamma^A = Y_{P,\gamma}^A \frac{S}{K_\gamma^S} =: Y_\gamma^A S.$$

Analogous production functions for metabolite B are simplified similarly.

In addition to linearizing all Hill functions, we impose assumptions A1 - A3 from

section 4.2 and assume symmetric initial conditions,

$$X_a(0) = X_b(0),\ A_a(0) = B_b(0),\ A_b(0) = B_a(0),\ A_{ext}(0) = B_{ext}(0).$$

We impose one more simplifying assumption on this system, that production rates of both A and B for the cheater and the rate of producing B for the A-cooperator are both zero, i.e. $Y_\emptyset^A = Y_b^A = 0$.

The simplified model is a system of nine ordinary differential equations.

$$\frac{dX_\emptyset}{dt} = (\mu_\emptyset - d)X_\emptyset \tag{6.1}$$

$$\frac{dX_{ab}}{dt} = (\mu_{ab} - d)X_{ab} \tag{6.2}$$

$$\frac{dX_a}{dt} = (\mu_a - d)X_a \tag{6.3}$$

$$\frac{dA_{ext}}{dt} = -JA_{ext} + (T_\emptyset^A X_\emptyset + T_{ab}^A X_{ab} + (T_a^A + T_b^A)X_a) \tag{6.4}$$

$$\frac{dA_\emptyset}{dt} = \beta(-Y_D^A \mu_\emptyset - T_\emptyset^A) - (\mu_\emptyset - d)A_\emptyset \tag{6.5}$$

$$\frac{dA_{ab}}{dt} = \beta(Y_{ab}^A S - Y_D^A \mu_{ab} - T_{ab}^A) - (\mu_{ab} - d)A_{ab} \tag{6.6}$$

$$\frac{dA_a}{dt} = \beta(Y_a^A S - Y_D^A \mu_a - T_a^A) - (\mu_a - d)A_a \tag{6.7}$$

$$\frac{dA_b}{dt} = \beta(-Y_D^A \mu_a - T_b^A) - (\mu_a - d)A_b \tag{6.8}$$

$$\begin{aligned}\frac{dS}{dt} &= J(S_{in} - S) - \frac{2}{Y_{A/S}} S(Y_\emptyset^A X_\emptyset + Y_{ab}^A X_{ab} + (Y_a^A + Y_b^A)X_a) \\ &\quad - \frac{1}{Y_{X/S}}(\mu_\emptyset X_\emptyset + \mu_{ab} X_{ab} + 2\mu_a X_a)\end{aligned} \tag{6.9}$$

where

$$\mu_{\emptyset} = \mu_m A_{\emptyset}^2 S$$

$$\mu_{ab} = \mu_m A_{ab}^2 S$$

$$\mu_a = \mu_m A_a A_b S$$

$$T_{\emptyset}^A = q(A_{\emptyset} - A_{ext})$$

$$T_{ab}^A = q(A_{ab} - A_{ext})$$

$$T_a^A = q(A_a - A_{ext})$$

$$T_b^A = q(A_b - A_{ext}).$$

6.2 Steady State Solutions

We solve the above system at steady state and use the eigenvalues of the associated Jacobian to analyze the behavior of the simplified system. There are seven possible steady states for this simplified passive transport model:

1. D: population collapse: $X_{ab} = 0$, $X_{\emptyset} = 0$, $X_a = 0$.
2. WT: pure wild type population, $X_{ab} > 0$, $X_{\emptyset} = 0$, $X_a = 0$.
3. CO: pure cooperator consortium: $X_{ab} = 0$, $X_{\emptyset} = 0$, $X_a > 0$.
4. WT/CH: coexistence of wild type and cheaters: $X_{ab} > 0$, $X_{\emptyset} > 0$, $X_a = 0$.
5. WT/CO: coexistence of wild type and cooperators: $X_{ab} > 0$, $X_{\emptyset} = 0$, $X_a > 0$.
6. CH/CO: coexistence of cheaters and cooperators: $X_{ab} = 0$, $X_{\emptyset} > 0$, $X_a > 0$.
7. WT/CH/CO: coexistence of all phenotypes: $X_{ab} > 0$, $X_{\emptyset} > 0$, $X_a > 0$.

Steady state from equations (6.1) - (6.9) is given as:

$$0 = (\mu_\emptyset - d)X_\emptyset \tag{6.10}$$

$$0 = (\mu_{ab} - d)X_{ab} \tag{6.11}$$

$$0 = (\mu_a - d)X_a \tag{6.12}$$

$$0 = -JA_{ext} + (T^A_\emptyset X_\emptyset + T^A_{ab}X_{ab} + (T^A_a + T^A_b)X_a) \tag{6.13}$$

$$0 = \beta(-Y^A_D\mu_\emptyset - T^A_\emptyset) - (\mu_\emptyset - d)A_\emptyset \tag{6.14}$$

$$0 = \beta(Y^A_{ab}S - Y^A_D\mu_{ab} - T^A_{ab}) - (\mu_{ab} - d)A_{ab} \tag{6.15}$$

$$0 = \beta(Y^A_a S - Y^A_D\mu_a - T^A_a) - (\mu_a - d)A_a \tag{6.16}$$

$$0 = \beta(-Y^A_D\mu_a - T^A_b) - (\mu_a - d)A_b \tag{6.17}$$

$$0 = J(S_{in} - S) - \frac{2}{Y_{A/S}}S(Y^A_\emptyset X_\emptyset + Y^A_{ab}X_{ab} + (Y^A_a + Y^A_b)X_a) \tag{6.18}$$
$$- \frac{1}{Y_{X/S}}(\mu_\emptyset X_\emptyset + \mu_{ab}X_{ab} + 2\mu_a X_a).$$

We note that when a population is assumed to be zero, i.e. $X_\gamma = 0$ for some $\gamma \in \{\emptyset, ab, a\}$, the corresponding internal concentration equation is no longer relevant.

Theorem 2. *For a generic set of parameters, there are no coexistence steady states, WT/CH, WT/CO, CH/CO, WT/CH/CO, in the simplified passive transport model.*

Proof. We consider two cases:

1. *Wild type and cheater coexistence (WT/CH):* If we have positive wild type and cheater populations, i.e. $X_\emptyset > 0, X_{ab} > 0$, then from equations (6.10) and (6.11) we have that $\mu_\emptyset = \mu_{ab} = d$. In terms of our simplified growth functions this is

$$\mu_m A^2_\emptyset S = \mu_m A^2_{ab} S = d, \tag{6.19}$$

which implies

$$A_{\emptyset} = A_{ab}.$$

Since passive transport is a function of these equal internal concentrations and the external resource is shared by all strains, the transport rates by wild type and cheaters will be equal,

$$T^A_{\emptyset} = T^A_{ab}. \tag{6.20}$$

With $\mu_{\emptyset} = \mu_{ab} = d$, equations (6.14) and (6.15) simplify to

$$\begin{aligned} 0 &= -Y^A_D d - T^A_{\emptyset} \\ 0 &= Y^A_{ab} S - Y^A_D d - T^A_{ab}, \end{aligned}$$

When coupled with (6.20), this implies

$$Y^A_{ab} S - Y^A_D d = -Y^A_D d.$$

This can only be true if either $Y^A_{ab} = 0$ or $S = 0$. The production rate for the wild type strain, Y^A_{ab}, is positive. Thus $S = 0$. Since the decay rate, d, of the population is positive and internal concentrations must be greater than or equal to zero, $\mu_m A^2_{ab} S = d$ from (6.19) implies that $S \neq 0$, and we have a contradiction. Therefore, neither WT/CH nor WT/CH/CO steady states exist for the simplified passive transport model.

2. *Coexistence of either wild type or cheater population with cooperators:* We assume that we have positive cooperator population, i.e. $X_a > 0$, and show that neither wild type nor cheater populations can be positive at the same time. Assume first that the wild type population is also positive, $X_{ab} > 0$.

Equations (6.11) and (6.12) then give $\mu_{ab} = \mu_a = d$, or

$$\mu_m A_{ab}^2 S = \mu_m A_a A_b S = d.$$

This implies $S > 0$ and by cancellation,

$$A_{ab}^2 = A_a A_b > 0.$$

From equation (6.15) we find

$$A_{ext} = \frac{1}{q}(Y_D^A d - Y_{ab}^A S + q A_{ab}). \tag{6.21}$$

Equations (6.16) and (6.17) give

$$A_a = \frac{1}{q}(Y_a^A S - Y_D^A d + q A_{ext})$$
$$A_b = \frac{1}{q}(q A_{ext} - Y_D^A d),$$

into which we can substitute the result in equation (6.21) to find

$$A_a = \frac{1}{q}(Y_a^A S - Y_{ab}^A S + q A_{ab})$$
$$A_b = \frac{1}{q}(q A_{ab} - Y_{ab}^A S).$$

When we substitute this result into $A_{ab}^2 = A_a A_b$ we get

$$\begin{aligned} A_{ab}^2 &= \frac{1}{q^2}(Y_a^A S - Y_{ab}^A S + qA_{ab})(qA_{ab} - Y_{ab}^A S) \\ &= \frac{1}{q^2}(qY_a^A S A_{ab} - Y_a^A Y_{ab}^A S^2 - qY_{ab}^A S A_{ab} + (Y_{ab}^A S)^2 + (qA_{ab})^2 - qY_{ab}^A S A_{ab}) \\ &= \frac{1}{q^2}((qA_{ab})^2 + qY_a^A S A_{ab} - qY_{ab}^A S A_{ab} - qY_{ab}^A S A_{ab} - Y_a^A Y_{ab}^A S^2 + (Y_{ab}^A S)^2) \\ &= A_{ab}^2 + \frac{1}{q}(Y_a^A - 2Y_{ab}^A) S A_{ab} + \frac{Y_{ab}^A}{q^2}(-Y_a^A + Y_{ab}^A) S^2. \end{aligned}$$

Since $S > 0$ and $A_{ab} > 0$, in order for this to be true both

$$\begin{aligned} Y_a^A &= 2Y_{ab}^A \\ Y_a^A &= Y_{ab}^A. \end{aligned}$$

This in turn, is only true if $Y_a^A = Y_{ab}^A = 0$, which contradicts the fact that producers have positive production rates, $Y_a^A > 0, Y_{ab}^A > 0$. Thus, wild type cannot coexist with cooperators. The proof is similar if we assume that the cheater population is positive. Therefore, neither WT/CO nor CH/CO steady states exist for the simplified passive transport model.

Comparing these two cases with the list of potential equilibria we se that the only possible steady states for the simplified passive transport system are WT, CO, or D. This finishes the proof of the theorem.

□

We now provide either an explicit solution or a procedure for explicitly solving for each of the equilibria WT, CO and D.

Theorem 3. *In the simplified passive transport system, at steady state D of population collapse for all $\gamma \in \{\emptyset, ab, a\}$, we have*

$$X_\gamma = 0, \quad A_{ext} = 0, \quad \text{and } S = S_{in}.$$

Internal concentrations, A_γ, $\gamma \in \emptyset, ab, a, b$ are the nonnegative roots of equations (6.14) through (6.17) respectively.

Proof. Equations (6.10) - (6.12) are satisfied by $X_\gamma = 0$. External concentration $A_{ext} = 0$ satisfies equation (6.13) when all populations are zero. Internal concentration of metabolite is not applicable when the population is zero and thus, equations (6.14) - (6.17) are not relevant to our system at steady state D. Initial conditions near D that converge to population collapse will have a population whose internal concentrations converge to nonnegative roots of equations (6.14) - (6.17) . We find S as stated in the theorem from equation (6.18). □

6.2.1 Wild Type (WT) Steady State

The wild type steady, WT, with pure wild type population is found using the procedure outlined below. We first find each variable in terms of A_{ab}. We then construct a function of A_{ab} whose roots can be used to find the values of the steady state solutions. Solutions are not guaranteed to exist or be unique, depending on the values chosen for the parameters. Here is the outline of the solution procedure:

1. If we assume $X_{ab} > 0, X_\emptyset = 0$, and $X_a = 0$ equations (6.10) and (6.12) are satisfied and equation (6.11) gives $\mu_{ab} = d$ which can be solved for $S = f_1(A_{ab})$.

2. Equation (6.18) is solved for $X_{ab} = f_2(S)$.

3. Equation (6.15) is solved for $A_{ext} = f_3(A_{ab}, S)$.

4. Functions f_1, f_2 and f_3 are then all substituted into equation (6.13) to give $f_4(A_{ab}) = 0$, which can then be solved for A_{ab}. The solution to this equation is the root of a fifth order polynomial. Thus, there is no guarantee of a positive root or uniqueness.

6.2.2 Cooperator (CO) Steady State

The procedure for solving for cooperator steady state, CO, of pure cooperator consortia is more complicated because the A-cooperator does not have equal production rates of A and B like the wild type strain under symmetry assumptions. Thus, the internal concentration of A in the A-cooperator cell, A_a, will be different than the internal concentration of B in the A-cooperator cell, A_b; whereas, for the wild type strain under our symmetry assumptions, the two internal concentrations are equal. Here is the outline of the solution procedure:

1. We assume $X_a > 0$, $X_\emptyset = 0$, and $X_{ab} = 0$. Then equations (6.10) and (6.11) are satisfied and equation (6.12) gives $\mu_a = d$ which can be solved for $S = f_1(A_a, A_b)$.

2. Equation (6.18) is solved for $X_a = f_2(S)$.

3. Equation (6.17) is solved for $A_{ext} = f_3(A_b)$.

4. Equation (6.16) with $f_1(A_a, A_b)$ and $f_3(A_b)$ substituted in for S and A_{ext}, is a quadratic equation in A_a. We solve it for $A_a = f_{4+}(A_b)$, and $A_a = f_{4-}(A_b)$.

   Lemma 4. *Function $A_a = f_{4+}(A_b)$ is the only positive solution of equation (6.16) with $f_1(A_a, A_b)$ and $f_3(A_b)$ substituted in for S and A_{ext}, respectively.*

Proof. Equation (6.16) when $\mu_a = d$, as is the case in steady state CO, is given by

$$0 = Y_a^A S - Y_D^A d - q(A_a - A_{ext}).$$

When $f_1(A_a, A_b)$ is substituted in for S this gives

$$0 = Y_a^A \frac{d}{\mu_m A_a A_b} - Y_D^A d - q(A_a - A_{ext}),$$

which we rearrange to find

$$0 = Y_a^A d - Y_D^A d \mu_m A_a A_b - q(A_a - A_{ext})\mu_m A_a A_b.$$

This is quadratic in A_a with leading coefficient

$$-q\mu_m A_b < 0.$$

which is negative since parameters q and μ_m are assumed to be positive and A_b is a positive concentration at steady state CO. The constant term,

$$Y_a^A d > 0,$$

is positive because both production rate and decay rate are positive parameters. Thus, we are guaranteed to have only one positive real value for A_a given by

$$A_a = \frac{\mu_m A_b(q f_3(A_b) - Y_D^A d) + \sqrt{(\mu_m A_b(q f_3(A_b) - Y_D^A d))^2 + 4(q\mu_m A_b)(Y_a^A d)}}{2(q\mu_m A_b)}$$

which we will denote as $A_a = f_{4+}(A_b)$. □

5. Functions f_1, f_2, f_3 and f_{4+} are all substituted into equation (6.13) to give

$f_5(A_b) = 0$, which is solved for A_b. There is no guarantee of the existence or uniqueness of a positive solution. If a positive solution for A_b exists, then the procedure yields a steady state CO.

6.2.3 Numerical Evaluations of Steady States

Using Mathematica we apply the solving procedures listed above with our chosen parameters from section 4.3. The values of q and S_{in} are used as a parameter. We find implicit function $f_4(A_{ab}, q) = 0$ for WT and $f_5(A_b, q) = 0$ for CO for different values of S_{in}. In Fig 6.1 we plot $f_4(A_{ab}, q) = 0$ for various values of S_{in}. The value for A_{ab} seen in these graphs for various values of q and S_{in} can then be substituted into functions f_1, f_2, and f_3 to give the complete steady state solution WT. Positive solutions for A_{ab} are not guaranteed to exist or be unique, and if a solution does exist, there is no guarantee that f_1, f_2, and f_3 will yield positive values for other variables.

In Fig 6.2 we plot $f_5(A_b, q) = 0$ for various values of S_{in}. The value for A_{ab} seen in these graphs for various values of q and S_{in} can then be substituted into functions $f_1, f_2,, f_3$, and f_{4+} to give the complete steady state solution CO. Positive solutions for A_b are not guaranteed to exist or be unique, and if a solution does exist, there is no guarantee that $f_1, f_2,, f_3$, and f_{4+} will yield positive values for other variables.

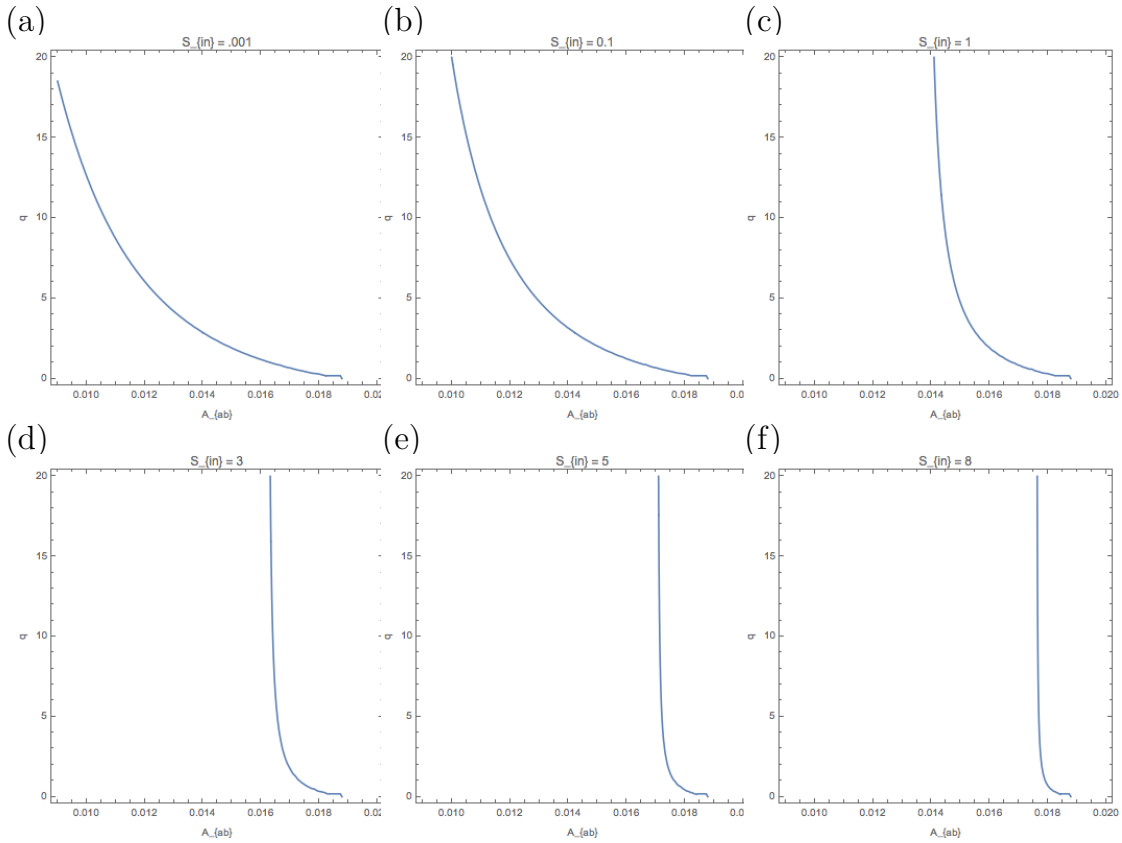

Figure 6.1: **WT: q vs. $\mathbf{A_{ab}}$** Graphs of $f_4(A_{ab}, q) = 0$ resulting from the solving proceedure for steady state WT. Graphs shown for $S_{in} = 0.001$ mM (a),$S_{in} = 0.1$ mM (b),$S_{in} = 1$ mM (c),$S_{in} = 3$ mM (d),$S_{in} = 5$ mM (e), and $S_{in} = 8$ mM (f). Solving for A_{ab} when q is fixed allows us to find all other variables by substitution. Positive solutions for other variables not guaranteed, and existing biologically relevant solutions for WT may not be stable.

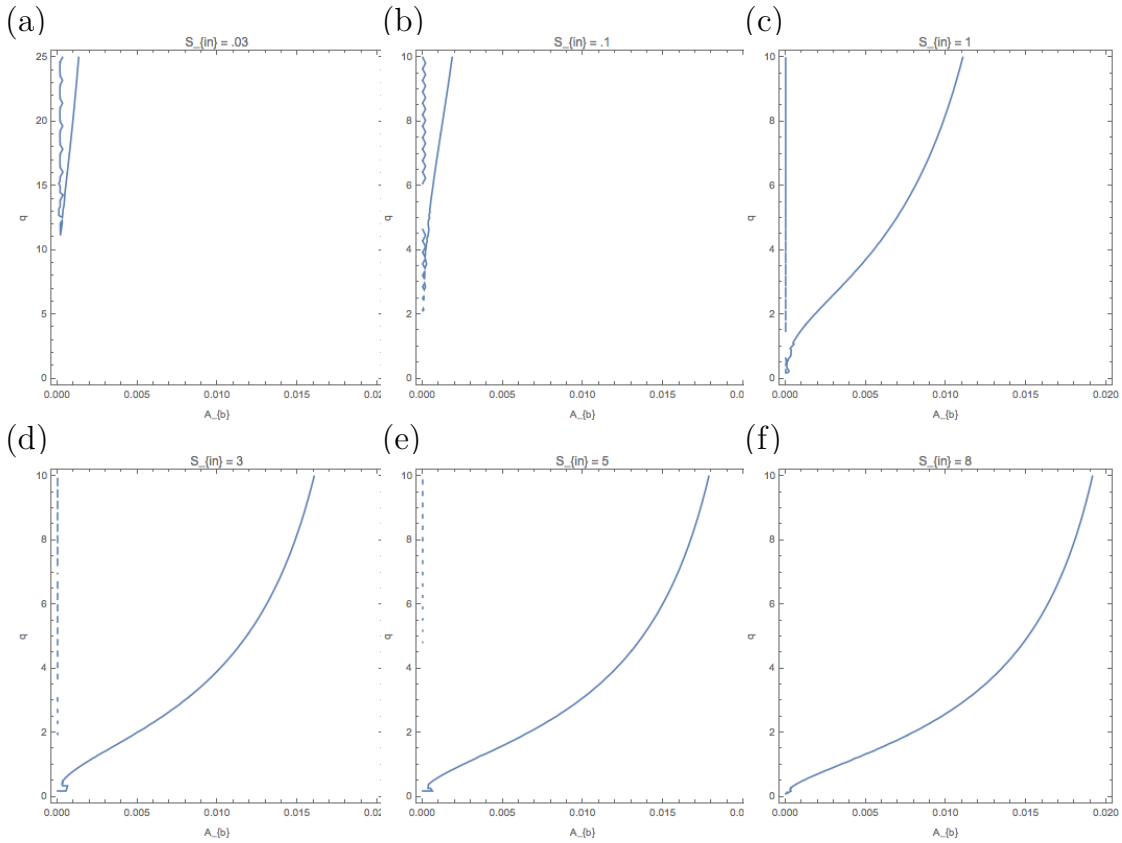

Figure 6.2: **CO: q vs. $\mathbf{A_b}$** Graphs of $f_5(A_b, q) = 0$ resulting from the solving procedure for steady state CO. Graphs shown for $S_{in} = 0.03$ mM (a),$S_{in} = 0.1$ mM (b),$S_{in} = 1$ mM (c),$S_{in} = 3$ mM (d),$S_{in} = 5$ mM (e), and $S_{in} = 8$ mM (f). Solving for A_b when q is fixed allows us to find all other variables by substitution. Positive solutions for other variables not guaranteed, and existing biologically relevant solutions for CO may not be stable.

6.3 Stability of Steady State Solutions

The Jacobian of the simplified passive transport system is shown in Fig 6.3. We use Mathematica to find the eigenvalues of the Jacobian evaluated at each steady state. When the real parts of all eigenvalues are negative, the steady state is stable. If any of the nine eigenvalues have positive real part the state is unstable.

We then compare the stability of steady states of the simplified model to the nonlinear passive transport model. We do not expect an exact match of behavior at the same parameter values, so we examine the qualitative behavior of the system for various q and S_{in} values. The results are summarized in Tables 6.1 and 6.2.

We first discuss qualitative similarities between the stable steady states of the simplified and nonlinear passive transport model. In both models, we see that for low transport rate only the WT state is stable. When substrate input concentration, S_{in}, is above 1 mM we have, for high transport rates, the pure cooperator state CO is stable. Intermediate levels of transport rate lead to bistability between WT and CO. The final steady state is determined by the initial conditions.

When substrate input levels are low and transport levels are moderate or high, both models have population collapse as the only stable steady state.

While the general qualitative trends are very similar between the simplified and nonlinear models, there are some important differences as well. One key difference is the lack of stability of state D in the simplified model for moderate to high substrate concentrations and transport levels. For the nonlinear model, we observe in section 5.1.2 that D is stable for moderate and high transport levels no matter the substrate input concentration.

To linearize our system near state D we consider the Jacobian from Fig 6.3 evaluated at state D (Fig 6.4). In order for D to be a stable steady state, the growth

rate must be smaller than parameter d for all strains γ. For moderate and high substrate concentrations, saturation of substrate in both growth and the metabolite production functions provides an upper bound for the growth function given in 3.1:

$$\mu_\gamma = \mu_{max,\gamma} \frac{A_\gamma}{K_\gamma^A + A_\gamma} \frac{B_\gamma}{K_\gamma^B + B_\gamma} \frac{S}{K_\gamma^S + S}. \tag{6.22}$$

When the cells reach saturation levels in S this function is bounded above by

$$\mu_\gamma = \mu_{max,\gamma} \frac{A_\gamma}{K_\gamma^A + A_\gamma} \frac{B_\gamma}{K_\gamma^B + B_\gamma}. \tag{6.23}$$

Thus, when the internal concentrations of A and B for each strain γ are low the growth rate becomes smaller than decay rate d and the population will collapse. For the nonlinear passive transport model, any time the transport coefficient is above $q = 1.591 \frac{\text{L}}{\text{g·h}}$, an initial condition near state D will converge to D (section 5.1, Fig 5.1b regions III-VI).

In contrast to this behavior, the simplified growth rate is given by

$$\mu_\gamma = \mu_m A_\gamma B_\gamma S.$$

Since this function is not bounded in any of the variables, if A and B are small, a high concentrations of substrate S can compensate for low A and B, allowing the growth rate to stay above the decay rate d. In such a case the population will not collapse. Thus, for the linearized system a substrate input concentration S_{in} above a minimum threshold prevents steady state D from being stable.

S_{in} mM	$q\ \frac{\text{L}}{\text{g·h}}$				
	0.001	1	3	5	10
8	WT	WT	WT,CO	CO	CO
5	WT	WT	WT,CO	WT,CO	CO
3	WT	WT	WT,CO	WT,CO	CO
1	WT	WT	WT	WT,CO	CO
0.1	WT	WT	WT	WT	WT
0.001	WT	WT	WT	D	D

Table 6.1: **Stability of steady states - Simplified model** Summary of stable steady states for simplified passive transport model. State WT is the only stable state for low transport, $q = 0.001\ \frac{\text{L}}{\text{g·h}}$ and $q = 1\ \frac{\text{L}}{\text{g·h}}$. Bistability occurs for moderate transport, $q = 3\ \frac{\text{L}}{\text{g·h}}$ and $q = 5\ \frac{\text{L}}{\text{g·h}}$, and moderate to high substrate input concentration, $S > 1$. At high transport $q > 5$, for $S > 1$ there is monostability of cooperator state CO, and for low substrate concentration, $S < 0.1$, population collapse D.

S_{in} mM	$q\ \frac{\text{L}}{\text{g·h}}$				
	0.001	1	3	5	10
8	WT	WT	WT,CO,D	CO,D	CO,D
5	WT	WT	WT,CO,D	CO,D	CO,D
3	WT	WT	WT,CO,D	WT,CO,D	CO,D
1	WT	WT	WT,D	WT,CO,D	CO,D
0.1	WT	WT	D	D	D
.001	WT	WT	D	D	D

Table 6.2: **Stability of steady states - Nonlinear model** Summary showing stable steady states for nonlinear passive transport model. State WT is the only stable state for low transport, $q = 0.001\ \frac{\text{L}}{\text{g·h}}$ and $q = 1\ \frac{\text{L}}{\text{g·h}}$. Bistability occurs for transport, $q > 1$, and moderate to high substrate input concentration, $S > 1$. At high transport $q > 5$, for $S > 1$ there is bistability of cooperator state CO and population collapse D, and for low substrate concentration, $S < 1$, population collapse D.

$$
\begin{pmatrix}
\mu_{ab}-d & 0 & 0 & 0 & \cdots \\
0 & \mu_{\emptyset}-d & 0 & 0 & \cdots \\
0 & 0 & \mu_a-d & 0 & \cdots \\
(A_{ab}-A_{ext})q & (A_{\emptyset}-A_{ext})q & (A_a-A_{ext})q+(A_b-A_{ext})q & -J-qX_{\emptyset}-2qX_a-qX_{ab} & \cdots \\
0 & 0 & 0 & \beta q & \cdots \\
0 & 0 & 0 & \beta q & \cdots \\
0 & 0 & 0 & \beta q & \cdots \\
0 & 0 & 0 & \beta q & \cdots \\
-\frac{\mu_{ab}}{Y_{X/S}}-\frac{2SY_{ab}^A}{Y_{A/S}} & -\frac{\mu_{\emptyset}}{Y_{X/S}}-\frac{2S}{Y_{A/S}} & -\frac{2Y_a^AS}{Y_{A/S}}-\frac{2\mu_a}{Y_{X/S}} & 0 & \cdots
\end{pmatrix}
$$

$$
\begin{pmatrix}
\cdots & 2A_{ab}\mu_m SX_{ab} & 0 & 0 & \cdots \\
\cdots & 0 & 2A_{\emptyset}\mu_m SX_{\emptyset} & 0 & \cdots \\
\cdots & 0 & 0 & A_b\mu_m SX_a & \cdots \\
\cdots & qX_{ab} & qX_{\emptyset} & qX_a & \cdots \\
\cdots & -3\mu_{ab}+d+\beta(-q-2A_{ab}\mu_m SY_D^A) & 0 & 0 & \cdots \\
\cdots & 0 & -3\mu_{\emptyset}+d+\beta(-q-2A_{\emptyset}\mu_m SY_D^A) & 0 & \cdots \\
\cdots & 0 & 0 & d-2\mu_a+\beta(-q-A_b\mu_m SY_D^A) & \cdots \\
\cdots & 0 & 0 & -\beta\mu_m SY_D^AA_b-A_b^2\mu_m S & \cdots \\
\cdots & -\frac{2A_{ab}\mu_m SX_{ab}}{Y_{X/S}} & -\frac{2A_{\emptyset}\mu_m SX_{\emptyset}}{Y_{X/S}} & -\frac{2A_b\mu_m SX_a}{Y_{X/S}} & \cdots
\end{pmatrix}
$$

$$
\begin{pmatrix}
\cdots & 0 & A_{ab}^2\mu_m X_{ab} \\
\cdots & 0 & A_{\emptyset}^2\mu_m X_{\emptyset} \\
\cdots & A_a\mu_m SX_a & A_aA_b\mu_m X_a \\
\cdots & qX_a & 0 \\
\cdots & 0 & \beta\left(Y_{ab}^A-A_{ab}^2\mu_m Y_D^A\right)-A_{ab}^3\mu_m \\
\cdots & 0 & \beta\left(-A_{\emptyset}^2\mu_m Y_D^A\right)-A_{\emptyset}^3\mu_m \\
\cdots & -\beta\mu_m SY_D^AA_a-A_a^2\mu_m S & \beta(Y_a^A-A_aA_b\mu_m Y_D^A)-A_a^2A_b\mu_m \\
\cdots & d-2\mu_a+\beta(-q-A_a\mu_m SY_D^A) & \beta(-A_aA_b\mu_m Y_D^A)-A_aA_b^2\mu_m \\
\cdots & -\frac{2A_a\mu_m SX_a}{Y_{X/S}} & -J-\frac{2(X_{\emptyset}+X_aY_a^A+X_a+X_{ab}Y_{ab}^A)}{Y_{A/S}}-\frac{\mu_mX_{\emptyset}A_{\emptyset}^2+2A_aA_b\mu_mX_a+A_{ab}^2\mu_mX_{ab}}{Y_{X/S}}
\end{pmatrix}
$$

Figure 6.3: **Jacobian Matrix for Simplified Passive Model** Jacobian matrix for the simplified passive transport model. Eigenvalues of the Jacobian evaluated at each steady state are used to determine stability of the steady state.

$$
\begin{pmatrix}
\mu_{ab}-d & 0 & 0 & 0 & 0 & 0 \\
0 & \mu_{\emptyset}-d & 0 & 0 & 0 & 0 \\
0 & 0 & \mu_a-d & 0 & 0 & 0 \\
A_{ab}q & A_{\emptyset}q & A_aq+A_bq & -J & 0 & 0 \\
0 & 0 & 0 & \beta q & -3\mu_{ab}+d+\beta(-q-2A_{ab}\mu_m S_{in}Y_D^A) & 0 \\
0 & 0 & 0 & \beta q & 0 & -3\mu_{\emptyset}+d+\beta(-q-2A_{\emptyset}\mu_m S_{in}Y_D^A) \\
0 & 0 & 0 & \beta q & 0 & 0 \\
0 & 0 & 0 & \beta q & 0 & 0 \\
-\frac{\mu_{ab}}{Y_{X/S}}-\frac{2S_{in}Y_{ab}^A}{Y_{A/S}} & -\frac{\mu_{\emptyset}}{Y_{X/S}}-\frac{2S_{in}}{Y_{A/S}} & -\frac{2Y_a^AS_{in}}{Y_{A/S}}-\frac{2\mu_a}{Y_{X/S}} & 0 & 0 & 0
\end{pmatrix}
$$

$$
\begin{pmatrix}
\cdots & 0 & 0 & 0 \\
\cdots & 0 & 0 & 0 \\
\cdots & 0 & 0 & 0 \\
\cdots & 0 & 0 & 0 \\
\cdots & 0 & 0 & \beta\left(Y_{ab}^A-A_{ab}^2\mu_mY_D^A\right)-A_{ab}^3\mu_m \\
\cdots & 0 & 0 & \beta\left(-A_{\emptyset}^2\mu_mY_D^A\right)-A_{\emptyset}^3\mu_m \\
\cdots & d-2\mu_a+\beta(-q-A_b\mu_mS_{in}Y_D^A & -\beta\mu_mSY_D^AA_a-A_a^2\mu_mS & \beta(Y_a^A-A_aA_b\mu_mY_D^A)-A_a^2A_b\mu_m \\
\cdots & -\beta\mu_mS_{in}Y_D^AA_b-A_b^2\mu_mS_{in} & d-2\mu_a+\beta(-q-A_a\mu_mSY_D^A) & \beta(-A_aA_b\mu_mY_D^A)-A_aA_b^2\mu_m \\
\cdots & 0 & 0 & -J
\end{pmatrix}
$$

Figure 6.4: **Jacobian Matrix for Simplified Passive Model at D** Jacobian matrix for the simplified passive transport model evaluated at steady state D.

REFERENCES CITED

[1] Mathematica 11.0, 2016.

[2] M. Archetti and I. Scheuring. Trading public goods stabilizes interspecific mutualism. *Journal of Theoretical Biology*, 318:58 – 67, 2013.

[3] A. Beck and R. Carlson. Synthetic consortia engineered for push and pull dynamics show conditional optimality over metabolic generalist. *In prep.*

[4] A. Beck and R. Carlson. Unpublished data.

[5] A. Beck, K. Hunt, H. Bernstein, and R. Carlson. Chapter 15 - interpreting and designing microbial communities for bioprocess applications, from components to interactions to emergent properties. In C. A. Eckert and C. T. Trinh, editors, *Biotechnology for Biofuel Production and Optimization*, pages 407 – 432. Elsevier, Amsterdam, 2016.

[6] A. Beck, K. Pintar, D. Schepens, A. Schrammeck, T. Johnson, A. Bleem, H. Bernstein, T. Gedeon, J. Heys, and R. Carlson. Escherichia coli co-metabolizes glucose and lactate for enhanced growth, In Prep.

[7] G. S. Becker and K. M. Murphy. The division of labor, coordination costs, and knowledge*. *The Quarterly Journal of Economics*, 107(4):1137–1160, 1992.

[8] B. D. Bennett, E. H. Kimball, M. Gao, R. Osterhout, S. J. V. Dien, and J. D. Rabinowitz. Absolute metabolite concentrations and implied enzyme active site occupancy in escherichia coli. *Nature Chemical Biology*, 5:593–599, 2009.

[9] I. Berman-Frank, P. Lundgren, and P. Falkowski. Nitrogen fixation and photosynthetic oxygen evolution in cyanobacteria. *Research in Microbiology*, 154(3):157 – 164, 2003.

[10] R. Boyd. Culture and the evolution of human cooperation. *Philosophical Transactions of the Royal Society B: Biological Sciences*, 364:3281–8, 2009.

[11] J. J. Bull and W. R. Harcombe. Population dynamics constrain the cooperative evolution of cross-feeding. *PLOS ONE*, 4(1):1–7, 01 2009.

[12] R. Carlson and F. Srienc. Fundamental escherichia coli biochemical pathways for biomass and energy production: Identification of reactions. *Biotechnology and Bioengineering*, 85(1):1–19, 2004.

[13] O. Ciofu, L. F. Mandsberg, T. Bjarnsholt, T. Wassermann, and N. Hiby. Genetic adaptation of pseudomonas aeruginosa during chronic lung infection of patients with cystic fibrosis: strong and weak mutators with heterogeneous genetic backgrounds emerge in muca and/or lasr mutants. *Microbiology*, 156(4):1108–1119, 2010.

[14] C. De Mazancourt and M. W. Schwartz. A resource ratio theory of cooperation. *Ecology Letters*, 13(3):349–359, 2010.

[15] E. Doedel, A. Champneys, F. Dercole, T. Fairgrieve, Y. Kuznetsov, B. Oldeman, R. Paffenroth, B. Sandstede, X. Wang, and C. Zhang. Xppaut/auto, 1996. https://indy.cs.concordia.ca/auto/.

[16] H. Dourado, V. G. Maurino, and M. J. Lercher. Enzymes and substrates are balanced at minimal combined mass concentration in vivo. *bioRxiv*, 2017.

[17] B. Ermentrout, Author and A. Mahajan, Reviewer. Simulating, analyzing, and animating dynamical systems: A guide to xppaut for researchers and students, 2003.

[18] J. Free. *Insect pollination of crops*. Academic Press, London, 2 edition, 1993.

[19] D. J. Gage. Infection and invasion of roots by symbiotic, nitrogen-fixing rhizobia during nodulation of temperate legumes. *Microbiol. Mol. Biol. Rev.*, 68(2):280–300, Jun 2004.

[20] G. F. Gauze. *The struggle for existence*. Baltimore,The Williams and Wilkins company, 1934.

[21] G. F. Gauze. The struggle for existence. *Proceedings of the Royal Society of London B: Biological Sciences*, 2002.

[22] I. Gudelj, M. Kinnersley, P. Rashkov, K. Schmidt, and F. Rosenzweig. Stability of cross-feeding polymorphisms in microbial communities. *PLOS Computational Biology*, 12(12):1–17, 12 2016.

[23] G. Guillermo. Improvement of escherichia coli production strains by modification of the phosphoenolpyruvate:sugar phosphotransferase system. *Microbial Cell Factories*, 4:14, 2005.

[24] C. W. Ha, Y. Y. Lam, and A. J. Holmes. Mechanistic links between gut microbial community dynamics, microbial functions and metabolic health. *World J. Gastroenterol.*, 20(44):16498–16517, Nov 2014.

[25] G. Hardin. The competitive exclusion principle. *Science*, 3409(131):1292–1297, 1960.

[26] I. Ispolatov, M. Ackermann, and M. Doebeli. Division of labour and the evolution of multicellularity. *Proc. R. Soc. B*, 279:1768–1776, 2012.

[27] C. A. Kearns, D. W. Inouye, and N. M. Waser. Endangered mutualisms: The conservation of plant-pollinator interactions. *Annual Review of Ecology and Systematics*, 29(1):83–112, 1998.

[28] M. Kinnersley, J. W. Wenger, G. Sherlock, and F. R. Rosenzweig. *Rapid Evolution of Simple Microbial Communities in the Laboratory*, pages 107–120. Springer Berlin Heidelberg, Berlin, Heidelberg, 2011.

[29] T. Kuritz. Cyanobacteria as agents for the control of pollution by pesticides and chlorinated organic compounds. *J. Appl. Microbiol.*, 85 Suppl 1:186S–192S, Dec 1998.

[30] T. Kuritz and C. P. Wolk. Use of filamentous cyanobacteria for biodegradation of organic pollutants. *Appl. Environ. Microbiol.*, 61(3):1169, Mar 1995.

[31] M. Levert, O. Zamfir, O. Clermont, O. Bouvet, S. Lespinats, M. C. Hipeaux, C. Branger, B. Picard, C. Saint-Ruf, F. Norel, T. Balliau, M. Zivy, H. Le Nagard, S. Cruvellier, B. Chane-Woon-Ming, S. Nilsson, I. Gudelj, K. Phan, T. Ferenci, O. Tenaillon, and E. Denamur. Molecular and evolutionary bases of within-patient genotypic and phenotypic diversity in escherichia coli extraintestinal infections. *PLOS Pathogens*, 6(9):1–19, 09 2010.

[32] H. Liu, R. Ramnarayanan, and B. E. Logan. Production of electricity during wastewater treatment using a single chamber microbial fuel cell. *Environmental Science & Technology*, 38(7):2281–2285, 2004.

[33] H. Lodish, A. Berk, S. Zipursky, and et al. *Molecular Cell Biology*. W. H. Freeman, New York, 2000.

[34] C. R. MacLean and I. Gudelj. Resource competition and social conflict in experimental populations of yeast. *Nature*, 441:498–501, 2006.

[35] K. Manch, L. Notley-McRobb, and T. Feremci. Mutational adaptation of escherichia coli to glucose limitation involves distinct evolutionary pathways in aerobic and oxygen-limited environments. *Genetics*, 153:5–12, 1999.

[36] MATLAB. *R2016a*. The MathWorks, Inc., Natick, Massachusetts, 2016.

[37] M. T. Mee, J. J. Collins, G. M. Church, and H. H. Wang. Syntrophic exchange in synthetic microbial communities. *Proc Natl Acad Sci U S A*, 111(20):E2149–E2156, 2014.

[38] J. J. Minty, M. E. Singer, S. A. Scholz, C.-H. Bae, J.-H. Ahn, C. E. Foster, J. C. Liao, and X. N. Lin. Design and characterization of synthetic fungal-bacterial consortia for direct production of isobutanol from cellulosic biomass. *Proceedings of the National Academy of Sciences*, 110(36):14592–14597, 2013.

[39] S. Møller, C. Sternberg, J. B. Andersen, B. B. Christensen, J. L. Ramos, M. Givskov, and S. Molin. In situ gene expression in mixed-culture biofilms: evidence of metabolic interactions between community members. *Appl. Environ. Microbiol.*, 64(2):721–732, Feb 1998.

[40] B. E. Morris, R. Henneberger, H. Huber, and C. Moissl-Eichinger. Microbial syntrophy: interaction for the common good. *FEMS Microbiology Reviews*, 37(3):384–406, 2013.

[41] F. C. Neidhardt and J. L. Ingraham. *Physiology of the Bacterial Cell: A molecular approach*. Sinauer Associates Inc, 1990.

[42] S. Pande, F. Kaftan, S. Lang, A. Svatos, S. Germerodt, and C. Kost. Privatization of cooperative benefits stabilizes mutualistic cross-feeding interactions in spatially structured environments. *The ISME Journal*, 10(6):1413–1423, 2016.

[43] S. Pande, H. Merker, K. Bohl, M. Reichelt, S. Schuster, L. F. de Figueiredo, C. Kaleta, and C. Kost. Fitness and stability of obligate cross-feeding interactions that emerge upon gene loss in bacteria. *The ISME Journal*, 8(5):953–962, 2014.

[44] S. Pirt. The maintenance energy of bacteria in growing cultures. *Proceedings of the Royal Society of London B: Biological Sciences*, 163(991):224–231, 1965.

[45] R. Popa, P. K. Weber, J. Pett-Ridge, J. A. Finzi, S. J. Fallon, I. D. Hutcheon, K. H. Nealson, and D. G. Capone. Carbon and nitrogen fixation and metabolite exchange in and between individual cells of anabaena oscillarioides. *The ISME Journal*, 1:354, 2007.

[46] R. F. Rosenzweig, R. R. Sharp, D. S. Treves, and J. Adams. Microbial evolution in a simple unstructured environment: genetic differentiation in escherichia coli. *Genetics*, 137(4):903–917, 1994.

[47] V. Rossetti, B. E. Schirrmeister, M. V. Bernasconi, and H. C. Bagheri. The evolutionary path to terminal differentiation and division of labor in cyanobacteria. *Journal of Theoretical Biology*, 262(1):23 – 34, 2010.

[48] D. Schepens, A. E. Beck, J. J. Heys, T. Gedeon, and R. P. Carlson. *Advances in Systems and Synthetic Biology*, chapter The Benefits of Resource Partitioning and Division of Labor in Microbial Consortia, pages 137–148. EDP Sciences Publishing, 2017.

[49] I. Schomburg, A. Chang, S. Placzek, C. Shngen, M. Rother, M. Lang, C. Munaretto, S. Ulas, M. Stelzer, A. Grote, M. Scheer, and D. Schomburg. Brenda in 2013: Integrated reactions, kinetic data, enzyme function data, improved disease classification: New options and contents in brenda. *Nucleic Acids Research*, 41:D764–72, 2013.

[50] S. Schuster, L. F. de Figueiredo, A. Schroeter, and C. Kaleta. Combining metabolic pathway analysis with evolutionary game theory. explaining the occurrence of low-yield pathways by an analytic optimization approach. *Biosystems*, 105(2):147 – 153, 2011. Proceedings of the workshop.

[51] H. Seligmann. Cost-minimization of amino acid usage. *Journal of Molecular Evolution*, 56(2):151–161, Feb 2003.

[52] E. C. Seth and M. E. Taga. Nutrient cross-feeding in the microbial world. *Frontiers in Microbiology*, 5:350, 2014.

[53] D. Sivasubramaniam and A. E. Franks. Bioengineering microbial communities: Their potential to help, hinder and disgust. *Bioengineered*, 7(3):137–144, Apr 2016.

[54] ThomasPfeiffer and SebastianBonhoeffer. Evolution of cross-feeding in microbial populations. *The American Naturalist*, 163(6):E126–E135, 2004.

[55] D. Tilman. *Resource competition and community structure*. Princeton University Press, Princeton, 1982.

[56] M. Venters, R. P. Carlson, T. Gedeon, and J. J. Heys. Effects of spatial localization on microbial consortia growth. *PLOS ONE*, 12(1):1–20, 01 2017.

[57] V. Wigneswaran, C. I. Amador, L. Jelsbak, C. Sternberg, and L. Jelsbak. Utilization and control of ecological interactions in polymicrobial infections and community-based microbial cell factories. *F1000Research*, 5, 2016.

[58] X. Yang and J. Borland. A microeconomic mechanism for economic growth. *Journal of Political Economy*, 99(3):460–482, 1991.

[59] A. Zelezniak, S. Andrejev, O. Ponomarova, D. R. Mende, P. Bork, and K. R. Patil. Metabolic dependencies drive species co-occurrence in diverse microbial communities. *Proceedings of the National Academy of Sciences*, 112(20):6449–6454, 2015.

[60] X. Zhang and J. L. Reed. Adaptive evolution of synthetic cooperating communities improves growth performance. *PLOS ONE*, 9(10):1–12, 10 2014.

[61] A. R. Zomorrodi and D. Segre. Genome-driven evolutionary game theory helps understand the rise of metabolic interdependencies in microbial communities. *Nature Communications*, 8(1):1563, 2017.

APPENDICES

APPENDIX A

LABORATORY EXPERIENCE

As part of collaboration with members of the Biological and Chemical Engineering department here at Montana State University, I assisted in the measuring of some parameters through laboratory experiments. Our ultimate goal was to measure growth and inhibition of *E.coli* in batch cultures under various glucose and lactic acid concentrations. These data are part of the data being analyzed and fit with various growth and inhibition curves by our collaborators. Results are being prepared for publication [6].

A.1 Medium Recipes

LB agar plates for streaking were provided by collaborator Ashely Beck according to the following recipe:

1. $\frac{1}{2}$ LB Agar Plates, per $\frac{1}{2}$ liter:
   (a) 7.5 g Agar
   (b) 5 g LB broth
   (c) H_2O to $\frac{1}{2}$ liter mark

Elements of media were prepared by me according to the following recipes:

1. 5× M9 Stock, per 1 liter (filter sterilized or autoclaved):
   (a) 30 g - Na_2HPO_4
   (b) 15 g - KH_2PO_4
   (c) 5 g - NH_4Cl
   (d) 2.5 g - NaCl
2. Trace Metals Solution, per 1 liter (filter sterilized):
   (a) 0.55 g - $CaCl_2$ or 0.73 g $CaCl_2 \cdot 2H_2O$
   (b) 0.10 g - $MnCl_2 \cdot 4H_2O$
   (c) 0.17 g - $ZnCl_2$
   (d) 0.043 g - $CuCl_2 \cdot 2H_2O$
   (e) 0.06 g - $CoCl_2 \cdot 6H_2O$
   (f) 0.06 g - $Na_2MoO_4 \cdot 2H_2O$
   (g) 0.06 g - $Fe(NH_4)_2(SO_4)_2 \cdot 6H_2O$
   (h) 0.20 g - $FeCl_3 \cdot 6H_2O$

Experiments were run with both glucose and no glucose media for varying concentrations of lactic acid (added in the form of sodium lactate). All media was filter sterilized and pH adjusted to 7.

1. Glucose Media:
   1×M9 + 10g/L glucose liquid media + x g/L NaLactate , per $\frac{1}{2}$ liter:
   (a) 100 ml - 5× M9 Stock
   (b) 0.5 ml - 1 M $MgSO_4 \cdot 7H_2O$
   (c) 15 ml - trace metal solution
   (d) 50 ml - 100 g/L glucose stock
   (e) $4.73485x$ ml - 105.6 g/L NaLactate solution
   (f) remainder to 500 ml - ddH_2O

2. No Glucose Media:
   1×M9 + x g/L NaLactate , per $\frac{1}{2}$ liter:
   (a) 100 ml - 5× M9 Stock
   (b) 0.5 ml - 1 M $MgSO_4 \cdot 7H_2O$
   (c) 15 ml - trace metal solution
   (d) $4.73485x$ ml - 105.6 g/L NaLactate solution
   (e) remainder to 500 ml - ddH_2O

A.1.1 Shake Flask Culturing Protocol

All shake flasks were inoculated with *E.coli* (strain MG1655 WT) with the following shake flask culturing protocol.

1. Two days before experiment:
   Make a plate culture of the strain of interest. Remove sample from the -80°C freezer and streak a small amount onto a LB agar plate using a sterile pipette tip. Replace sample in the freezer asap.

2. One day before experiment:
   (a) Make experimental media. This is 1×M9 + (10 g/L glucose) + desired Lactic Acid concentration. Adjust pH, if needed, using HCl to 7. Record media pH.
   (b) Make an overnight culture from the plate culture. Fill a culturing tube with 7mL sterile experimental media (1×M9 + (10g/l glucose) + appropriate acid). If necessary, "Spike" this with 70 μL of LB Broth (100 g/l). Use a sterile pipette tip to remove some of the *E. coli* culture from the LB plate, and mix this into the media in the culturing tube. Vortex to mix well. Place the culturing tube in the shaking incubator, 37°C and 150 rpm.
   (c) Autoclave equipment. You will need sterile 1mL pipette tips and sterile shake flasks. Use three shake flasks (A, B, and C) per condition so that you have triplicate data.

3. Day of experiment:

   (a) *Start the laminar flow cabinet.* Sterilize with EtOH, allow to run at least 10 min before use.

   (b) *Start the spectrophotometer.* Turn on using switch at back of machine. Set the wavelength to 600 nm and allow the lamp to warm up at least 10 minutes. Set the blank using a cuvette of DI water.

   (c) *Prepare the shake flasks.* Using the electronic pipette (fitted with 25mL pipette), fill each sterile shake flask with 50 mL of the media of interest.

   (d) *Prepare the overnight culture.* Measure OD(600nm) from aliquot of overnight culture. In the flow cabinet, transfer the culture from the culture tube to a small Falcon tube. Place in the centrifuge and balance. Run for 8 min, 3700 rpm, 25°C. Remove Falcon tube and decant liquid, making sure not to dump out any of the cells in the bottom. Refill the tube with 7mL sterile experimental medium and vortex to wash the cells. Replace in centrifuge and run again at the same settings. Remove Falcon tube and decant liquid again. Refill with sterile medium so final OD(600nm) is approximately 0.5 and vortex to resuspend the cells. *DO NOT FORGET to do the above step!! It is critical to remove glucose and NaLac from the inoculum, as their presence can greatly affect your results.

   (e) *Inoculate flasks.* Then, using sterile 1mL pipettes, add 1mL of inoculum to each shake flask. Swirl the flask gently, and use another sterile 1mL pipette to move 1mL of culture from the shake flask to a cuvette. Take this cuvette to the spectrophotometer and measure/record the time and absorbance. Place the shake flask in the shaking incubator (37C and 150 rpm), and repeat the inoculation-absorbance procedure for each flask.

   (f) *Sampling.* Sample the shake flasks every 1-2 hours until stationary stage is reached (about 7 or 8 samples). Each sample measurement will include time, absorbance, and volume of sample taken. Remove the shake flask from the incubator and use a sterile pipette tip to transfer a 500μL volume to a cuvette. Measure absorbance at OD600 nm and record.

4. Clean up:
   Autoclave all of the culture-filled shake flasks on the liquid setting for at least 20 min. You can then pour sterilized culture waste down the drain and wash the glassware using a dilute soap solution. Rinse well with tap water, and then do a final rinse with DI water before drying (this prevents spotting).

A.2 Experimental Data

We provide details of all experimental data in supplemental spreadsheets and include the results of one experiment here. The following data was collected from

Time (h)	OD (600 nm)			
	A	B	C	Control
0.00	0.009	0.009	0.010	0
3.60	0.088	0.087	0.100	0
4.70	0.161	0.187	0.219	0
5.63	0.322	0.378	0.444	0
6.63	0.669	0.762	0.892	0
7.85	1.428	1.652	1.855	0
8.63	2.097	2.394	2.607	0
9.48	2.871	3.014	3.372	0

Table A.1: **Experimental Data -1XM9, 10 g/L glucose, and 4 g/L NaLactate** Batch culture data of *E. coli* grown in media - 1XM9, 10 g/L glucose, and 4 g/L sodium lactate, with starting pH 6.99. Optical density (600 nm) of population measured periodically until culture reached stationary phase.

	A	B	C	Average	StDev
$\mu \frac{1}{\mathrm{h}}$	0.6947	0.7187	0.7245	0.7127	0.0158

Table A.2: **Experimental Data -1XM9, 10 g/L glucose, and 4 g/L NaLactate** Batch culture data of *E. coli* grown in media - 1XM9, 10 g/L glucose, and 4 g/L sodium lactate, with starting pH 6.99. Optical density (600 nm) of population measured periodically until culture reached stationary phase.

batch culture of *E. coli* (strain MG1655 WT) using the above protocol and media- 1XM9, 10 g/L glucose, and 4 g/L sodium lactate, with starting pH of 7. Population density was recorded periodically using optical density given by a spectrophotometer with absorbance measured at OD 600 nm (Table A.1). Experiment was performed in triplicate with a control of media not inoculated.

Data was plotted and exponential growth was fitted to the four data points collected with fastest growth for each batch (Fig A.1).

Average exponential growth rate and standard deviation is computed from the growth rate for each batch culture obtained from the exponential fit (Table A.2).

Similar experiments were performed with various concentrations of sodium lactate and plotted (Fig A.2) to obtain a product inhibition curve for sodium lactate. Curve is being fit by collaborators and publication of data is in preparation [6]. See attached supplemental spreadsheets for other data collected for this curve and for data from experiments measuring the inhibition curve of sodium lactate with no glucose present in the media.

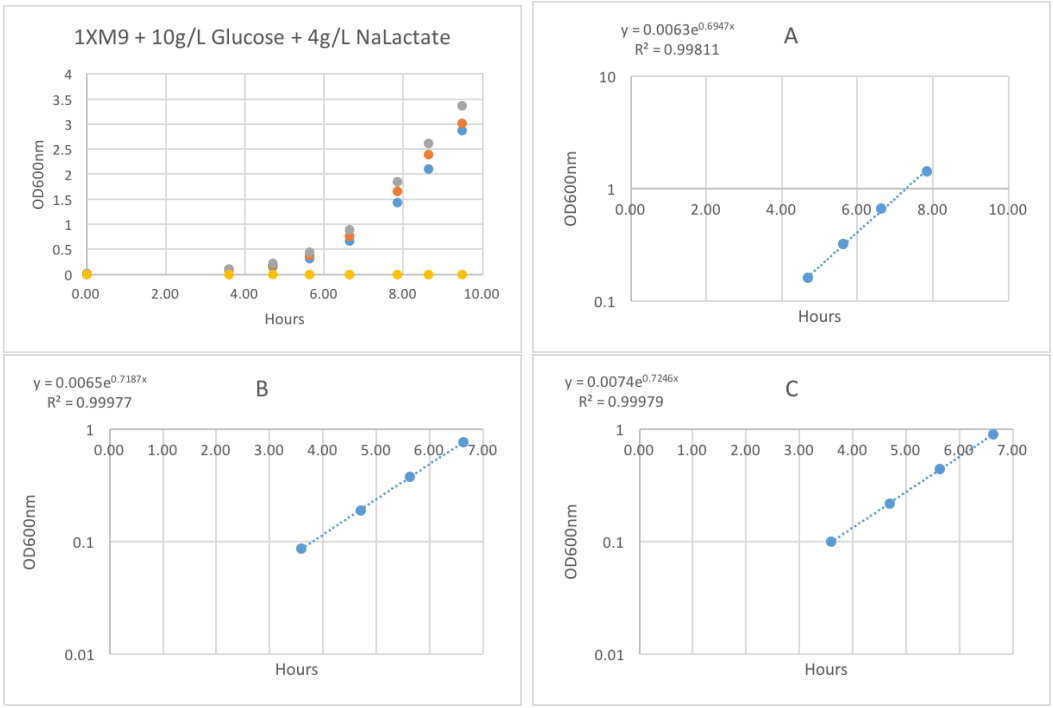

Figure A.1: **Plot of experimental data-1XM9, 10 g/L glucose, and 4 g/L NaLactate** Experimental data is plotted and exponential growth function is fit to the four data points collected with fastest growth for each batch.

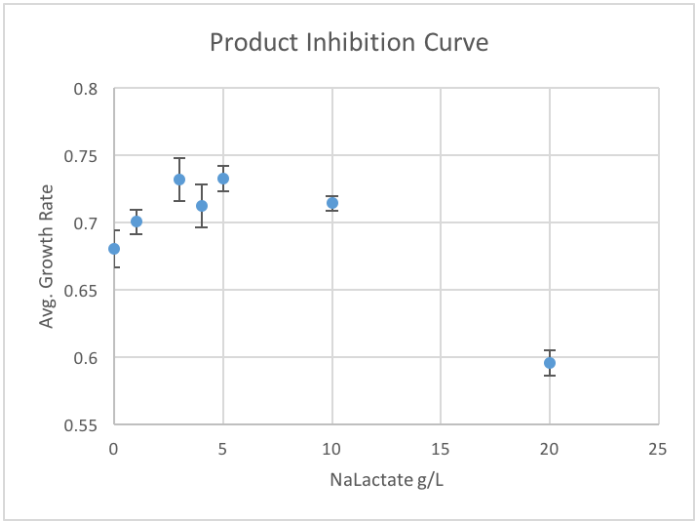

Figure A.2: **Product inhibition curve - Sodium lactate and glucose** Average growth rate and standard deviation plotted for various sodium lactate concentration.

APPENDIX B

SAMPLE XPP CODE

For the purposes of transparency and reproducibility, we provide here the *.ode code used for XPP [17]. Note that due to formatting requirements, variable and parameter names may appear differently in this code as compared to those used previously in this work.

```
init Xcheat=0.1, XWT=0.1, XcoA=0.1, Aext=0
init Acheat=0.01, AWT=0.01, AcoA=0.01, AcoB=0.01, S=0.001

params Sn=1, qA=9, d=.2, mum=.6, J=.19, beta=1000, YAX=.25, qsaCheat=0
params qsaWT=0.1, qsaCoA=.4, qsaCoB=0, YSX=15, KS=.001
params KA=.023, KAx=5.957, KAI=.00597, Ahat=.39, YSA=1.1

muCheat(Acheat,Acheat,S)=mum*Acheat/(KA+Acheat)*Acheat/(KA+Acheat)*S/(KS+S)
muWT(AWT,AWT,S)=mum*AWT/(KA+AWT)*AWT/(KA+AWT)*S/(KS+S)
muCoA(AcoA,AcoB,S)=mum*AcoA/(KA+AcoA)*AcoB/(KA+AcoB)*S/(KS+S)
muCoB(AcoB,AcoA,S)=mum*AcoB/(KA+AcoB)*AcoA/(KA+AcoA)*S/(KS+S)

RSX(Xcheat,XWT,XcoA)=YSX*(muCheat(Acheat,Acheat,S)*Xcheat+muWT(AWT,AWT,S)*X
WT+muCoA(AcoA,AcoB,S)*XcoA+muCoB(AcoB,AcoA,S)*XcoA)

TAcheat(Acheat,Aext)=qA*(Acheat-Aext)
TAWT(AWT,Aext)=qA*(AWT-Aext)
TAcoA(AcoA,Aext)=qA*(AcoA-Aext)
TAcoB(AcoB,Aext)=qA*(AcoB-Aext)

XWT'=(muWT(AWT,AWT,S)-d)*XWT
Xcheat'=(muCheat(Acheat,Acheat,S)-d)*Xcheat
XcoA'=(muCoA(AcoA,AcoB,S)-d)*XcoA
Aext'=-
J*Aext+TAcheat(Acheat,Aext)*Xcheat+TAWT(AWT,Aext)*XWT+TAcoA(AcoA,Aext)*XcoA
+TAcoB(AcoB,Aext)*XcoA
Acheat'=beta*(qsaCheat*S/(KS+S)-YAX*muCheat(Acheat,Acheat,S)-TAcheat(Acheat,Aext))-
Acheat*(muCheat(Acheat,Acheat,S)-d)
AWT'=beta*(qsaWT*S/(KS+S)-YAX*muWT(AWT,AWT,S)-TAWT(AWT,Aext))-
AWT*(muWT(AWT,AWT,S)-d)
AcoA'=beta*(qsaCoA*S/(KS+S)-YAX*muCoA(AcoA,AcoB,S)-TAcoA(AcoA,Aext))-
AcoA*(muCoA(AcoA,AcoB,S)-d)
AcoB'=beta*(qsaCoB*S/(KS+S)-YAX*muCoB(AcoB,AcoA,S)-TAcoB(AcoB,Aext))-
AcoB*(muCoB(AcoB,AcoA,S)-d)
S'=J*Sn-J*S-
2*YSA*(qsaCheat*S/(KS+S)*Xcheat+qsaWT*S/(KS+S)*XWT+qsaCoA*S/(KS+S)*XcoA+qsa
CoB*S/(KS+S)*XcoA)-RSX(Xcheat,XWT,XcoA)

@ maxstor=120000
@ total=10, dt=0.5, bounds=1000000
@ method=gear, toler=0.01, dtmin=0.00000000000001, dtmax=.001
@ xlo=0, xhi=10, ylo=-0.1, yhi=0.5

done
```

Figure B.1: Symmetric nonlinear passive transport model *.ode code

```
init Xcheat=0.1, XWT=0.1, XcoA=0.1, Aext=0
Acheat=0.01, AWT=0.01, AcoA=0.01, AcoB=0.01, S=0.001

params qA=10, Sn=5.6, d=.2, mum=.6, J=.19, beta=1000, YAX=.25, qsaCheat=0
params qsaWT=0.1, qsaCoA=.4, qsaCoB=0, YSX=15, KS=.001, KA=.023
params KAx=5.957, KAI=.00597, Ahat=.39, YSA=1.1

muCheat(Acheat,Acheat,S)=mum*Acheat/(KA+Acheat)*Acheat/(KA+Acheat)*S/(KS+S)
muWT(AWT,AWT,S)=mum*AWT/(KA+AWT)*AWT/(KA+AWT)*S/(KS+S)
muCoA(AcoA,AcoB,S)=mum*AcoA/(KA+AcoA)*AcoB/(KA+AcoB)*S/(KS+S)
muCoB(AcoB,AcoA,S)=mum*AcoB/(KA+AcoB)*AcoA/(KA+AcoA)*S/(KS+S)

RSX(Xcheat,XWT,XcoA)=YSX*(muCheat(Acheat,Acheat,S)*Xcheat+muWT(AWT,AWT,S)*XWT+muCoA(
AcoA,AcoB,S)*XcoA+muCoB(AcoB,AcoA,S)*XcoA)

TAcheat(Acheat,Aext)=(-qA/2*(Ahat-Acheat)/Ahat*Aext/(KAI+Aext))*tanh(Acheat/.01)+(-qA/2*(Ahat-
Acheat)/Ahat*Aext/(KAI+Aext))*tanh((Ahat-Acheat)/.01)+(qA/2*(Acheat-
Ahat)/Ahat*Acheat/(KAx+Acheat))*tanh(Acheat/.01)+(qA/2*(Acheat-
Ahat)/Ahat*Acheat/(KAx+Acheat))*tanh((Acheat-Ahat)/.01)

TAWT(AWT,Aext)=(-qA/2*(Ahat-AWT)/Ahat*Aext/(KAI+Aext))*tanh(AWT/.01)+(-qA/2*(Ahat-
AWT)/Ahat*Aext/(KAI+Aext))*tanh((Ahat-AWT)/.01)+(qA/2*(AWT-
Ahat)/Ahat*AWT/(KAx+AWT))*tanh(AWT/.01)+(qA/2*(AWT-Ahat)/Ahat*AWT/(KAx+AWT))*tanh((AWT-
Ahat)/.01)

TAcoA(AcoA,Aext)=(-qA/2*(Ahat-AcoA)/Ahat*Aext/(KAI+Aext))*tanh(AcoA/.01)+(-qA/2*(Ahat-
AcoA)/Ahat*Aext/(KAI+Aext))*tanh((Ahat-AcoA)/.01)+(qA/2*(AcoA-
Ahat)/Ahat*AcoA/(KAx+AcoA))*tanh(AcoA/.01)+(qA/2*(AcoA-
Ahat)/Ahat*AcoA/(KAx+AcoA))*tanh((AcoA-Ahat)/.01)

TAcoB(AcoB,Aext)=(-qA/2*(Ahat-AcoB)/Ahat*Aext/(KAI+Aext))*tanh(AcoB/.01)+(-qA/2*(Ahat-
AcoB)/Ahat*Aext/(KAI+Aext))*tanh((Ahat-AcoB)/.01)+(qA/2*(AcoB-
Ahat)/Ahat*AcoB/(KAx+AcoB))*tanh(AcoB/.01)+(qA/2*(AcoB-
Ahat)/Ahat*AcoB/(KAx+AcoB))*tanh((AcoB-Ahat)/.01)

XWT'=(muWT(AWT,AWT,S)-d)*XWT
Xcheat'=(muCheat(Acheat,Acheat,S)-d)*Xcheat
XcoA'=(muCoA(AcoA,AcoB,S)-d)*XcoA
Aext'=-
J*Aext+TAcheat(Acheat,Aext)*Xcheat+TAWT(AWT,Aext)*XWT+TAcoA(AcoA,Aext)*XcoA+TAcoB(AcoB
,Aext)*XcoA
Acheat'=beta*(qsaCheat*S/(KS+S)-YAX*muCheat(Acheat,Acheat,S)-TAcheat(Acheat,Aext))-
Acheat*(muCheat(Acheat,Acheat,S)-d)
AWT'=beta*(qsaWT*S/(KS+S)-YAX*muWT(AWT,AWT,S)-TAWT(AWT,Aext))-
AWT*(muWT(AWT,AWT,S)-d)
AcoA'=beta*(qsaCoA*S/(KS+S)-YAX*muCoA(AcoA,AcoB,S)-TAcoA(AcoA,Aext))-
AcoA*(muCoA(AcoA,AcoB,S)-d)
AcoB'=beta*(qsaCoB*S/(KS+S)-YAX*muCoB(AcoB,AcoA,S)-TAcoB(AcoB,Aext))-
AcoB*(muCoB(AcoB,AcoA,S)-d)
S'=J*Sn-J*S-
2*YSA*(qsaCheat*S/(KS+S)*Xcheat+qsaWT*S/(KS+S)*XWT+qsaCoA*S/(KS+S)*XcoA+qsaCoB*S/(KS+S)
*XcoA)-RSX(Xcheat,XWT,XcoA)

@ maxstor=12000
@ total=20, dt=0.5, bounds=1000000
@ method=gear, toler=0.1, dtmin=0.0000000001, dtmax=.01
@ xlo=0, xhi=20, ylo=-0.1, yhi=0.5

done
```

Figure B.2: Symmetric nonlinear active transport model *.ode code

```
init Xcheat=0.1, XWT=0.1, XcoA=0.1, Aext=0
init Acheat=0.01, AWT=0.01, AcoA=0.01, AcoB=0.01, S=0.001

params qA=10, Sn=5.6, d=.2, mum=.6, J=.19, beta=1000, YAX=.25, qsaCheat=0
params qsaWT=0.1, qsaCoA=.4, qsaCoB=0, YSX=15, KS=.001, KA=.023, KAx=5.957
params KAI=.00597, Ahat=.39, YSA=1.1, a=3546, b=556, alpha=1000

cheat(S)=a*(beta*qsaCheat*S/(KS+S))+2*b*sqrt(beta*qsaCheat*S/(KS+S))+a*(beta*qsaCheat*S/(KS
+S))+2*b*sqrt(beta*qsaCheat*S/(KS+S))
wt(S)=a*(beta*qsaWT*S/(KS+S))+2*b*sqrt(beta*qsaWT*S/(KS+S))+a*(beta*qsaWT*S/(KS+S))+2*b*
sqrt(beta*qsaWT*S/(KS+S))
coA(S)=a*(beta*qsaCoA*S/(KS+S))+2*b*sqrt(beta*qsaCoA*S/(KS+S))+a*(beta*qsaCoB*S/(KS+S))+
2*b*sqrt(beta*qsaCoB*S/(KS+S))
coB(S)=a*(beta*qsaCoB*S/(KS+S))+2*b*sqrt(beta*qsaCoB*S/(KS+S))+a*(beta*qsaCoA*S/(KS+S))+
2*b*sqrt(beta*qsaCoA*S/(KS+S))

Avg(S)=(cheat(S)+wt(S)+coA(S)+coB(S))/4
Main(S)=alpha*wt(S)
TotAvg(S)=Avg(S)+Main(S)

Ccheat(S)=TotAvg(S)/(cheat(S)+Main(S))
Cwt(S)=TotAvg(S)/(wt(S)+Main(S))
CcoA(S)=TotAvg(S)/(coA(S)+Main(S))
CcoB(S)=TotAvg(S)/(coB(S)+Main(S))

muCheat(Acheat,Acheat,S)=Ccheat(S)*mum*Acheat/(KA+Acheat)*Acheat/(KA+Acheat)*S/(KS+S)
muWT(AWT,AWT,S)=Cwt(S)*mum*AWT/(KA+AWT)*AWT/(KA+AWT)*S/(KS+S)
muCoA(AcoA,AcoB,S)=CcoA(S)*mum*AcoA/(KA+AcoA)*AcoB/(KA+AcoB)*S/(KS+S)
muCoB(AcoB,AcoA,S)=CcoB(S)*mum*AcoB/(KA+AcoB)*AcoA/(KA+AcoA)*S/(KS+S)

RSX(Xcheat,XWT,XcoA)=YSX*(muCheat(Acheat,Acheat,S)*Xcheat+muWT(AWT,AWT,S)*XWT+mu
CoA(AcoA,AcoB,S)*XcoA+muCoB(AcoB,AcoA,S)*XcoA)

TAcheat(Acheat,Aext)=qA*(Acheat-Aext)
TAWT(AWT,Aext)=qA*(AWT-Aext)
TAcoA(AcoA,Aext)=qA*(AcoA-Aext)
TAcoB(AcoB,Aext)=qA*(AcoB-Aext)

XWT'=(muWT(AWT,AWT,S)-d)*XWT
Xcheat'=(muCheat(Acheat,Acheat,S)-d)*Xcheat
XcoA'=(muCoA(AcoA,AcoB,S)-d)*XcoA
Aext'=-
J*Aext+TAcheat(Acheat,Aext)*Xcheat+TAWT(AWT,Aext)*XWT+TAcoA(AcoA,Aext)*XcoA+TAcoB(
AcoB,Aext)*XcoA
Acheat'=beta*(qsaCheat*S/(KS+S)-YAX*muCheat(Acheat,Acheat,S)-TAcheat(Acheat,Aext))-
Acheat*(muCheat(Acheat,Acheat,S)-d)
AWT'=beta*(qsaWT*S/(KS+S)-YAX*muWT(AWT,AWT,S)-TAWT(AWT,Aext))-
AWT*(muWT(AWT,AWT,S)-d)
AcoA'=beta*(qsaCoA*S/(KS+S)-YAX*muCoA(AcoA,AcoB,S)-TAcoA(AcoA,Aext))-
AcoA*(muCoA(AcoA,AcoB,S)-d)
AcoB'=beta*(qsaCoB*S/(KS+S)-YAX*muCoB(AcoB,AcoA,S)-TAcoB(AcoB,Aext))-
AcoB*(muCoB(AcoB,AcoA,S)-d)
S'=J*Sn-J*S-
2*YSA*(qsaCheat*S/(KS+S)*Xcheat+qsaWT*S/(KS+S)*XWT+qsaCoA*S/(KS+S)*XcoA+qsaCoB*S/(
KS+S)*XcoA)-RSX(Xcheat,XWT,XcoA)

@ maxstor=12000
@ total=100, dt=0.5, bounds=1000000
@ method=gear, toler=0.01, dtmin=0.00000000000001, dtmax=.01
@ xlo=0, xhi=100, ylo=-0.1, yhi=0.5

done
```

Figure B.3: Symmetric nonlinear passive transport model with cost scaling *.ode code

```
init Xcheat=0.1, XWT=0.1, XcoA=0.1, Aext=0
init Acheat=0.01, AWT=0.01, AcoA=0.01, AcoB=0.01, S=0.001

params qA=2, alpha=500, Sn=5.6, d=.2, mum=.6, J=.19, beta=1000, YAX=.25, qsaCheat=0
params qsaWT=0.1, qsaCoA=.4, qsaCoB=0, YSX=15, KS=.001, KA=.023, KAx=5.957
params KAI=.00597, Ahat=.39, YSA=1.1, a=3546, b=556

cheat(S)=a*(beta*qsaCheat*S/(KS+S))+2*b*sqrt(beta*qsaCheat*S/(KS+S))+a*(beta*qsaCheat*S/(KS+S))+2*b*sqrt(b
eta*qsaCheat*S/(KS+S))
wt(S)=a*(beta*qsaWT*S/(KS+S))+2*b*sqrt(beta*qsaWT*S/(KS+S))+a*(beta*qsaWT*S/(KS+S))+2*b*sqrt(beta*qsaW
T*S/(KS+S))
coA(S)=a*(beta*qsaCoA*S/(KS+S))+2*b*sqrt(beta*qsaCoA*S/(KS+S))+a*(beta*qsaCoB*S/(KS+S))+2*b*sqrt(beta*q
saCoB*S/(KS+S))
coB(S)=a*(beta*qsaCoB*S/(KS+S))+2*b*sqrt(beta*qsaCoB*S/(KS+S))+a*(beta*qsaCoA*S/(KS+S))+2*b*sqrt(beta*q
saCoA*S/(KS+S))

Avg(S)=(cheat(S)+wt(S)+coA(S)+coB(S))/4
Main(S)=alpha*wt(S)
TotAvg(S)=Avg(S)+Main(S)

Ccheat(S)=TotAvg(S)/(cheat(S)+Main(S))
Cwt(S)=TotAvg(S)/(wt(S)+Main(S))
CcoA(S)=TotAvg(S)/(coA(S)+Main(S))
CcoB(S)=TotAvg(S)/(coB(S)+Main(S))

muCheat(Acheat,Acheat,S)=Ccheat(S)*mum*Acheat/(KA+Acheat)*Acheat/(KA+Acheat)*S/(KS+S)
muWT(AWT,AWT,S)=Cwt(S)*mum*AWT/(KA+AWT)*AWT/(KA+AWT)*S/(KS+S)
muCoA(AcoA,AcoB,S)=CcoA(S)*mum*AcoA/(KA+AcoA)*AcoB/(KA+AcoB)*S/(KS+S)
muCoB(AcoB,AcoA,S)=CcoB(S)*mum*AcoB/(KA+AcoB)*AcoA/(KA+AcoA)*S/(KS+S)

RSX(Xcheat,XWT,XcoA)=YSX*(muCheat(Acheat,Acheat,S)*Xcheat+muWT(AWT,AWT,S)*XWT+muCoA(AcoA,Aco
B,S)*XcoA+muCoB(AcoB,AcoA,S)*XcoA)

TAcheat(Acheat,Aext)=(-qA/2*(Ahat-Acheat)/Ahat*Aext/(KAI+Aext))*tanh(Acheat/.01)+(-qA/2*(Ahat-
Acheat)/Ahat*Aext/(KAI+Aext))*tanh((Ahat-Acheat)/.01)+(qA/2*(Acheat-
Ahat)/Ahat*Acheat/(KAx+Acheat))*tanh(Acheat/.01)+(qA/2*(Acheat-
Ahat)/Ahat*Acheat/(KAx+Acheat))*tanh((Acheat-Ahat)/.01)

TAWT(AWT,Aext)=(-qA/2*(Ahat-AWT)/Ahat*Aext/(KAI+Aext))*tanh(AWT/.01)+(-qA/2*(Ahat-
AWT)/Ahat*Aext/(KAI+Aext))*tanh((Ahat-AWT)/.01)+(qA/2*(AWT-
Ahat)/Ahat*AWT/(KAx+AWT))*tanh(AWT/.01)+(qA/2*(AWT-Ahat)/Ahat*AWT/(KAx+AWT))*tanh((AWT-
Ahat)/.01)

TAcoA(AcoA,Aext)=(-qA/2*(Ahat-AcoA)/Ahat*Aext/(KAI+Aext))*tanh(AcoA/.01)+(-qA/2*(Ahat-
AcoA)/Ahat*Aext/(KAI+Aext))*tanh((Ahat-AcoA)/.01)+(qA/2*(AcoA-
Ahat)/Ahat*AcoA/(KAx+AcoA))*tanh(AcoA/.01)+(qA/2*(AcoA-Ahat)/Ahat*AcoA/(KAx+AcoA))*tanh((AcoA-
Ahat)/.01)

TAcoB(AcoB,Aext)=(-qA/2*(Ahat-AcoB)/Ahat*Aext/(KAI+Aext))*tanh(AcoB/.01)+(-qA/2*(Ahat-
AcoB)/Ahat*Aext/(KAI+Aext))*tanh((Ahat-AcoB)/.01)+(qA/2*(AcoB-
Ahat)/Ahat*AcoB/(KAx+AcoB))*tanh(AcoB/.01)+(qA/2*(AcoB-Ahat)/Ahat*AcoB/(KAx+AcoB))*tanh((AcoB-
Ahat)/.01)

XWT'=(muWT(AWT,AWT,S)-d)*XWT
Xcheat'=(muCheat(Acheat,Acheat,S)-d)*Xcheat
XcoA'=(muCoA(AcoA,AcoB,S)-d)*XcoA
Aext'=-J*Aext+TAcheat(Acheat,Aext)*Xcheat+TAWT(AWT,Aext)*XWT+
TAcoA(AcoA,Aext)*XcoA+TAcoB(AcoB,Aext)*XcoA
Acheat'=beta*(qsaCheat*S/(KS+S)-YAX*muCheat(Acheat,Acheat,S)-TAcheat(Acheat,Aext))-
Acheat*(muCheat(Acheat,Acheat,S)-d)
AWT'=beta*(qsaWT*S/(KS+S)-YAX*muWT(AWT,AWT,S)-TAWT(AWT,Aext))-AWT*(muWT(AWT,AWT,S)-d)
AcoA'=beta*(qsaCoA*S/(KS+S)-YAX*muCoA(AcoA,AcoB,S)-TAcoA(AcoA,Aext))-AcoA*(muCoA(AcoA,AcoB,S)-d)
AcoB'=beta*(qsaCoB*S/(KS+S)-YAX*muCoB(AcoB,AcoA,S)-TAcoB(AcoB,Aext))-AcoB*(muCoB(AcoB,AcoA,S)-d)
S'=J*Sn-J*S-2*YSA*(qsaCheat*S/(KS+S)*Xcheat+qsaWT*S/(KS+S)*XWT+
qsaCoA*S/(KS+S)*XcoA+qsaCoB*S/(KS+S)*XcoA)-RSX(Xcheat,XWT,XcoA)

@ maxstor=12000
@ total=20, dt=0.5, bounds=1000000
@ method=gear, toler=0.01, dtmin=0.000000000001, dtmax=.01
@ xlo=0, xhi=20, ylo=-0.1, yhi=0.5

done
```

Figure B.4: Symmetric nonlinear active transport model with cost scaling *.ode code